

ALMA MATER STUDIORUM - UNIVERSITÀ DI BOLOGNA

SCUOLA DI INGEGNERIA

DIPARTIMENTO di
INGEGNERIA DELL'ENERGIA ELETTRICA E DELL'INFORMAZIONE
"Guglielmo Marconi"
DEI

**LAUREA MAGISTRALE IN
TELECOMMUNICATIONS ENGINEERING**

TESI DI LAUREA
in
Optical Fiber System

Feasible predistortion loop for the linearization of
Radio-over-Fiber system based on 850 nm Vertical
Cavity Surface Emitting Laser and standard G.652 fiber

CANDIDATO

Lorenzo Baschieri

RELATORE

Chiar.mo Prof. Giovanni Tartarini

CORRELATORE

Ing. Jacopo Nanni

Anno Accademico 2019/2020

Sessione III

For those who have always believed in me and supported me during this wonderful journey.

I will make you proud.

Summary

- ABSTRACT:** 6
- INTRODUCTION**..... 7
- CHAPTER 1**..... 11
 - 1.1) USE OF COUPLER** 11
 - 1.2) ANALYSIS OF THE BIMODALITY**..... 19
 - 1.2.1) MATHEMATICAL MODEL** 20
 - 1.2.2) CONSIDERATION ON THE PROPOSED SOLUTION:** 23
 - 1.2.3) CONCLUSION OF THE PRELIMINARY TEST** 24
 - 1.3) NOTCHES IN FREQUENCY** 24
 - 1.3.1) INTERMODAL DISPERSION ANALYSYS**..... 25
 - 1.4) MATLAB MODELLING FOR BIMODALITY EVALUATION**..... 30
 - 1.5) 300 m CASE ANALYSIS** 35
 - 1.5.1) COUPLER 50-50**..... 36
 - 1.5.2) COUPLER 90-10**..... 38
 - 1.5.3) COUPLER 99-01**..... 41
 - 1.5.3) CONCLUSION ON 300 m** 43
 - 1.6) 2 KM ANALYSIS** 45
 - 1.6.1) COUPLER 50-50**..... 46
 - 1.6.2) COUPLER 90-10**..... 48
 - 1.6.3) COUPLER 99-01**..... 51
 - 1.6.4) MEASURE COMPARISON**..... 54
 - 1.7) CONCLUSION ON THE TWO MEASURMENTS SET**..... 54
 - 1.8) 5 um TEST**..... 55
 - 1.8.1) CONSIDERATION ON 5 um SMF**..... 58
 - 1.9) CONCLUSION** 59
- CHAPTER 2 DIGITAL PREDISTORTION**..... 60
 - 2.1) OVERVIEW ON PREDISTORTION** 60

2.1.1) LINEARIZATION METHODS	63
2.2) BEHAVIORAL MODELLING OF ROF LINK	65
2.2.1) MODEL ARCHITECTURE	66
2.2.2) NL SYSTEMS	67
2.2.3) DIRECT LEARNING ARCHITECTURE	68
2.3) MODELLING OF MEMORY EFFECTS	71
2.3.1) MEMORY STRUCTURES	72
2.3.2) WIENER MODEL	74
2.3.3) MEMORY POLYNOMIAL	75
2.3.4) GENERALIZED MEMORY POLYNOMIAL	76
2.3.5) COMPUTATIONAL COMPLEXITY	76
2.4) ESTIMATION ALGORITHMS	76
2.5) MATLAB MODEL	79
2.5.1) GMP FUNCTION	82
2.5.2) SIMULATION OF RoF SYSTEM	83
2.5.3) POST AND PREDISTORTER OPERATION	84
2.5.4) DATA POST-PROCESSING FIGURE	85
CHAPTER 3: REALIZATION OF THE FINAL SYSTEM	88
3.1) LTE FRAME GENERATOR	88
3.1.1) OFDM/OFDMA	89
3.1.2) FRAME FORMAT	92
3.1.3) ALLOCATION BANDWIDTH	92
3.1.4) PHYSICAL CHANNEL	93
3.1.5) PHYSICAL SIGNAL	93
3.2) TRANSMITTER LTE	94
3.3) RECEIVER LTE	96
3.3.1) RECEIVER SOFTWARE	99
3.4) MERGING PROGRAMS	101

3.5) TRAINING OF THE ALGORITHM	103
3.5.1) MOTIVATION	104
3.6) IMPACT OF PA GAIN CHOICES	107
3.6.1) LINEARIZATION G1	109
3.6.2) LINEARIZATION AT G2	111
3.7) EXPERIMENTAL RESULTS	112
3.7.1) INTERMEDIATE LINK	112
3.7.2) FINAL LINK COUPLER 50-50	116
3.7.3) FINAL LINK COUPLER 90-10	121
3.7.4) TEST 256 QAM IN DIRECT PATH	123
CONCLUSION:	127
BIBLIOGRAFY	130

ABSTRACT:

The main purpose of the work is to investigate a low-cost solution for systems designed for the distribution of the RF signal employing the Radio Over Fiber technology, including the additional feature of digital predistortion in order to improve the performance of the system, the overall quality and to support higher order modulation format already present in the LTE standard, e.g. 256 QAM.

In this work has been used a Vertical Cavity Surface Emitting Laser (VCSEL) single mode laser operating at 850 nm and the standard single mode fiber G-652, since this combination, is very interesting from a cost point of view, being one of the cheapest possible solution that can be implemented.

The main problem is due to the fact that, using this kind of lasers in a fiber like G-652, that has been realized to work at wavelength higher than 1260 nm, problems of bimodality arise.

So, in practice, what we can see inside the single mode fiber is something similar to the two rays model, where we can see the effect of constructive and destructive interference due to the interaction of the two modes LP01 and LP11 entering inside the fiber link.

This dangerous effect has been studied and modelled, in order to better understand its behaviour. Some solutions already exist, for example inserting a small branch of 5 μm diameter fiber (SMF 5) which is truly single mode at 850 nm, before the standard G-652 fiber being able to filter out the mode LP11 and letting pass only the desired mode LP01.

In this work we have tested a different solution with respect to the use of SMF 5 μm , based on commercial 1310nm/1550nm couplers, which are theoretically able to separate the modes at 850 nm making possible, similar to the use of SMF 5 μm , the realization of the RoF link based on G-652 fiber and 850 nm VCSEL with the additional feature of the laser response pre-distortion.

Once this analysis is performed and a model is extracted, we move on to digital predistortion. The final goal of this second part is the realization of a system using the coupler as studied before, but in a more sophisticated way.

Given a generic input signal, each coupler has two different paths, the direct and the feedback one. Our goal is to use the coupler at the laser section, the direct path will be used to feed the

single mode fiber G-652, instead the feedback part will be used in order to digitally pre-distort the laser itself.

The improvements in the performance given by the system are presented in terms of NMSE (nominal mean square error), ACPR (adjacent channel power ratio), EVM (error vector magnitude) and spectral regrowth reduction.

This system is attractive because is a low-cost solution with high performance in term of quality of the link that we can achieve using the digital predistortion.

Another important aspect is that we could implement the same coupler to work in a via with 850 nm and on the other input section use the standard 1550 nm, like presented in figure 1:

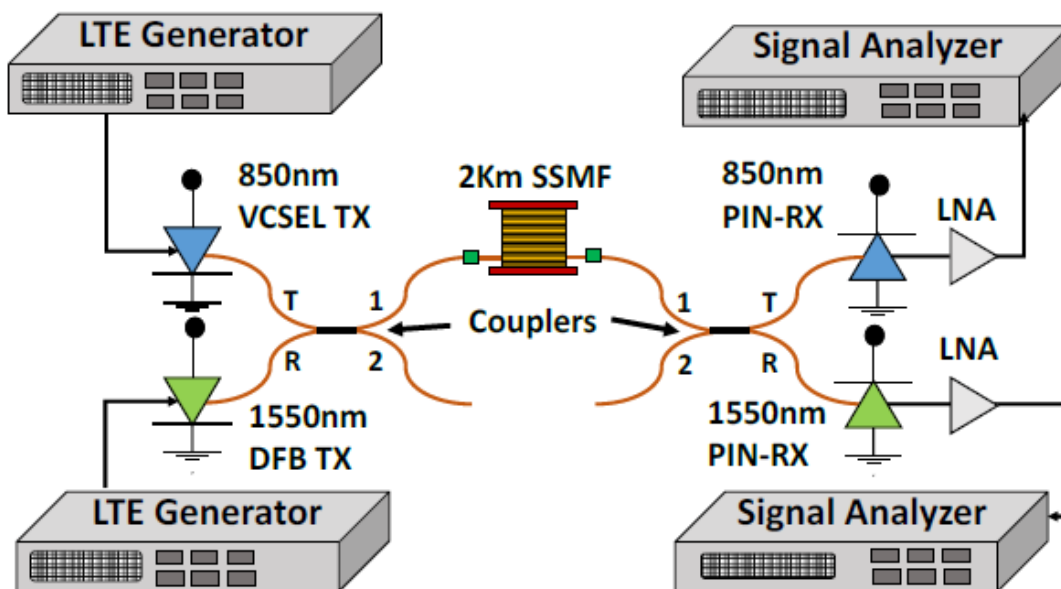


Figure 1: multi-service WDM 850nm/1550nm RoF system [4].

INTRODUCTION

The Radio Over Fiber is one of the most used technology since it presents low attenuation, low complexity, low cost, easy installation, immunity to electromagnetic interference, high capacity, low consumption and can work with all the protocols, so it represents an optimal solution even for future technology [9].

The scope of the analysis in this work is related to the current and future telecommunications networks, that need always more capacity since the number of connected devices increase

exponentially. Another key aspect is the minimization of the cost and power consumption implementation [7].

To achieve those results, VDN (very dense network) and DAS (distributed antenna system) are widely implemented.

DAS can be seen basically as a unique macro cell that has the purpose to extend the coverage using a lot of Radio Access Points (RAPs). VDN instead is a sort of DAS but, each RAP now is an independent small cell; the intelligence is still located in a remote unite [1].

This topology allows network function virtualization (NFV) and software defined network (SDN) so represents a very attractive applicative scenario.

DAS and VDN are actually very similar, the differences are the number of elements. In figure 2 we can see an example of this architecture:

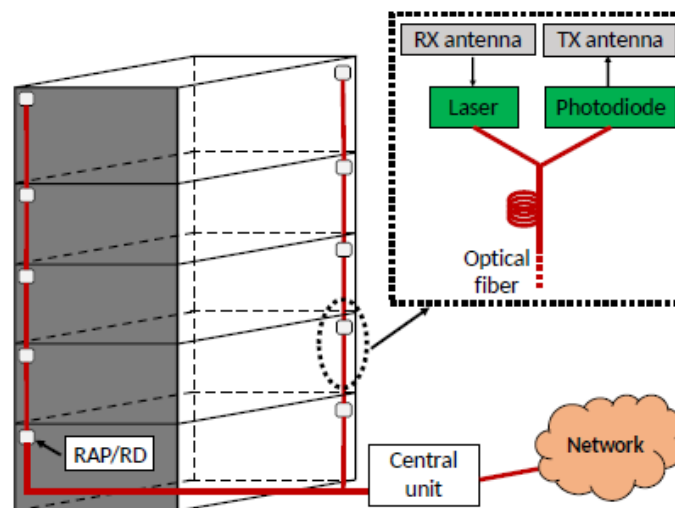


Figure 2: example of an in-building Analog Radio over Fiber system infrastructure. In this case it presents only one central unit and many RAPs, that are exploited by the users for distributing the downlink signal. [1]

One of the classical DAS infrastructures rely on Analog RoF (ARoF) technology, that is simple and has good performance. This technical solution leads to power efficient network; in fact, the power on each cell is maintained to low levels but there are a lot of those small cells, so keeping low the cost is a fundamental aspect.

For what concern the optical part, Distributed Feedback Laser (DFB) are the most implemented at 1310 nm and 1550 nm but in a case of VDN where a lot of cell and laser should be employed, it would be better to adopt VCSEL instead of DFB. The reason of this change in optical

transmitter is due to the fact vertical cavity surface emitting lasers show a much lower threshold current, up to 10 times less than a DFB, and keep high conversion efficiency. [1-3]

Another important aspect is the size, in fact the VCSEL are very small and this decrease the cost of testing step since it can be realized directly on the silica wafers. Furthermore, vertical emitting lasers show a better coupling to the optical fiber with respect to the edge emitting laser like DFB. Nowadays the use of VCSEL for telecommunications is limited to baseband data transmission and it is implemented in data centre for example.

The typical links in data centre exploit multi-transverse mode VCSEL for distance up to 100 m using multimode fibers [1]. The research field is trying to use it also for ARoF transmission for medium and short distance in DAS and home area network (HAN).

From an applicative point of view the performance are good, but to maintain low the cost, it is fundamental to use Standard Single Mode Fiber G-652 as optical transmission channel, but using the VCSEL at 850 nm. The only problem stands in the fact that SSMF shows a bimodal behaviour at 850 nm which produces notches in the modulation bandwidth of the RoF link, spaced in an inversely proportional manner with respect to the length of the fiber strand.

Another fundamental sector where this technology can be implemented is in the realization of short and medium Mobile Front-Haul connections for the LTE and 5G cellular network. It is fundamental to find an efficient countermeasure to the bimodality that occurs in order to maintain a high-quality service. We can see an example in the figure 3:

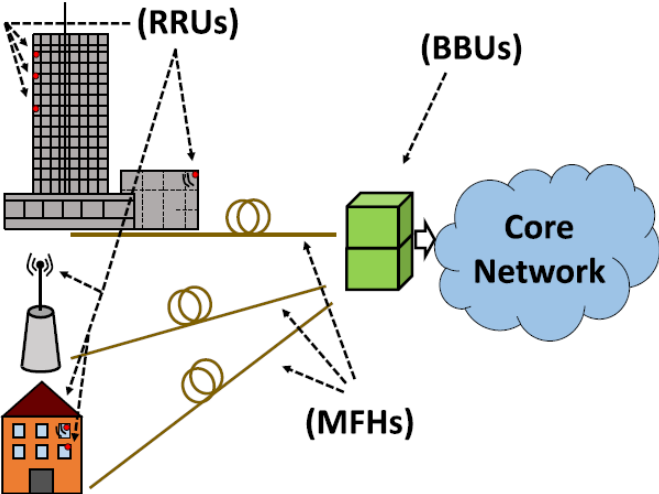


Figure 3: example of a centralized architecture of radio access network. RRU (remote radio unit), MFH (mobile front haul), BBU (baseband unit). [2]

One of the best features introduced by the RoF is the agnosticity with respect to the particular standard and modulation format; this makes this technique optimal for future developments and will have a primary role for the 5G [9].

The general trend in the architecture of 4G and 5G is the splitting of the digital processing section from the radio access section.

For this reason, the BBU (baseband unit) or DU (digital unit) section can be centralized, and this is better from the point of view of installation cost and maintenance; it also improves the spectral efficiency since the centralized structure makes the use of cooperative algorithm available.

The radio access section can have a lot of elements indicated as RRU or RRH (radio resource units/ heads) installed in a capillary way, creating a VDN architecture. There are different possible technologies for the implementation of the MFH. One of the most powerful solution is the ARoF. The advantages of this solution are the low complexity in the RRU stages. For this reason, the ARoF technology represents a solid solution for the coverage in Non-Line-of-Sight environment such as urban environment, shopping malls, stations, stadium etc...

This solution can also be very useful for the practical realization of MFH in cooperation with digital radio over fiber (DRoF).

Since the infrastructure has a very big number of entities and network cells, the implementation must be as simple and as less power consuming as possible.

In this view, VCSEL operating at 850 nm represents a very good solution for telecommunications systems because of the low cost and low power consumption.

A possible solution is to use long wavelength VCSEL that emits at 1310 or 1550 nm where the single mode fiber can operate in a single mode behaviour.

This idea is good for long distance MFH, since the single mode fiber shows a low attenuation in the second and third windows, but those kind of long wave VCSEL has a higher cost with respect to the one operating at 850 nm, so for shorter MFH it does not represent the optimal solution in term of cost.

For the realization of short and medium range MFH a different solution is investigated and will be presented in the next chapter using single mode fiber (SMF) 5 μ m, a particular fiber with a smaller core with respect to the SSMF, in order to counterbalance the bimodal behaviour and

also reduce the fluctuation of the received power due to modal noise and intermodal dispersion effects [3]. Then the same analysis will be repeated with a coupler to check if somehow can act as a mode filter.

CHAPTER 1

1.1) USE OF COUPLER

The most employed solution, as countermeasure for the bimodal behaviour of the single mode fiber SSMF operating at 850 nm, is to use a small core fiber SMF 5 μm in order to apply a modal filtering to the system. Actually, this is a solid way to cancel out the bimodality, but for our work, we try to find out a different technical solution using the commercial coupler designed to operate at 1550 nm. This solution has become very attractive because it solves the problem of bimodality but allows also to new features that will be analysed in this section. From a practical point of view the use of coupler allows to apply digital predistortion just after the transmitting laser and this, represents for sure an important aspect for the realization of the final system implementing DPD on the feedback branch of the coupler.

A point to be considered is that in the last years the internet traffic has increase exponentially and the researchers have put their effort on how to increase the transmission capacity of the optical system. One of the keys to improve the capacity is the Mode Division Multiplexing (MDM) employing multicore fibers or different optical modes in the optical fibers, but the relative delay between the different modes introduce some limitation for long links. This limit of multi-mode fibers has put the attention on the developing of fiber that support just a small number of modes as technology to increase the system capacity [5].

For those kind of system, mode converters and mode multiplexer/demultiplexer are the key technology to combine and divide the signals. Recently, the use of a coupler at 1550 for MDM system has been proposed; in this case the mode LP01 and LP11 propagates in SSMF, anyway those modes have a high differential delay so modal coupling become negligible for SSMF link. We can appreciate the concept of MDM link in the following figure:

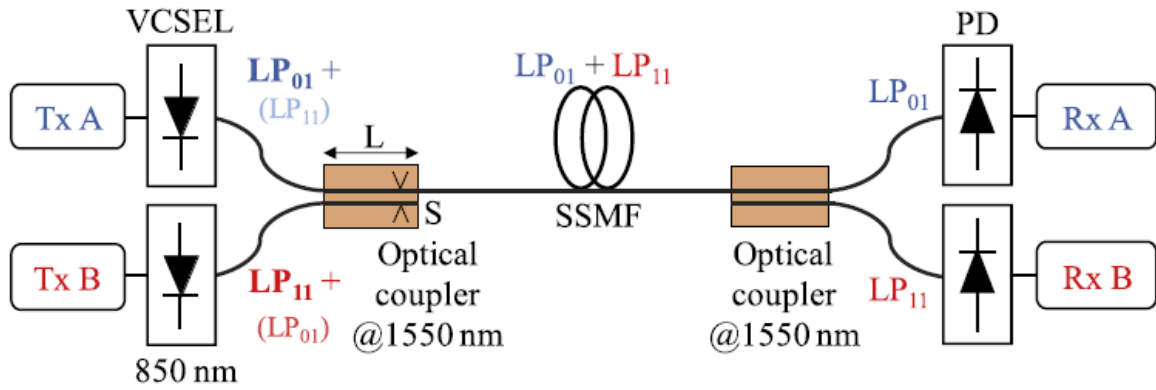


Figure 4: MDM transmission using standard single-mode couplers as multiplexer/demultiplexer at 850 nm [5].

It basically consists in two transmitting lasers operating at 850 nm in a SSMF link. Both modes will be couple together using a commercial optical coupler designed to operate at 1550 nm. The basic idea is to multiplex the LP₀₁ in the upper branch and the LP₁₁ on the lower one. The residual mode, LP₁₁ of the upper branch, and LP₀₁ of the lower one, will be drive to the other coupler output and eventually discarded. At receiving side, the same coupler act as demultiplex to divide the two via to the corresponding PIN receiver.

The coupler can be schematized as follow:

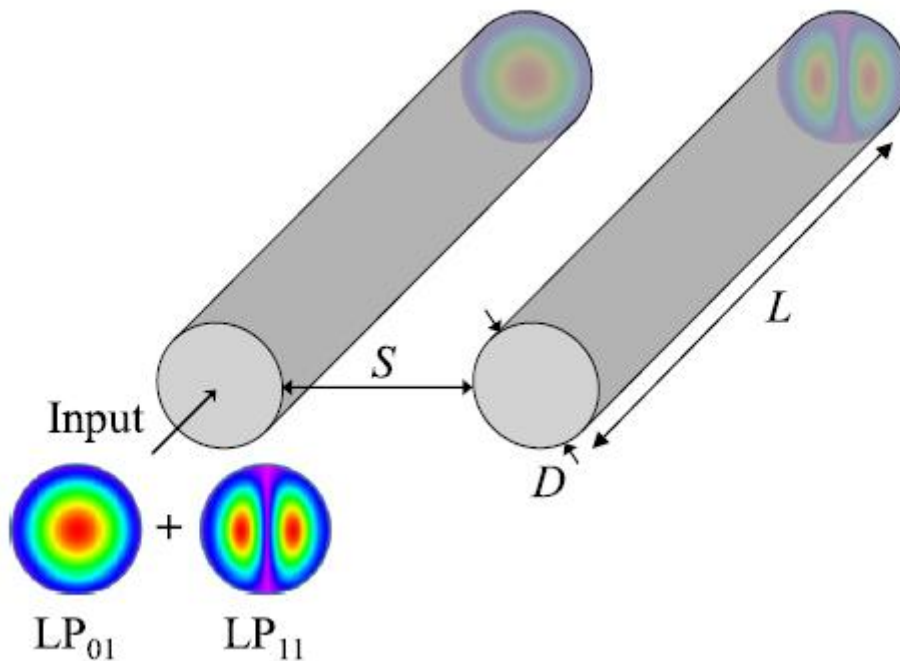


Figure 5: 3D sketch of the structure of the fiber coupler device [5].

The structure is defined by three main parameters:

- D, diameter.
- S, separation between cores.
- L, coupling length.

The power is exchanged periodically between both modes with a coupling length $L_C = \frac{\pi}{2\beta_c}$

Different structures can be tested playing with the three parameters D, S and L, in general if the gap increases, the mutual coupling is reduced, and therefore a longer coupling length is required. The maximum separation between cores for having maximum coupling is around 9 μm . In general, the commercial coupler designed to work at 1550 nm have a separation shorter than 9 μm . The solution just presented show an important application of the coupler designed for 1550 nm in the 850 nm system, anyway this is not the feature for our interest.

The important aspect of the coupler we are interested in, is the filtering mode properties when excited at 850 nm, and the possibility to integrate it in the current developed infrastructure to deploy low-cost system operating in the first optical window.

As we have seen, VCSEL operating at 850 nm are low-cost and low-power but, usually, are employed in graded index multimode fibers scenarios for short distance connections.

Anyway, the use of SSMF is interesting since the infrastructure is already deployed in many environments for distribution of wireless signals. Furthermore, for future applications requiring higher performances there will be no need of replacing it thanks to their single mode operation.

There are also negative aspects to deal with, for example the necessity to minimize the modal dispersion and modal noise caused by the bimodal propagation taking place inside the SSMF at 850 nm. In general, it is fundamental to prevent the simultaneous propagation of the two modes LP01 and LP11 inside the SSMF in order to reduce both modal dispersion and modal noise. The solution of placing a small core fiber SMF 5 μm is good from a mode filtering point of view but, this solution, does not provide easy integration of 850 nm system in already existing infrastructure, which support services at second or third window. Anyway, the use of commercial 1550 nm coupler fed at 850 nm open a new scenario since it is able to filter out or separate the LP01 and LP11 modes and allows also the integration of 850 nm system with already existing ones operating in the third window [4].

For the evaluation of the efficiency of the 1550 nm coupler a simplified two-mode model is adopted, the efficiency is evaluated by the total losses introduced and the amount of power of LP11 with respect to the fundamental mode LP01. In the evaluation procedure is sufficient to consider only the modal dispersion, so we neglect the contribution of modal noise. In fact, if the power of higher mode is reduced, also the fluctuation due to modal noise will be reduced.

The model considered in the study of the coupler is a generic RF signal $I_{RF, in} * \cos(\omega_{RF}t)$.

In this formulation the value $I_{RF, in}$ represents the current amplitude that directly modulate the VCSEL single mode operating at 850 nm. Because of the electromagnetic and geometric properties of the SSMF, we consider that two electrical fields propagate inside the SSMF. The expression of those field is:

$$\vec{E}_i = E_{0, IN} e^{-\frac{\alpha}{2}L} * A_i \sqrt{1 + m * \cos[\omega_{RF}(t - \check{\tau}_i L)]} e^{j[\omega_o t - \beta_i L]} \vec{e}_i$$

Where $E_{0, IN} = \sqrt{\frac{\eta}{c} * (I_{bias} - I_{th})}$ represents the total electric field amplitude at the input section of the SSMF. In this formulation η represents the slope-efficiency, α represents the fiber attenuation in neper/m, m is the optical modulation index that is defined as $m = \frac{I_{RF}}{(I_{bias} - I_{th})}$, ω_o represents the optical carrier, c is a variable that takes into account the possible losses between the laser and the SSMF link. The value $\check{\tau}_i$ represents the group delay-per-meter. An important assumption is the normalization of the power coefficients: $A_1^2 + A_2^2 = 1$.

At the end of the SSMF a photo-current is detected by the receiving photodiode and can be evaluated as follow:

$$i_{PD} = \int_{S_{PD}} |\vec{E}_1 + \vec{E}_2|^2 dS$$

Where S_{PD} is the surface of the PIN receiver. Then we consider that the output surface of SSMF is aligned with the surface of the receiver, leading to a situation where the two modes are orthogonal each other so we can simplify the problem as follow:

$$\begin{aligned} i_{PD} &= i_{PD, DC} + i_{PD, RF} \\ &= E_0^2 + E_0^2 m * \{A_1^2 \cos[\omega_{RF}(t - \check{\tau}_1 L)] + A_2^2 \cos[\omega_{RF}(t - \check{\tau}_2 L)]\} \end{aligned}$$

We focus on the component at RF of the photocurrent and we also assume a perfect matching between the SSMF and the photodiode so it is possible to evaluate the gain:

$$G_{RF} = \frac{\langle i^2_{PD,RF} \rangle}{I^2_{RF,IN}} \propto \frac{\{A_1^2 \cos[\omega_{RF}(t - \check{\tau}_1 L)] + A_2^2 \cos[\omega_{RF}(t - \check{\tau}_2 L)]\}}{C^2}$$

It is also reasonable to assume as working condition that the principal mode LP01 carries always more power than LP11 $\rightarrow A_1 \geq A_2$

In order to test experimentally those concepts the following set up has been assembled [4], as we can see in the following figure:

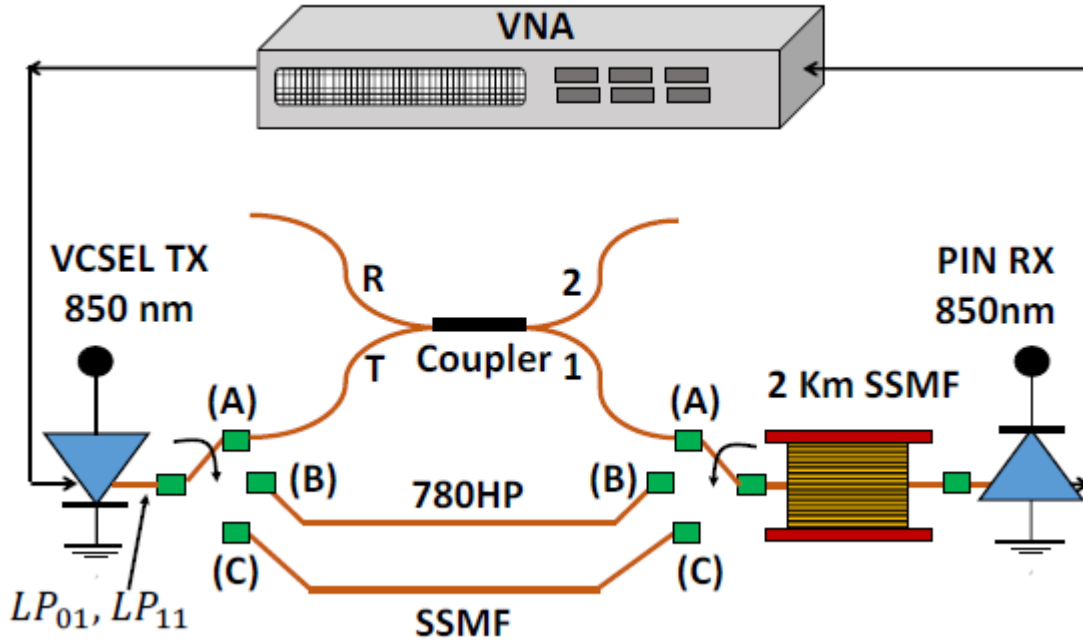


Figure 6: Experimental set up for the characterization of the multi-service WDM 850/1550 nm system [4].

The VNA has been used to generate the signal and evaluate the G_{RF} of the optical link. As we can understand by the figure, three different situations have been considered:

- A : 1550 nm coupler 50-50.
- B : short span of truly single mode fiber.
- C : direct connection to the SSMF.

In an analogue way of the measure performed in the following section, a de-embedding procedure is applied and to each measure is subtracted the back-to-back system response in order to characterize the optical part of the system.

Comparison between the three different measures performed:

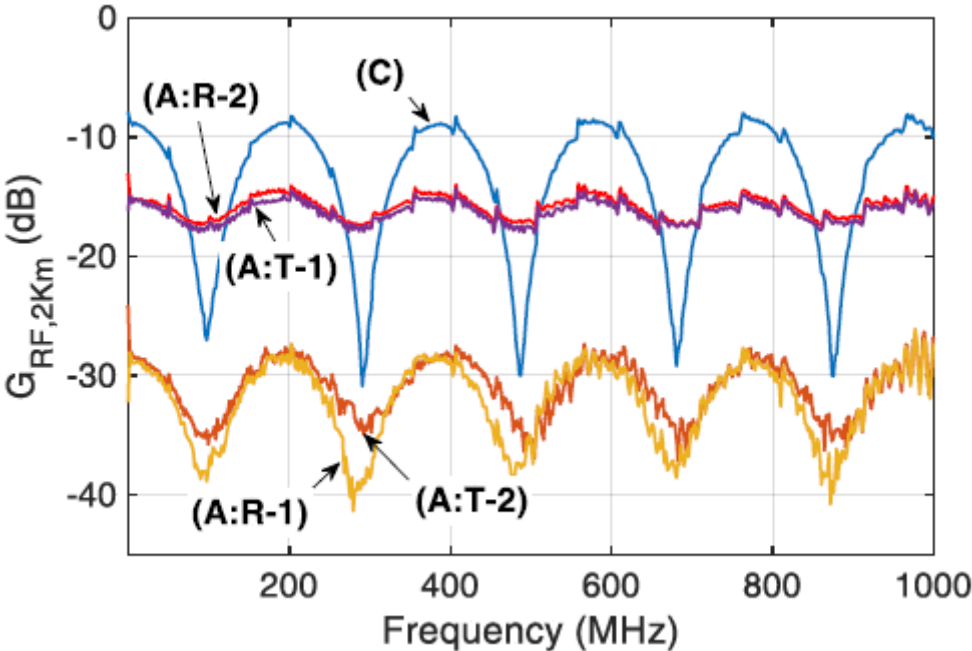


Figure 7: characterization of normalized gain G_{RF} for case C and A. [4]

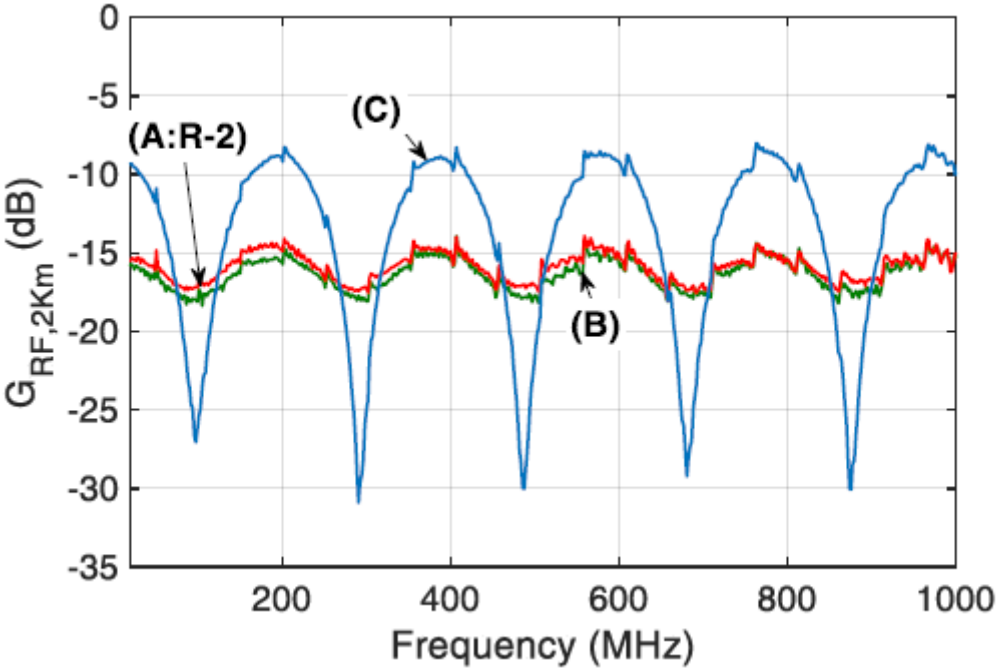


Figure 8: comparison of A-R2, B and C. [4]

The results can be collected as follow:

case	$A1^2$	$A2^2$
A \rightarrow T1	0.87	0.13
A \rightarrow T2	0.75	0.25
A \rightarrow R1	0.75	0.25
A \rightarrow R2	0.87	0.13
B	0.9	0.1
C	0.57	0.43

Tab 1: tab of the power coefficients in the different configurations. [4]

This tab confirms the advantage of using the 1550 nm coupler with respect to the single mode fiber since, the filtering mode capability, is almost the same, but the coupler can be also exploited for the realization of more sophisticated system, integrating the 850 nm and 1550 nm together.

This idea can be schematized in the following system:

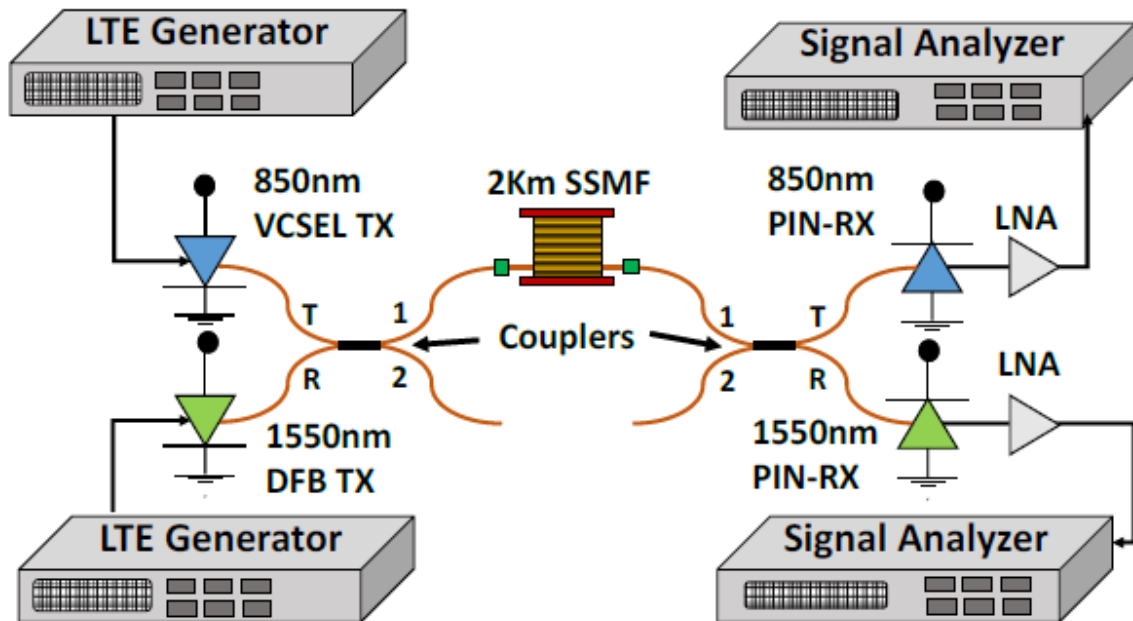


Figure 9: Experimental setup for the characterization of the multi-service WDM 850nm/1550 nm RoF system[4].

The system is divided in two part, the upper one, operating using a VCSEL at 850 nm, and the lower part, using a DFB laser at 1550 nm, both directly connected to commercial 1550 nm coupler 50/50. The common port (1) of the first coupler is connected to the SSMF link, where the filtered 850 nm signal and the 1550 nm signal propagate independently. At the end of SSMF the same coupler is used to split the two paths toward the two photodiodes. Note that the final coupler is used in reverse way with respect to the first one exploiting the reciprocity of this

device. The presence of the two coupler allows to separate the two paths but, at the same time, cause also an optical loss of 6 dB for the channel operating at 1550 nm. This loss is acceptable because the DFB laser can support more power than the VCSEL so the system can work.

The performance of each path is evaluated in term of EVM varying the input power using an LTE signal having bandwidth of 20 MHz.

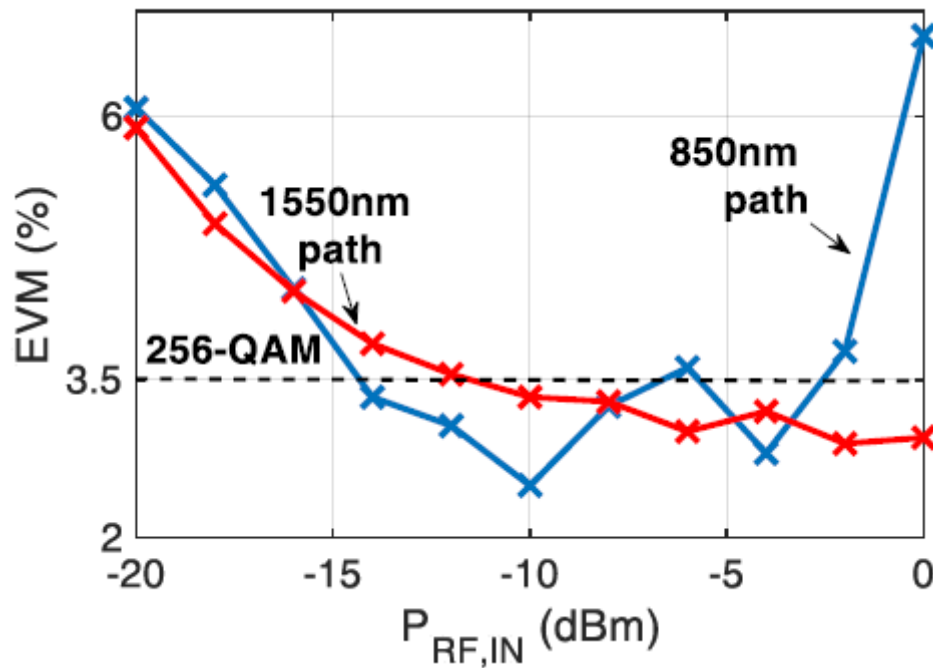


Figure 10: Performance results in terms of EVM for the two multiplexed 850 nm and 1550 nm systems [4].

From the extracted results is possible to appreciate that, the branch operating at 850 nm, has a sharp increase of the EVM for high input power, this phenomenon is given by the fact that VCSEL has a much lower dynamic range with respect to the DFB lasers, anyway this problem can be mitigated applying the DPD algorithms on the signal coming out from the unused port of the first coupler, as we do for the realization of the final system.

In conclusion the coupler is able to act as mode filter, but also to realize a system operating in the first and third window, opening also the possibility to exploit the unused port of the first coupler as feed-back loop in order to improve the performance of the 850 nm branch in term of EVM.

1.2) ANALYSIS OF THE BIMODALITY

There are different short range optical connections, for both digital high-bit-rate or analog signal, that exploit 850 nm vertical-cavity-emitting laser as optical source together with the single mode fiber SSMF.

This solution presents an interesting feature in term of reduced cost and energy consumption, but we have a considerable bandwidth reduction due to intermodal dispersion rising by the fact that there are two propagating modes. The multimodal propagation generates also undesired fluctuations of the received signal due to modal noise [3].

In general, VCSEL are utilized with Multimode Fiber standard but cost a little more than the SSMF. Furthermore, SSMF is less sensitive to bends and many offices and houses are already equipped with it.

VCSEL laser are low-cost components and has small consume since it has a very small active volume that carry to a very small threshold current for activation. Obviously since they are very small, they cannot emit high amount of optical power since its small operating volume has a limited number of electrons.

For these reasons, the use of VCSEL and SSMF is limited to short / medium distances, anyway a lot of new applicative scenarios require short distances to be covered so its applicative interest it is not compromised.

The analog modulation of VCSEL by an RF signal allows a transparent and robust transmission and this become very useful for a lot of different applications.

However, even for short range link the different propagating modes show a different group velocity and this causes the intermodal dispersion leading to band limitation in case of analog RoF or error vector magnitude increase for digital links.

The two modes have mutual phase differences because, their propagation constants, are affected in a different way by the external changes such as temperature. The differences rise the phenomenon of modal noise which cause a fluctuation on the received power.

The key evaluation of transmission quality is the frequency response of the link.

$$G = \log_{10} \frac{P_{RF, out}}{P_{RF, in}}$$

The undesired fluctuation due to modal noise can be evaluated considering the variance of G , or in alternative its standard deviation σ_G .

The problem of mitigation of these impairments has been studied in different ways. One of the most attractive solution aim to insert a fiber loops of short diameter as a mode filter in the beginning and at the end of fiber SSMF G-652. [3]

This method is simple and low cost but has repeatability problem and the effectiveness has been carried out without considering the impact of modal noise.

The insertion of a short span of 5 μm core fiber that is truly single mode at 850 nm at the end of SSMF strand is proposed [3]. Anyway, this simple solution causes an increase of modal noise.

Another possible solution is to put the 5 μm fiber strand between the laser and the single mode fiber SSMF. We will see the differences in the next sections.

1.2.1) MATHEMATICAL MODEL

The electromagnetic problem is the modelling of multimodal propagation in the SSMF operating at 850 nm. Some approximations have to be considered in order to realize the model in a simple way.

A preliminary analysis on the SSMF's normalized frequency show its value are in a range from 3,2 to 4. Therefore, we can conclude that the number of excited modes is 2, we have LP01 and LP11 modes.

Thanks to those consideration a mathematical model has been extracted, as we can see in [3].

In order to do a complete analysis, we have highlighted that two modes go inside the SSMF strand, LP01 and LP11. Anyway, this statement is a simplification since the LP consist, in reality, in a group of two mode and four modes respectively.

The LP01 has inside the HE11 mode in its two polarizations, while LP11 has TE01, TM01 and HE21 in its two polarization.

In the formula presented at the beginning of this consideration we consider a situation where a complete coupling is present within the 2 groups, while coupling between them is considered to be negligible [3].

This consideration is given by the fact that we consider small environmental perturbation but actually, some mechanical stress can cause strong coupling between LP01 and LP11 even for short length.

The electrical field at the output section of the single mode fiber SSMF G-652, having length L1, can be expressed as follow:

$$\begin{aligned} \bar{E}(t, L1) \\ = \sum_{i=1}^{N_m} A_i \bar{e}_i(x, y) e^{j(2\pi f_0 t - \beta_i(t)L_1)} \sqrt{1 + m_i \cos(2\pi f_{RF}(t - \tau_i L_1))} e^{-j \frac{K_f I_{0in, RF}}{f_{RF}} \sin(2\pi f_{RF}(t - \tau_i L_1))} \end{aligned}$$

In this equation, $\bar{e}_i(x, y)$ represents the normalized field vector of the i-th mode, A_i represents its amplitude, $\beta(t)$ represent the phase constant and it's time variant, due to changes in the environment, e.g. temperature, and τ_i represents the group-delay-per-meter.

The ratio $\frac{K_f I_{0in, RF}}{f_{RF}}$ in the last line of the equation can be regarded as the phase modulation index of the optical wave, it is linked to the frequency chirp of the laser and we can indicate it as m_p . Finally, we denote as optical modulation index m_i with the following relation:

$$m_i = \frac{\eta_{RF} I_{0in, RF}}{\eta_0 (I_{bias} - I_{th})}$$

η_{RF} and η_0 represents respectively the RF current-power conversion efficiency and the current-power conversion efficiency at DC.

In [3], we can see that, to limit the bimodal behaviour a small patch of SMF 5 um, is inserted, for example at the end of the fiber span or at the beginning, so the model become as follow:

$$\begin{aligned} \bar{E}(t, L1 + L2) = \bar{e}_{i_{SMF5um}}(x, y) e^{j(2\pi f_0 t - \beta_{1_{SMF5um}}(t)L_2)} \sum_{i=1}^{N_m} A_i a_{i1} e^{-j[\beta_i(t)L_1]} * \\ * \sqrt{1 + m_i \cos(2\pi f_{RF}(t - \tau_i L_1 - \tau_{1_{SMF5um}} L_2))} * \\ * e^{-j m_p \sin(2\pi f_{RF}(t - \tau_i L_1 - \tau_{1_{SMF5um}} L_2))} \end{aligned}$$

L2 represents the length of the SMF 5 um span and tau1 SMF its time delay.

The quantity a_{i1} represents the overlap integral between the i -th mode of the SSMF and the LP01 mode of the SMF 5um. The integral is performed on the cross section of the SMF 5 um fiber.

$$a_{i1} = \int_{S_{SMF5um}} \bar{e}_i * \bar{e}_{1SMF5um}^* dS$$

We can note that due to the shapes of the fields of the fiber, in a case of ideal connection we should have $a_{11} = 1$ and $a_{21} = 0$. In the real case it is not like that because of imperfection in the connection (e.g. misalignments) so a value of a_{21} different from zero must be taken into account.

Once the electrical field expression is obtained, a formula for the extracted current at the photodiode can be assembled taking in consideration the relationship that link the electrical field and the current. The integral is performed on the PD surface.

$$i_{out}(t) = \int_{S_{PD}} |\bar{E}(t, L)|^2 dS$$

At this point it is just a matter of computation of the integrals so for the shake of simplicity we just report the final results in terms of RF components, anyway a complete analysis is present in [3].

$$\begin{aligned} i_{out, RF}(t) &= [A_C + B_C(t)] \cos(\omega_{RF}t) + [A_S + B_S(t)] \sin(\omega_{RF}t) \\ &= Real\{\tilde{I}_{out, RF}(t)e^{j\omega_{RF}t}\} \end{aligned}$$

Where the coefficients inside can be expressed by the following relation:

$$A_C = \sum_{i=1}^{N_m} m_I A_i^2 a_{i1}^2 b_{11SMF5um} \cos[2\pi f_{RF}(\tau_i L_1 + \tau_{1, SMF5um} L_2)]$$

$$A_S = \sum_{i=1}^{N_m} m_I A_i^2 a_{i1}^2 b_{11SMF5um} \sin[2\pi f_{RF}(\tau_i L_1 + \tau_{1, SMF5um} L_2)]$$

$$B_C(t) = 2A_1 A_2 a_{11} a_{21} b_{11SMF5um} C(t) \cos(2\pi f_{RF} \bar{\tau})$$

$$B_S(t) = 2A_1 A_2 a_{11} a_{21} b_{11SMF5um} C(t) \sin(2\pi f_{RF} \bar{\tau})$$

$$C(t) = m_I \cos(2\pi f_{RF} \Delta\tau) J_0(x) \cos(\Delta\beta(t)L_1) + 2J_1(x) \sin(\Delta\beta(t)L_1)$$

In those equation the value $b_{11SMF5um}$ is defined as:

$$b_{11SMF5um} = \int_{S_{PD}} |\bar{e}_{1SMF5um}|^2 dS$$

In the case with no SMF 5um at the end, I outRF assumes the formal aspect see at the beginning of this section and the term $b_{11SMF5um}$ has to be replaced by a b_{ij} defined as follow:

$$b_{ij} = \int_{S_{PD}} \bar{e}_i * \bar{e}_j^* dS \quad i, j = 1, 2.$$

Actually, if we consider a PD with infinite surface, the b coefficients can be considered as $b_{11}=b_{22}=1$ and $b_{12}=0$.

1.2.2) CONSIDERATION ON THE PROPOSED SOLUTION:

In [3], there are analysed different technical solution for the issue of bimodality, in particular four cases are put into evidence:

- **SSMF only:** it represents the basic case, here the effect of bimodality are presents and no countermeasure are taken. The received power shows the classical notches in frequency as we expected.
- **SSMF+SMF 5um:** in this case a strand of small diameter fiber is put on the output section in order to filter out the LP11 mode. This solution shows an increase in passband with respect to the basic case seen before. The improvement can be seen in the normalized gain in frequency $g = \langle G \rangle - \langle G \rangle_{\max}$ that is reduced in a significant way, passing from a $\Delta g = -34$ dB to -6 dB, but at the same time increase the modal noise, furthermore in the frequency near to the minima of g.
- **SMF 5um+SSMF+SMF5um:** a different configuration has been tested, putting another small diameter fiber also in the input section. This configuration improves the previous results, passing from a $\Delta g=6$ dB to less than 2 dB.
- **SMF 5um+SSMF:** this time the small diameter fiber is put only at the input section. In this case basically we reach the same Δg as before, but actually it shows some improvements with respect to the previous case. In fact, in term of power penalties due to insertion loss is better to have only one strand of SMF 5um at the beginning with respect to put it both at input and output section. This case represents also the best solution as noise figure, so in conclusion represents the most performing technical solution with respect to the others.

1.2.3) CONCLUSION OF THE PRELIMINARY TEST

During the test presented in this section it has been put into evidence the bimodal behaviour of the VCSEL 850 nm + SSMF configuration. This bimodality has an impact on the modal interference and modal noise. We can appreciate the behaviour in the measure of the link without any of the previously explained countermeasure in the following figure:

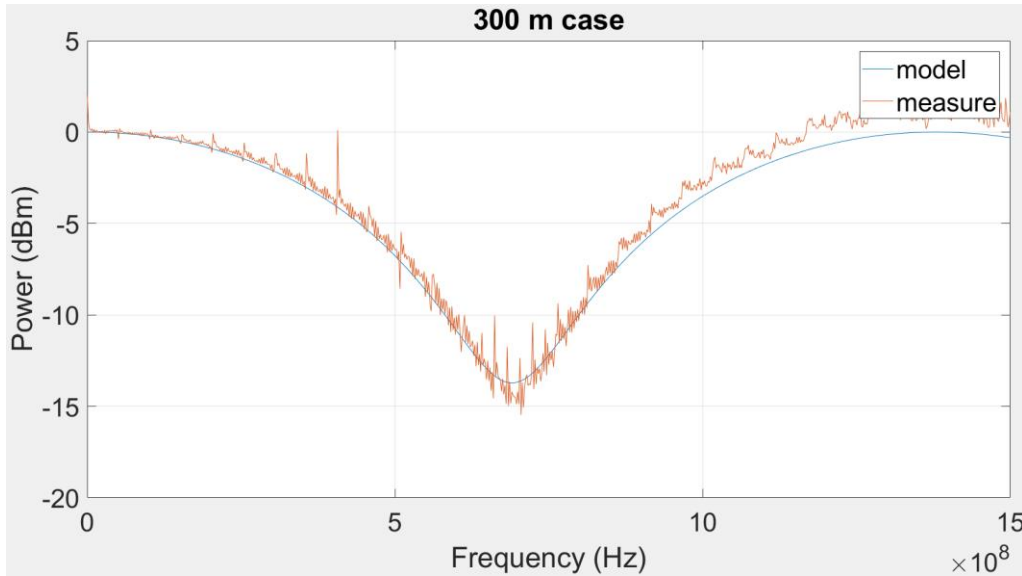


Figure 11: example of bimodal behaviour for a 300 m span.

An analytical model is proposed to characterize such system. It has been demonstrated that a mode filtering at the input section can reduce both modal interference and modal noise. In the case of 300 m SSMF span the bandwidth has improve from 250 MHz to 2500 MHz; instead, the standard deviation of modal noise is reduced to less than 2 dB. The analysis that has been carried out can be exploited for the realization of short-range link with high bit rate but, more important, is a low-cost solution.

1.3) NOTCHES IN FREQUENCY

As we have said in the introduction the bimodal behaviour shows some notches in the frequency in a similar way as the two rays model, even though we are dealing with guided propagation. More specific, the notches in the frequency show an inversional proportional respect to the fiber length. In order to better understand the mathematical behaviour of this effect, let consider a situation where the weight of the two propagating modes is the same so $A_1=A_2$. In this case we can formulate as follow:

$$\begin{aligned}
i_{out}(t) &= \sum_i^{N_m} A^2_i (1 + m_i * \cos (2\pi f_{RF}(t - \tau_i L_1)) = \\
&= 2A_1 + 2A_1 * m_i * \cos \left(2\pi f_{RF} \frac{(\tau_2 - \tau_1)L_1}{2} \right) * \cos \left(2\pi f_{RF} \left(\frac{2t - (\tau_1 + \tau_2)L_1}{2} \right) \right)
\end{aligned}$$

We have used the prosthapheresis function in order to achieve those results; now in order to find the notches we have to put the first cosine equal to zero.

The cosine at double frequency is ignored for the scope of our dissertation, furthermore we consider the first minima to proceed and the results are the following:

$$\begin{aligned}
\cos \left(2\pi f_{RF} \frac{(\tau_2 - \tau_1)L_1}{2} \right) &= 0 \\
2\pi f_{RF} * \frac{\Delta\tau L}{2} &= \frac{\pi}{2} \rightarrow \Delta\tau = \frac{1}{L f_{RF} * 2}
\end{aligned}$$

So, in general, we can formulate those equation for the minima of the output current [1]:

$$f_{min, k} = \frac{2k + 1}{2L \Delta\tau}$$

Hence, we can conclude that this relationship shows that for longer fiber we have more minima, so frequency is inversely proportional to L and in the same way, for increasing frequency we have more minima in parity of L.

1.3.1) INTERMODAL DISPERSION ANALYSYS

The scope of this analysis starts from some detrimental effect that we have observed in the first measure carried out. In order to characterize the effect, we have realized a direct measure (without coupler) of different SSMF span.

We have performed measure at 300m,1500m,3000m,5000m,6500m,8000m and 9500m.

All the measures were performed at 4.5 mA bias point of the VCSEL Optowell GS85 single mode. Note that all the following measures has been performed using the same laser.

The different measures were reported in a unique figure to make a comparison among them as follow:

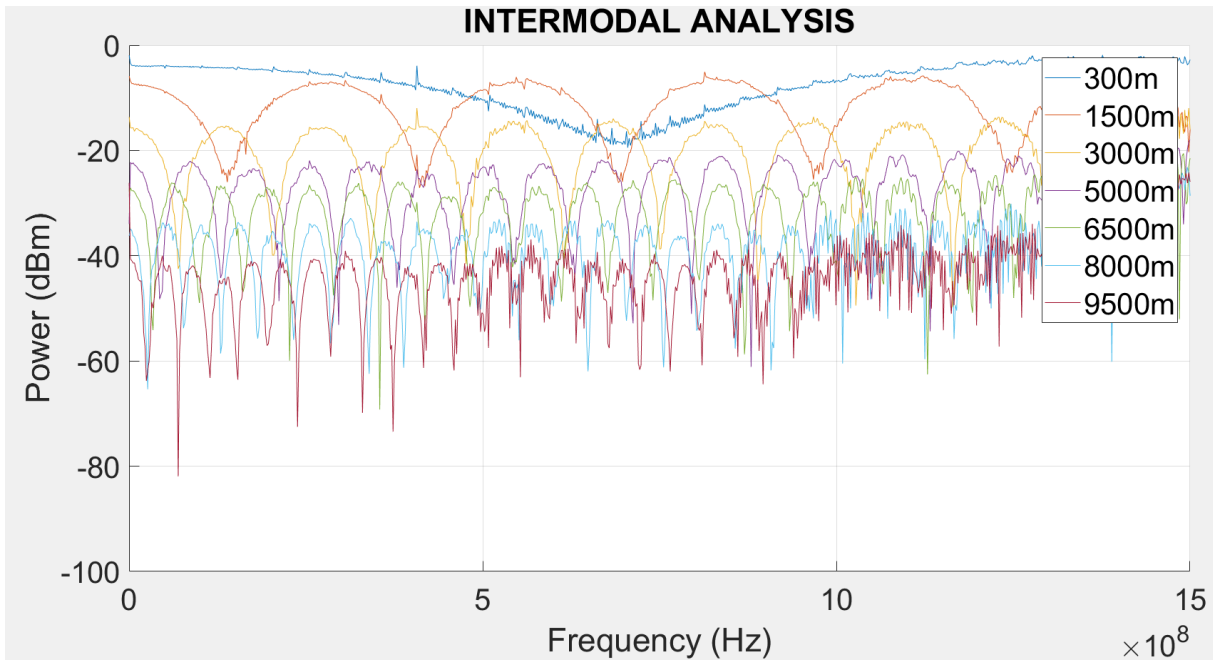
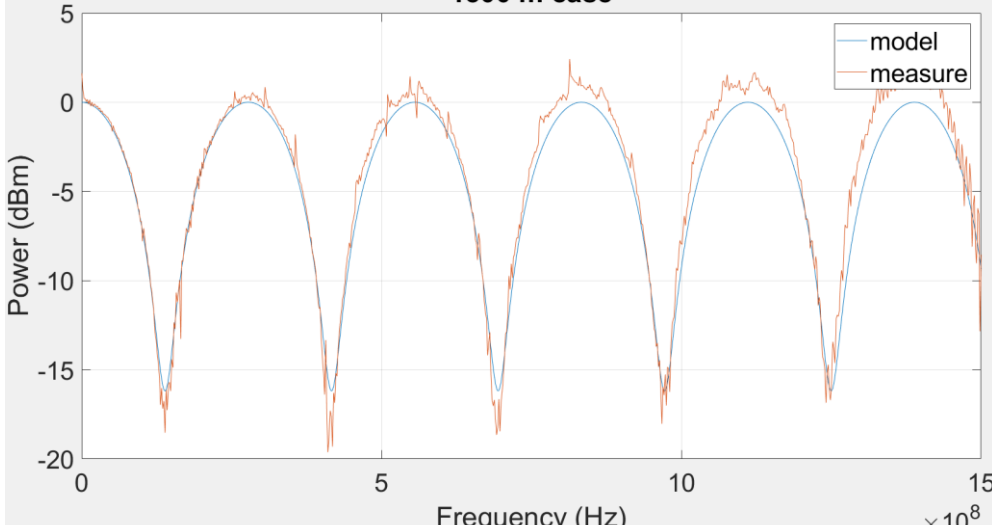
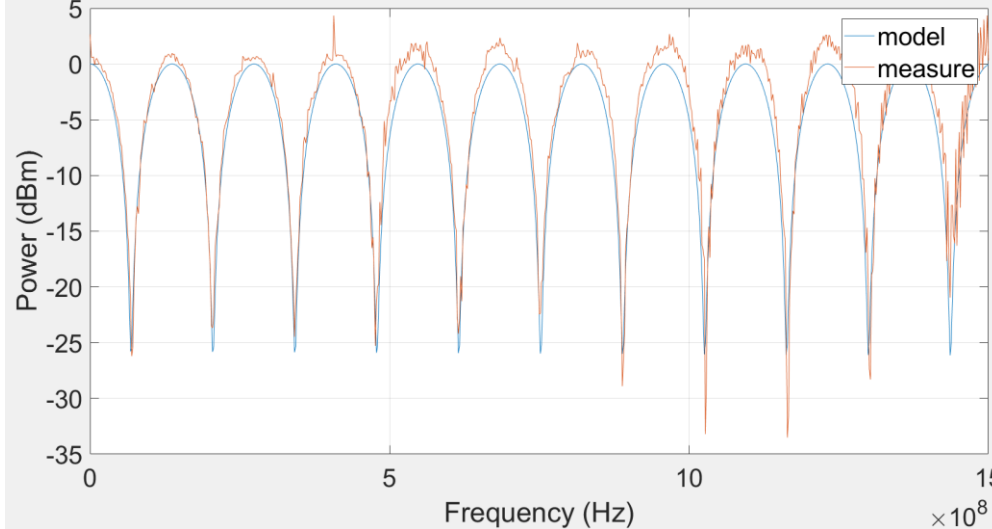
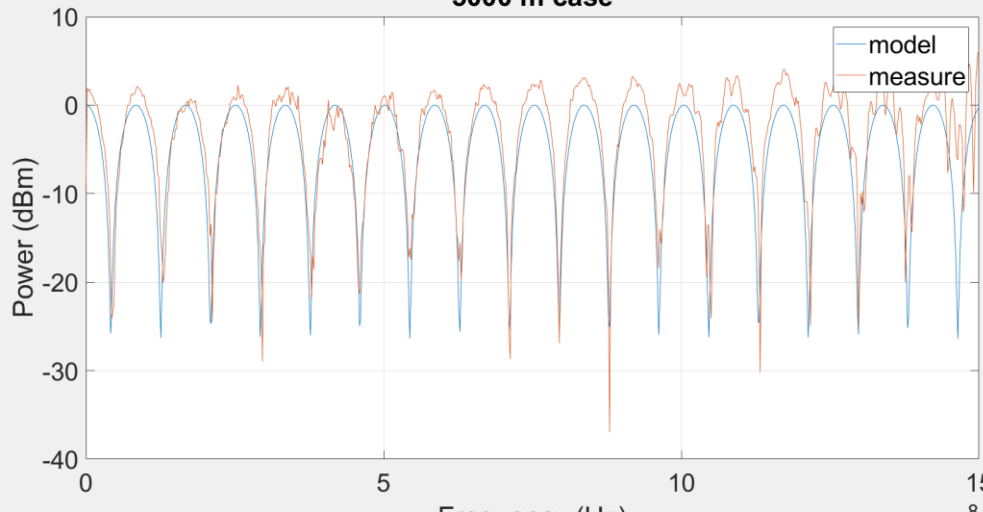
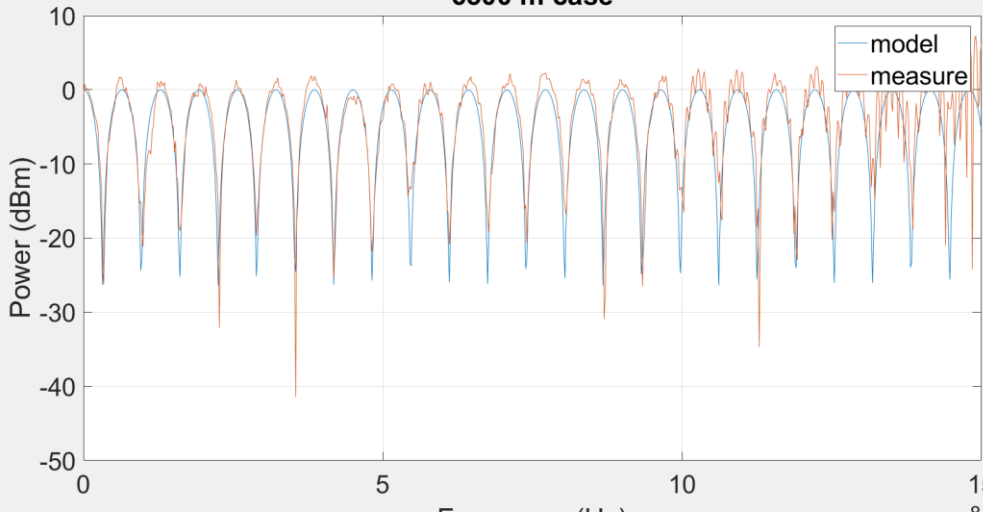


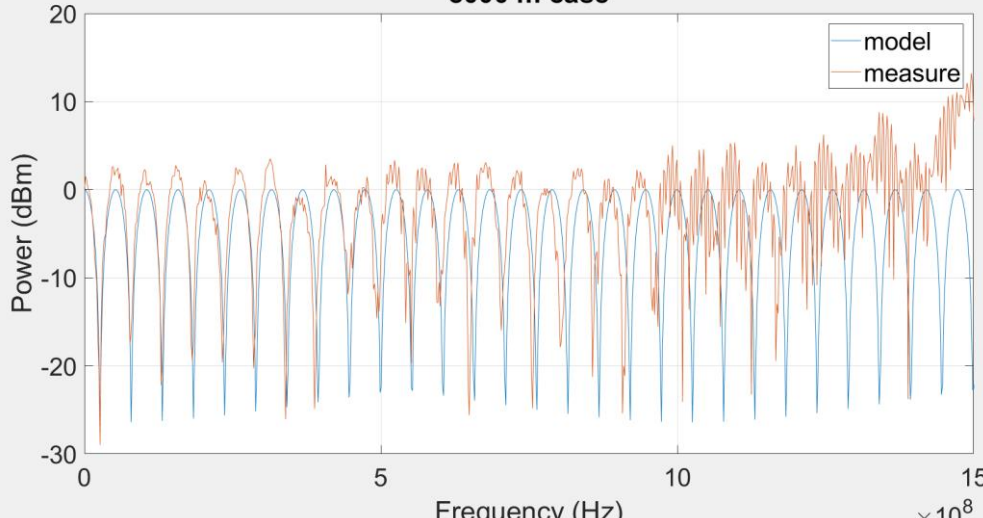
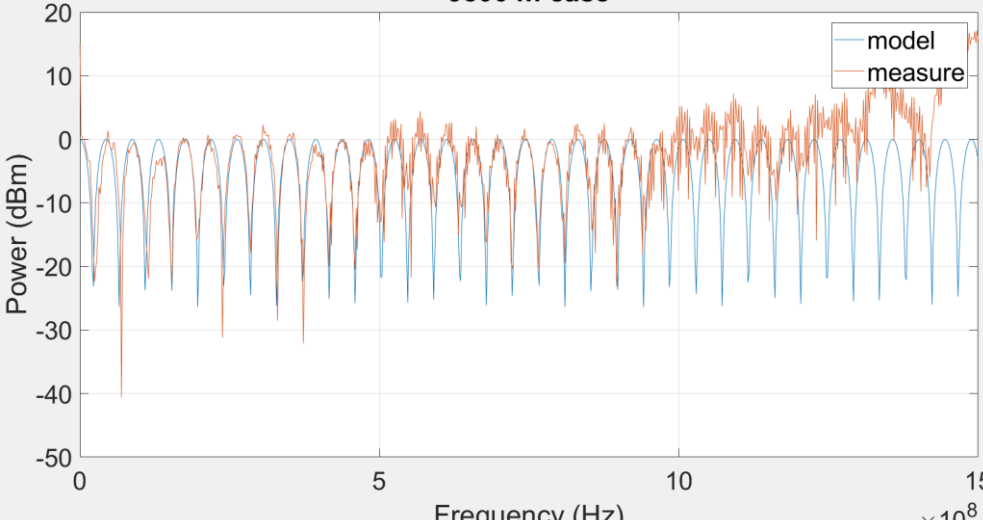
Figure 12: panoramic of the different measures from 300m up to 9500 m.

Now we focus on the different set of measurements:

LENGTH	GRAPHS
300 m	<p style="text-align: center;">300 m case</p>
Delta τ	<pre>l_span1=300; deltaTau1=1/(l_span1*2*6.9e8); deltaTau1=2.4155e-12 s</pre>

<p>1500m</p>	<p style="text-align: center;">1500 m case</p> 
<p>Delta τ</p>	<p> $l_span1=1500;$ $\text{deltaTau1}=9/(l_span1*2*1.25e9)$ In this case we pick the 5th maxima for the delta Tau evaluation $\text{deltaTau1}=2.4000e-12$ </p>
<p>3000m</p>	<p style="text-align: center;">3000 m case</p> 
<p>Delta τ</p>	<p> $l_span1=3000;$ $\text{deltaTau1}=19/(l_span1*2*1.3e9);$ in this case we have picked the 10th minima $\text{deltaTau1}=2.4359e-12$ </p>

<p>5000m</p>	<p style="text-align: center;">5000 m case</p> 
<p>Delta τ</p>	<pre>l_span1=5000; deltaTau1=19/(l_span1*2*7.95e8); even in this case we pick the 10th minima deltaTau1=2.3899e-12</pre>
<p>6500m</p>	<p style="text-align: center;">6500 m case</p> 
<p>Delta τ</p>	<pre>l_span1=6500; deltaTau1=19/(l_span1*2*6.11e8) even in this case we pick the 10th minima deltaTau1=2.3920e-12</pre>

<p>8000m</p>	<p style="text-align: center;">8000 m case</p> 
<p>Delta τ</p>	<pre>l_span1=8000; deltaTau1=1/(l_span1*2*2.63e7);</pre> <p>the interesting thing is that we use the first minima for delta Tau evaluation like the case of 300m and 1500m. This could be seen not in agreement with the previous cases, in fact we can note a little drift effect between the model and the measure. What is particular in this measure is that, even selecting the frequency where the first minima fall, we were lucky and we pick the correct frequency value. The reason why we were lucky will explained at the end of this tabs.</p> <pre>deltaTau1=2.3764e-12</pre>
<p>9500m</p>	<p style="text-align: center;">9500 m case</p> 
<p>Delta τ</p>	<pre>l_span1=9500; deltaTau1=37/(l_span1*2*8.1e8)</pre> <p>in this case we pick the 19th minima in order to have a precise evaluation of delta Tau</p> <pre>deltaTau1=2.4042e-12</pre>

The reason why we perform this analysis is due to the facts that, increasing the length of the fiber span we notice a strange drift effect in the value of $\Delta\tau$. Actually, the reason of this

misalignment was simply an accuracy factor. In fact, when we perform the measure of $\Delta\tau$ we select the frequency where the first minima of the measure occur. The measure is actually chosen by an ad hoc selection from the graph that we have just obtained, and this, generates an absolute error in the operation of selecting the frequency. The relative error is the absolute error, that it is always present and is supposed to be the same for each measure, divided by the frequency range from 0 to the selected frequency.

It is easy to understand that, if we pick a minima after the first one, for example the 10th minima, we have the same absolute error but the frequency range is 10 times with respect to the one we would have selecting the first minima.

In the case in the example the relative error will be 10 times smaller respect to the one of the first minima, so the accuracy is way better!

The interesting thing in the 8000m case is that in this case even choosing the first minima we were quite lucky since it was accurate; the reason stands in the fact the frequency of the first minima was picked almost correctly. Even though selecting a frequency from a following minima is always a better solution.

1.4) MATLAB MODELLING FOR BIMODALITY EVALUATION

In order to study and understand the behaviour of the bimodality that VCSEL 850 nm shows when a SSMF is used as optical channel we have developed a matlab model. This model basically attributes a weight for the 2 mode LP01 and LP11 that propagates inside the optical channel. A preliminary assumption, that will be demonstrated in the next section, is that the mode carrying the most power is always the principal mode LP01.

The analysis regards the use of the coupler instead of the SMF 5um fiber span in order to compensate the bimodality. This solution represents an attractive idea because can mitigate the problem of bimodal behaviour and also opens new applicative scenarios like feedback predistortion of the laser that will be investigated in the next chapters.

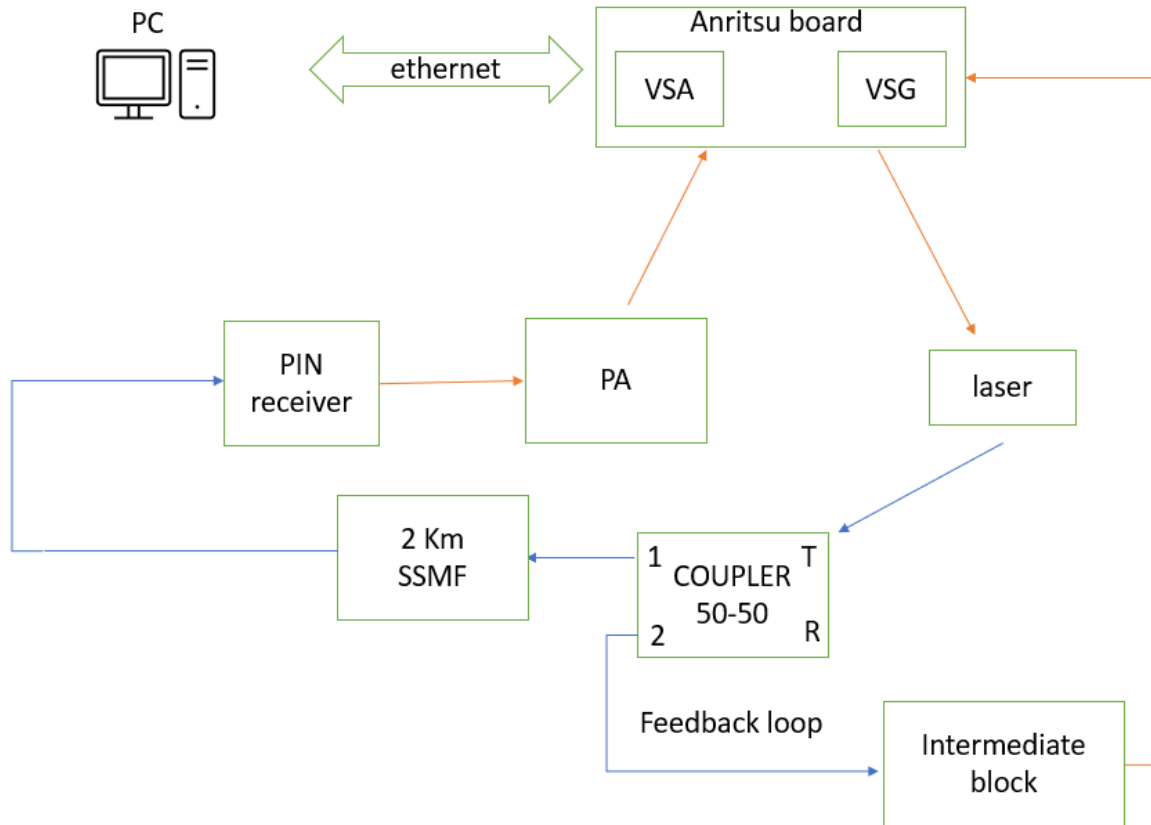


Figure 13: schematic of the experimental set up of the final system. The blue link represents optical connections, while the orange link represents the electrical ones. The red arrow represents electrical connections, the blue ones represent the optical connections.

All the coupler in our analysis are 1550 nm couplers and present two inputs, called T and R, and two output called 1 and 2. Note that the intermediate block, is actually a full receiving chain, including the PIN receiver, the power amplifier and the electronics that perform a demodulation and detection of the signal and do some elaboration on the baseband signal in order to apply the predistortion algorithm to the system. In addition to the previous features, the intermediate block has also to re-create the transmitting signal and modulate the transmitting laser. In our practical case we do not have any intermate block, in fact the Anritsu board adopted for our work, has only one receiving port. For the realization of the final set up in practice we have trained the algorithm using the feedback loop and using the receiving port of the Anritsu board for the receiving chain e for the transmission of the signal with the laser. Once the training is finished, we switch the connection from the feedback port of the coupler to the direct one (T1), then we have simply pre-distort the signal applying the coefficients evaluated in the feedback loop for the direct via.

All the measurements were carried out in the same way for each coupler (50-50, 90-10 and 99-01) and for each span of fiber, in our case 300 m and 2km.

The first measurement is always the one without coupler that represents the starting situation where the bimodal behaviour shows its notches. Once the starting measure is done, we measure the behaviour for the other four configurations of the coupler T1, T2, R1 and R2, in order to realize a complete analysis.

All the analysis has been carried out using a fixed scheme:

- Measurements
- Import the measurements to matlab
- Graphical representation of the four configurations of the coupler
- Weight modes analysis

The link can be schematized in figure as follow:

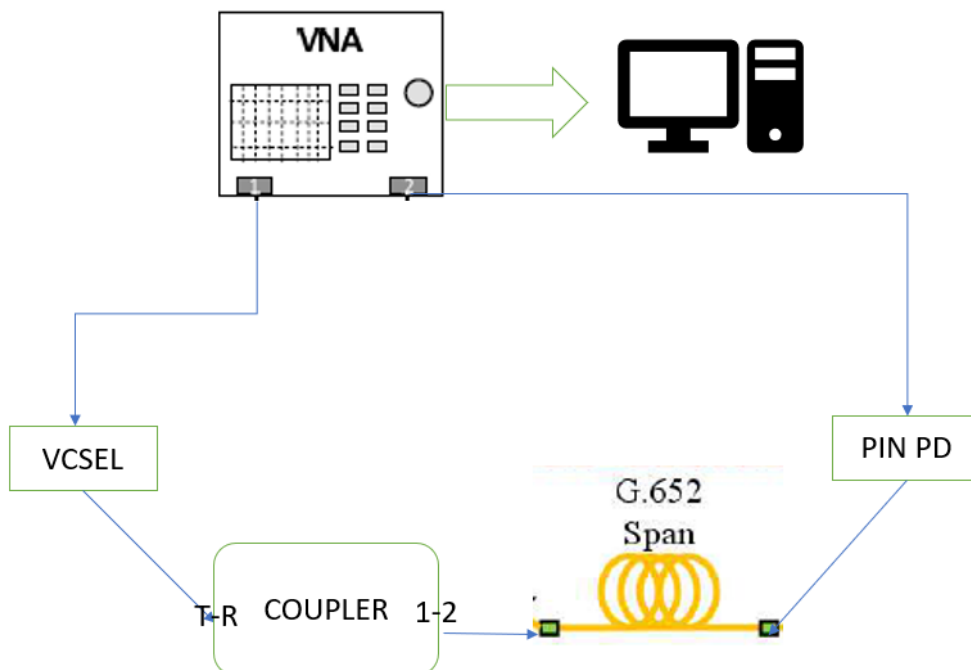


Figure 14: Schematic of the experimental set up implemented in the first measures.

We can see the VNA that is the origin and final point of the connection, then we have a VCSEL operating at 850 nm connected to a coupler 50-50 designed for operating at 1550 nm and

connected to a SSMF fiber. At receiving side, we denote a PIN rx operating at 12 V that is connected to the receiving port of the Anritsu.

The standard procedure is given as follow; we first load the file into matlab:

```
%% import data

close all
clear all

datab2b=importdata('VCSEL_sm_4.5ma_rxoptwell_b2b.s2p', ' ',5);
data300m=importdata('VCSEL_sm_4.5ma_rxoptwell_300m.s2p', ' ',5);
```

Then we extract the data from the matrix that is imported in the Matlab workspace and we extract the back-to-back(b2b) data and the data corresponding to the length we want to analyse. As we can see in the Matlab code we subtract to the measure at the given length the b2b measure in order to characterize the optical link, subtracting the behaviour of transmitter and receiver.

```
%% extraction of data from back2back
freqb2b=datab2b.data(:,1);
s21realb2b=datab2b.data(:,4);
s21imagb2b=datab2b.data(:,5);

s21magnitueb2b=abs(s21realb2b+i*s21imagb2b);
s21magb2bdb=mag2db(s21magnitueb2b);

%% extraction of data from new measure without coupler
freqBase=data300m.data(:,1);
s21realBase=data300m.data(:,4);
s21imagBase=data300m.data(:,5);

s21magnitueBase=abs(s21realBase+i*s21imagBase);
s21magBasedB=mag2db(s21magnitueBase);
diffBase=s21magBasedB-s21magb2bdb;
```

Then we proceed with the graphical representation of the data just put inside the simulator.

The core of the matlab program is the weight evaluation of the 2 mode that is carried out in an iterative way as we can appreciate in the matlab script that follows:

```
%% calculation of coefficient without coupler 300m
l_span1=300;
deltaTau1=1/(l_span1*2*6.9e8);

y=(cos(2*pi*freq300m* deltaTau1*(l_span1/2)));
```

```

figure
plot(freq300m,y.^2)

z=mag2db(abs(y));
figure
plot(freq300m, z);

tau1=5e-9;
tau2=deltaTau1+tau1;
%t=[0 : 1e-9 : 0.2];
t=linspace(0,0.00001, 1601);
a_1=1;
a_2=1;
modindex=1;

%for a_2 =[0:0.1:1]
    for i = (1:length(freq300m))
m(:,i)=(a_1)^2*(modindex * cos( 2*pi*freq300m(i)* ( t -
tau1*l_span1)))+(a_2)^2*(modindex * cos( 2*pi*freq300m(i)* ( t
- tau2*l_span1)));
        end
figure
plot(t, m(:,i));

for a_2=[0.6:0.01:0.63]
    a_1=sqrt(1-(a_2)^2);

Ac=modindex* (( a_1)^2 * cos(2*pi*freq300m* tau1* l_span1)+
(a_2)^2 * cos (2*pi*freq300m*tau2*l_span1));
As=modindex* (( a_1)^2 * sin(2*pi*freq300m* tau1* l_span1)+
(a_2)^2 * sin (2*pi*freq300m*tau2*l_span1));

envelopemod=sqrt(Ac.^2+As.^2);
envelopnorm=envelopemod/envelopemod(1);
envelopnormdB=mag2db(envelopnorm);

figure
plot(freq300m,envelopnormdB);
hold on
delta1db=diffBase300m - diffBase300m(10);
plot(freq300m,delta1db);
end

```

For sake of simplicity we consider the modulation index m_i equal to 1. This simplification makes sense because we normalize the measurement. Note that the m_i just consider is different from the m variable present in the code.

The mathematical model is developed as we have analysed in the section 1.1.1; the value $m(:,i)$ represents the total output current, instead the A_c and A_s value represents the real and imaginary part of the envelope of I_{outRF} .

The value a_1 and a_2 represents the weights of the and their square value represent the actual power splitting ratio of the 2 mode LP01 and LP11 and will be indicated as A_1 and A_2 .

Those coefficients are in a strict relation with each other, in fact we assume a normalization condition such that $A_1^2 + A_2^2 = 1$ as we can see inside the second for loop where the iterative procedure is realized.

Basically, it is a fitting problem in which we play with the coefficients A_1 and A_2 such that, the modelled curve, fit in the best possible way with respect to the measured value; this way we can characterize the weights of the two propagating modes and understand if the coupler acts somehow as a mode filtering or not.

Then a complete analysis using the 3 couplers previously mentioned is carried out for 300 m and 2 km case.

1.5) 300 m CASE ANALYSIS

The second analysis has been carried out for the 300 m case SSMF span. Differently from the previous set of measures, from this point, in all the measure a coupler will be present. In particular, we have performed a complete analysis of the three couplers in its four configurations. The final goal of this part is to extract a value of the weights of the 2 modes entering inside the SSMF fiber. All the three couplers analysed operate at 1550 nm so will not act as we could expect for the 850 nm case. The first study case is the coupler 50-50. The analysis performed will be the same for each case.

1.5.1) COUPLER 50-50

In figure 15 and 16 we observe the behaviour of the normalized link and the non-normalized one respectively:



Figure 15: normalized measure.

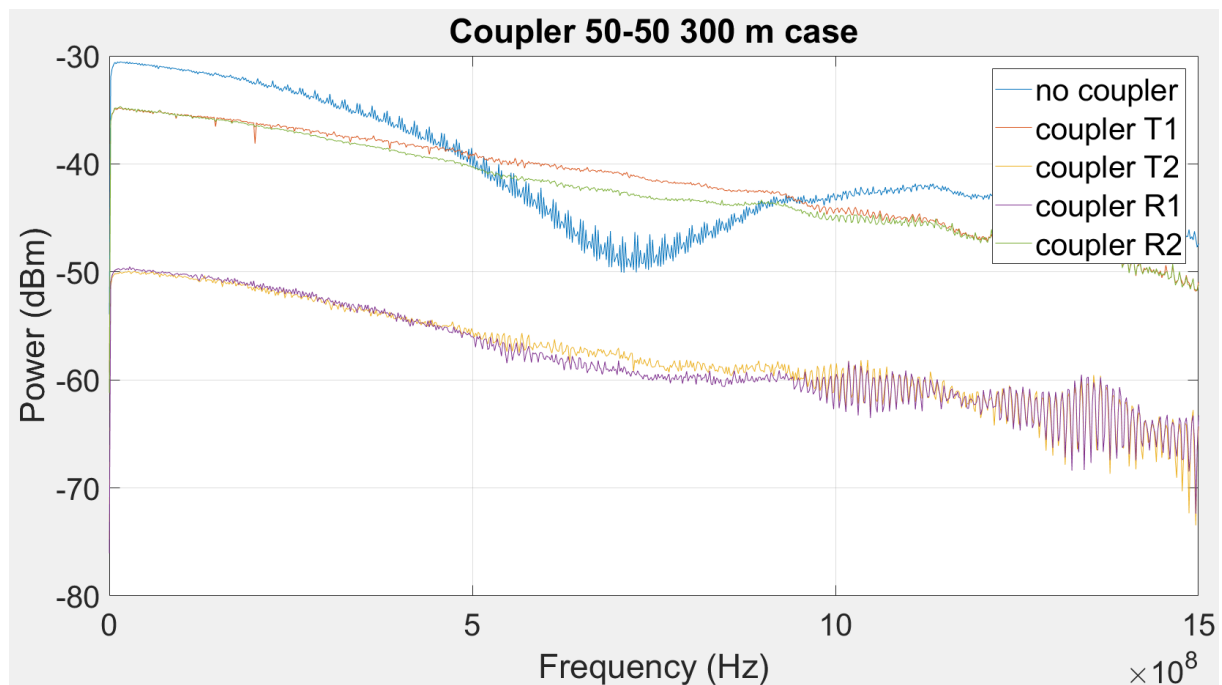
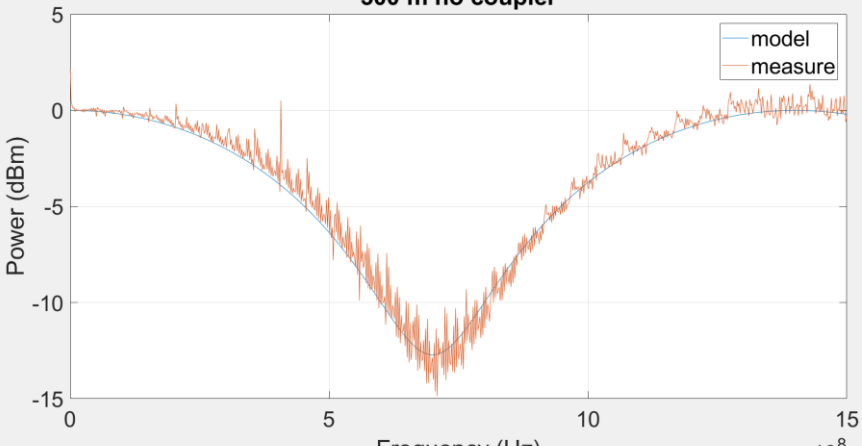
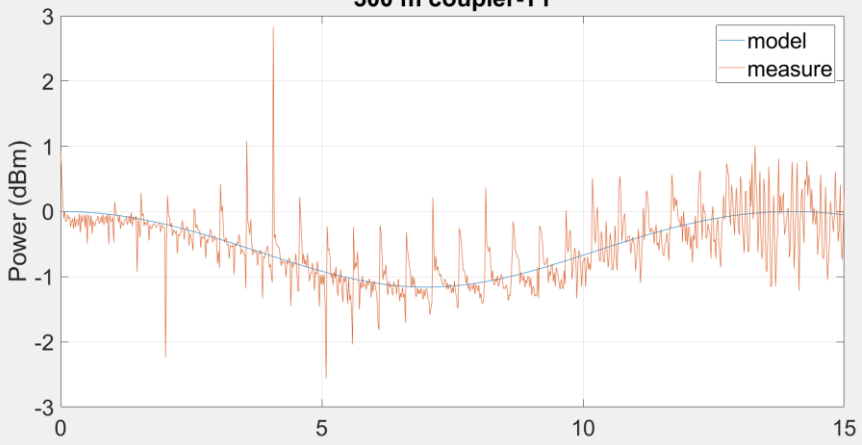
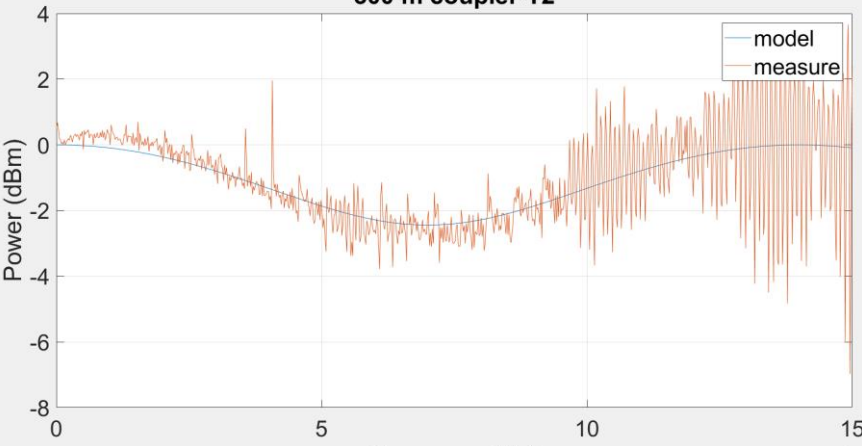
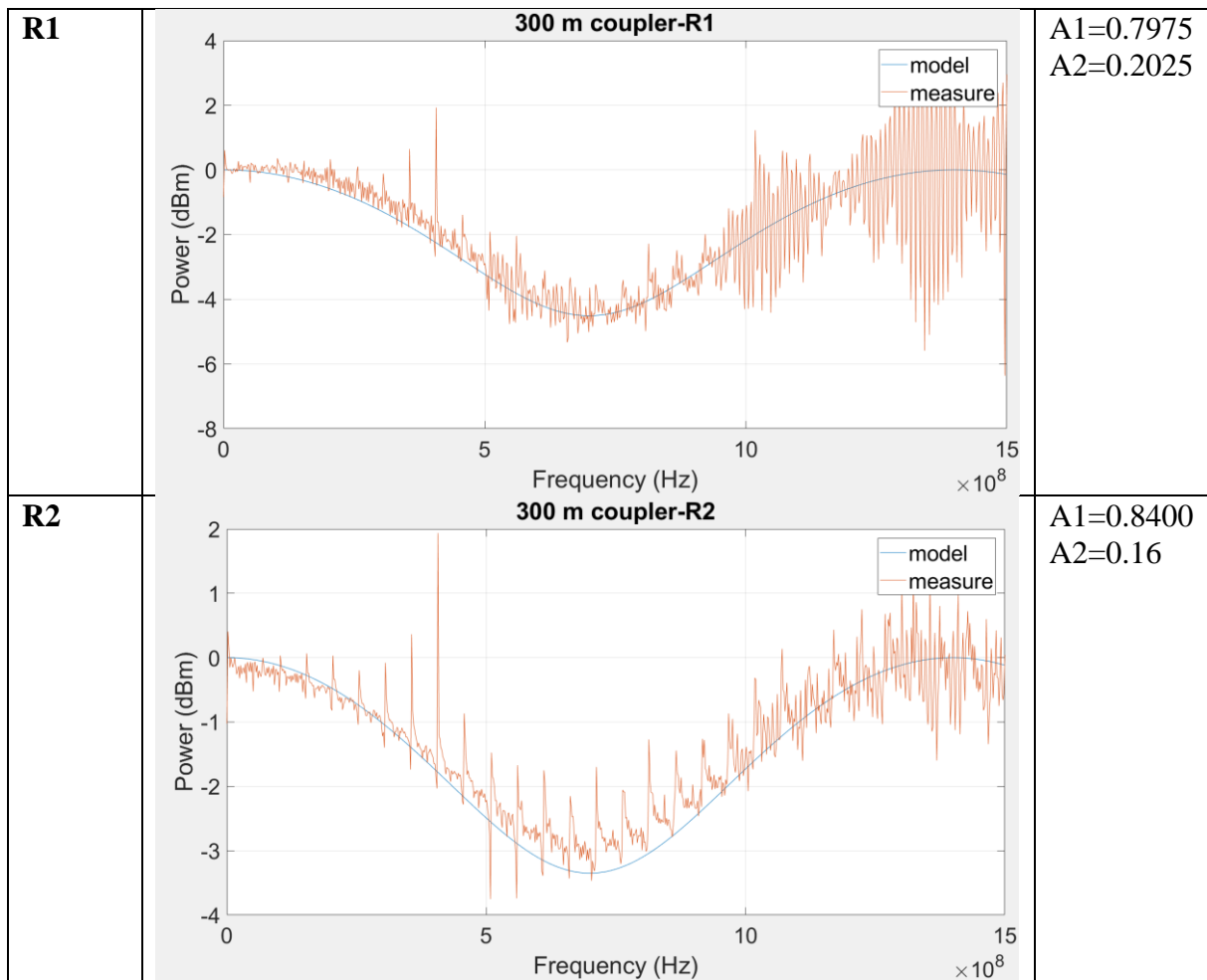


Figure 16: Non-normalized measure.

Now we proceed the analysis with the 4 configurations of the coupler:

case	Graph	Power weights
No coupler		A1=0.6156 A2=0.3844
T1		A1=0.9682 A2=0.0318
T2		A1=0.8775 A2=0.1225



1.5.2) COUPLER 90-10

As before we start the analysis with the graph of the normalized and non-normalized curve; then the different configuration will be taken into account.

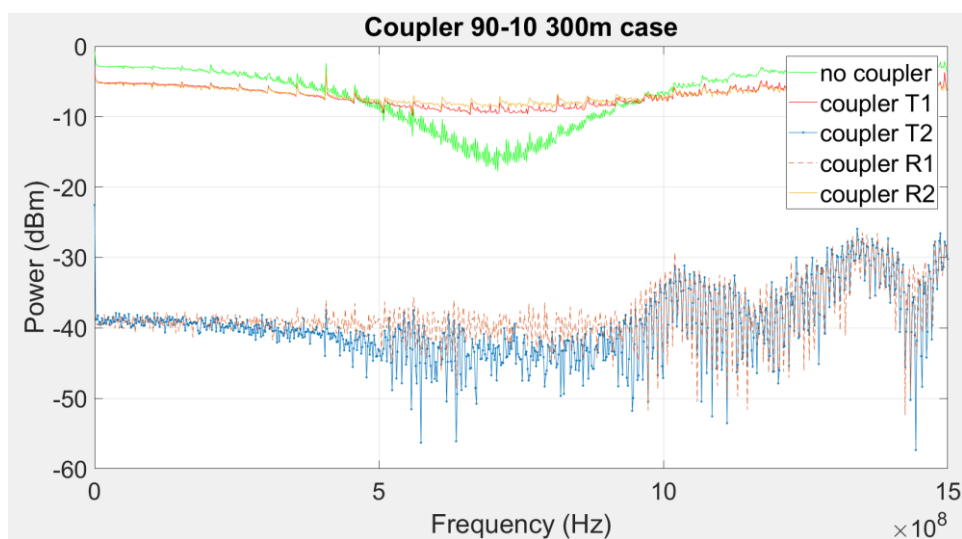


Figure 17: normalized measure.

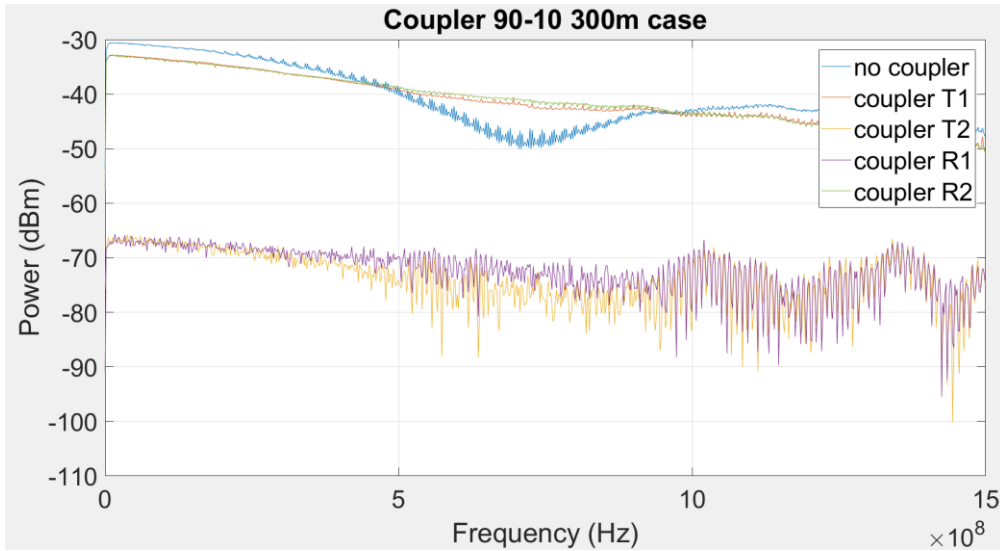


Figure 18: Non-normalized measure.

Analysis of the different configurations:

case	graph	Power weights
No coupler		A1=0.6156 A2=0.3844
T1		A1=0.7975 A2=0.2025

T2	<p style="text-align: center;">300 m case coupler-T2</p>	<p>A1=0.84 A2=0.16</p>
R1	<p style="text-align: center;">300 m coupler-R1</p>	<p>A1=0.96 A2=0.04</p>
R2	<p style="text-align: center;">300 m coupler-R2</p>	<p>A1=0.84 A2=0.16</p>

1.5.3) COUPLER 99-01

As before we start the analysis with the graph of the normalized and non-normalized curve; then the different configuration will be taken into account.

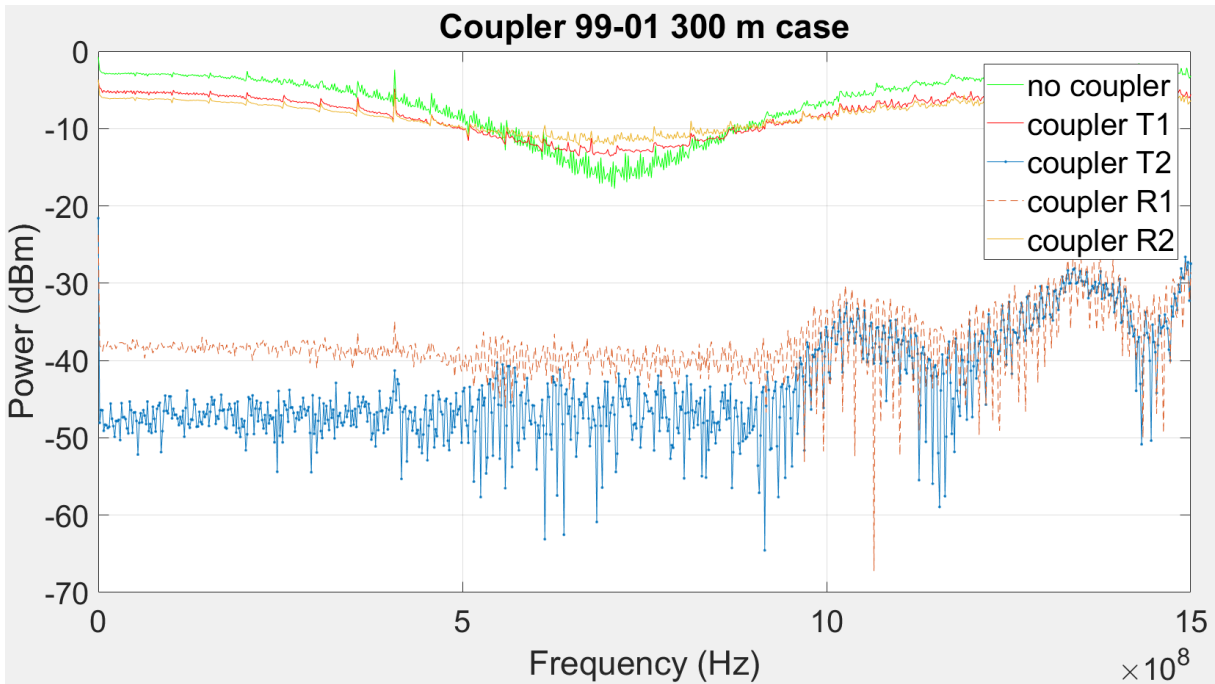


Figure 19: normalized curve.

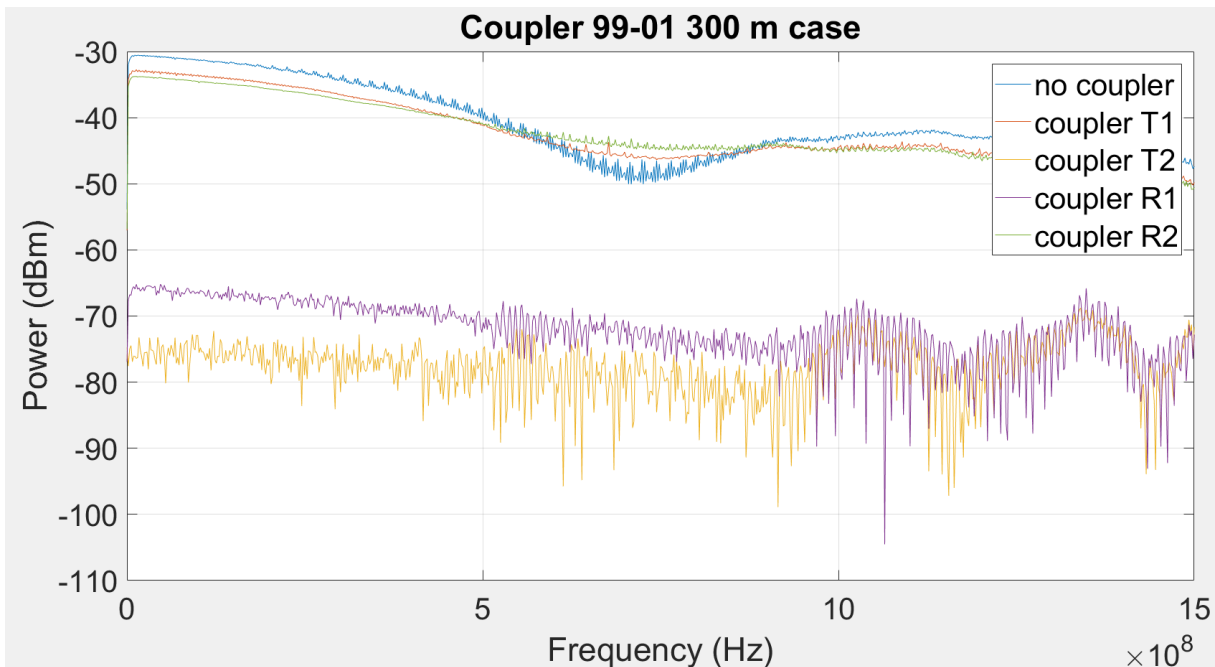
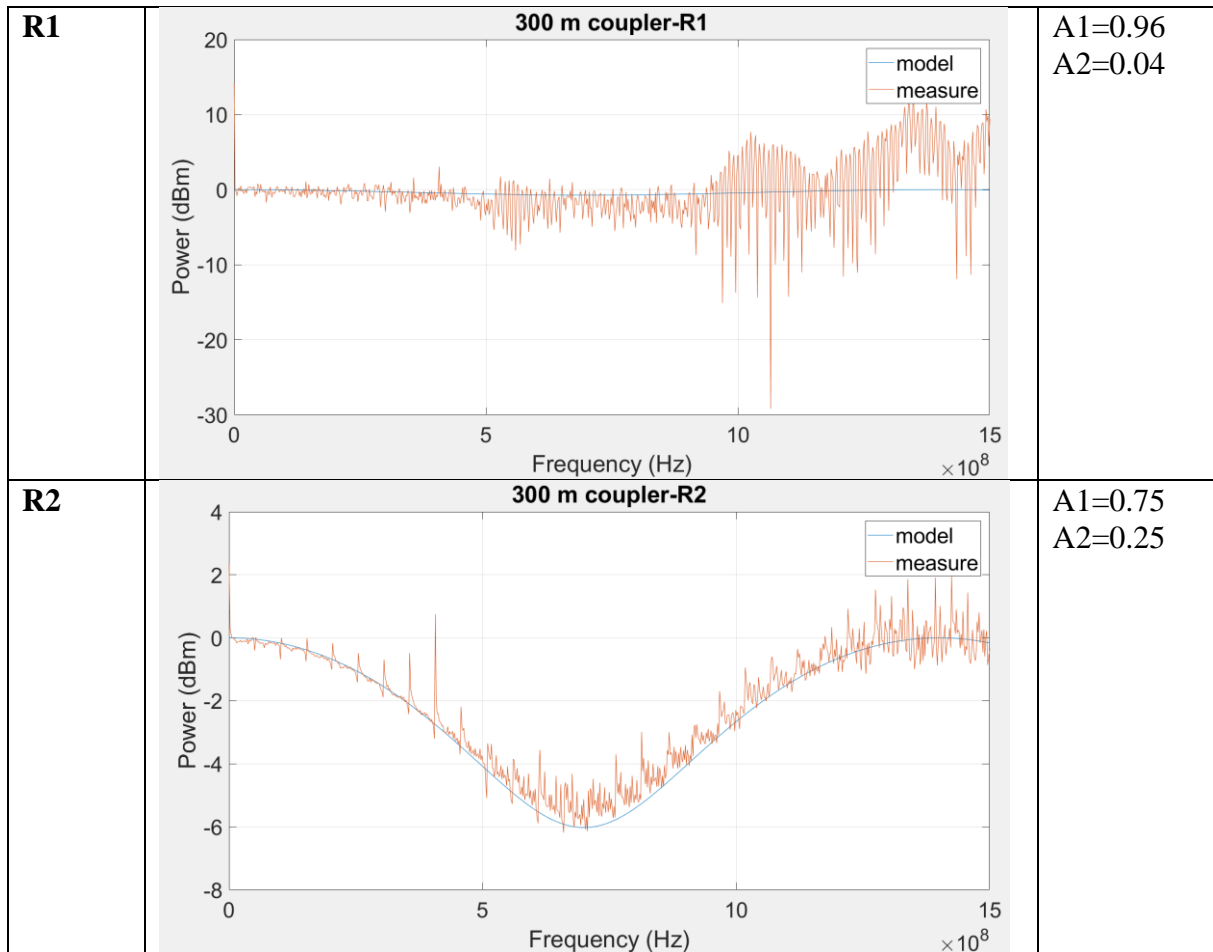


Figure 20: Non-normalized curve.

Analysis of the different configurations:

case	graph	Power weights
No coupler		A1=0.6156 A2=0.3844
T1		A1=0.6975 A2=0.3025
T2		A1=0.96 A2=0.04



1.5.3) CONCLUSION ON 300 m

Actually, the measures carried out were a lot more but here are presented the last set of measure that represents the more accurate case analysis. In fact, from the first sets of measure we have notice that in order to guarantee an accurate result, we have to fix all the fiber span, in order not to move since each movement can stimulate in a different way the two mode presents inside.

For the shake a completeness we have collected al the results in an excel file, with a column for the coefficients used in the algorithm and a column for the power coefficients that are the square of the previous ones.

The collected results are the following:

comparison measure 50-50 coupler				
T1	0,9165	0,839972	0,9682	0,937411
	0,4	0,16	0,25	0,0625
T2	0,9798	0,960008	0,9367	0,877407
	0,2	0,04	0,35	0,1225
R1	0,866	0,749956	0,893	0,797449
	0,5	0,25	0,45	0,2025
R2	0,9682	0,937411	0,9367	0,877407
	0,25	0,0625	0,35	0,1225

Tab 2: it shows a comparison between two set of measures with coupler 50-50, the first and third column represent the splitting coefficients, the second and fourth represent their square value also called power splitting.

comparison measure 90-10 coupler				
T1	0,893	0,797449	0,893	0,797449
	0,45	0,2025	0,45	0,2025
T2	0,9165	0,839972	0,9165	0,839972
	0,4	0,16	0,4	0,16
R1	0,9682	0,937411	0,9798	0,960008
	0,25	0,0625	0,2	0,04
R2	0,9165	0,839972	0,9165	0,839972
	0,4	0,16	0,4	0,16

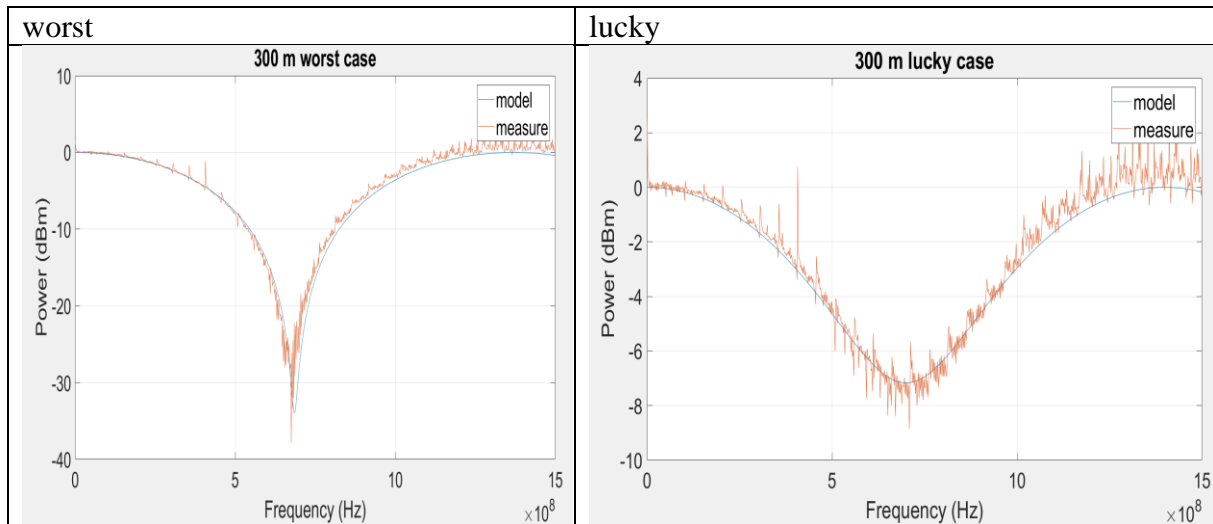
Tab 3: it shows a comparison between two set of measures with coupler 90-10, the first and third column represents the splitting coefficients, the second and fourth represent their square value also called power splitting.

comparison measures 99-01 coupler								
	1		2		worst	lucky		
T1	0,9682	0,937411	0,8352	0,697559	0,893	0,797449	0,8352	0,697559
	0,25	0,0625	0,55	0,3025	0,45	0,2025	0,55	0,3025
T2	0,9798	0,960008	0,9798	0,960008	0,9798	0,960008	0,9798	0,960008
	0,2	0,04	0,2	0,04	0,2	0,04	0,2	0,04
R1	0,9798	0,960008	0,9897	0,979506	0,9798	0,960008	0,9798	0,960008
	0,2	0,04	0,2	0,04	0,2	0,04	0,2	0,04
R2	0,9165	0,839972	0,866	0,749956	0,9165	0,839972	0,866	0,749956
	0,4	0,16	0,5	0,25	0,4	0,16	0,5	0,25

Tab 4: it shows a comparison between two set of measures with coupler 99-01, the first, third, fifth and seventh column represents the splitting coefficients, the second, fourth, sixth and eighth represent their square value also called power splitting.

For the last coupler (99-01) we have performed also a further analysis for the worst and lucky case.

For worst we intend a case where the 2 mode LP01 and LP11 carries actually the same amount of power, for lucky we mean a case where the mode LP01 is dominant as we can see in the table:



1.6) 2 KM ANALYSIS

Now the same analysis just seen is repeated with the 2 km SSMF fiber strand. The results are collected as before:

1. Coupler 50-50
2. Coupler 90-10
3. Coupler 99-01

1.6.1) COUPLER 50-50

The first results collected are as before the normalized and non-normalized measured of the different configurations:

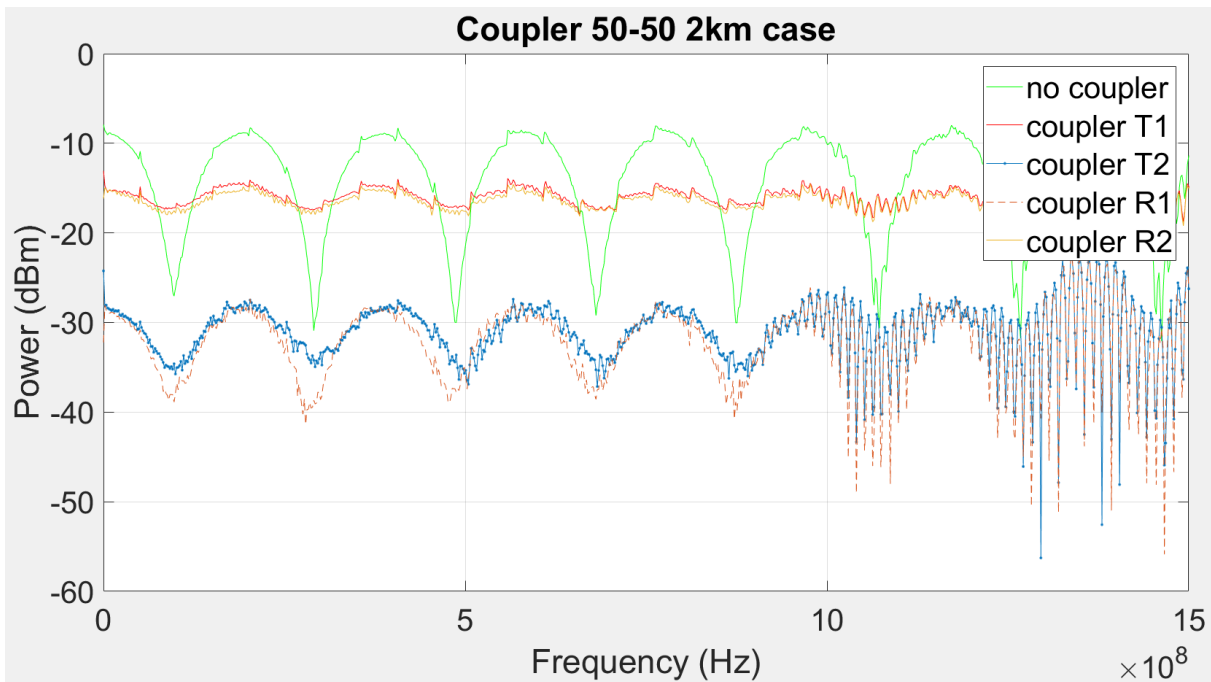


Figure 21: normalized measure 2 km case.

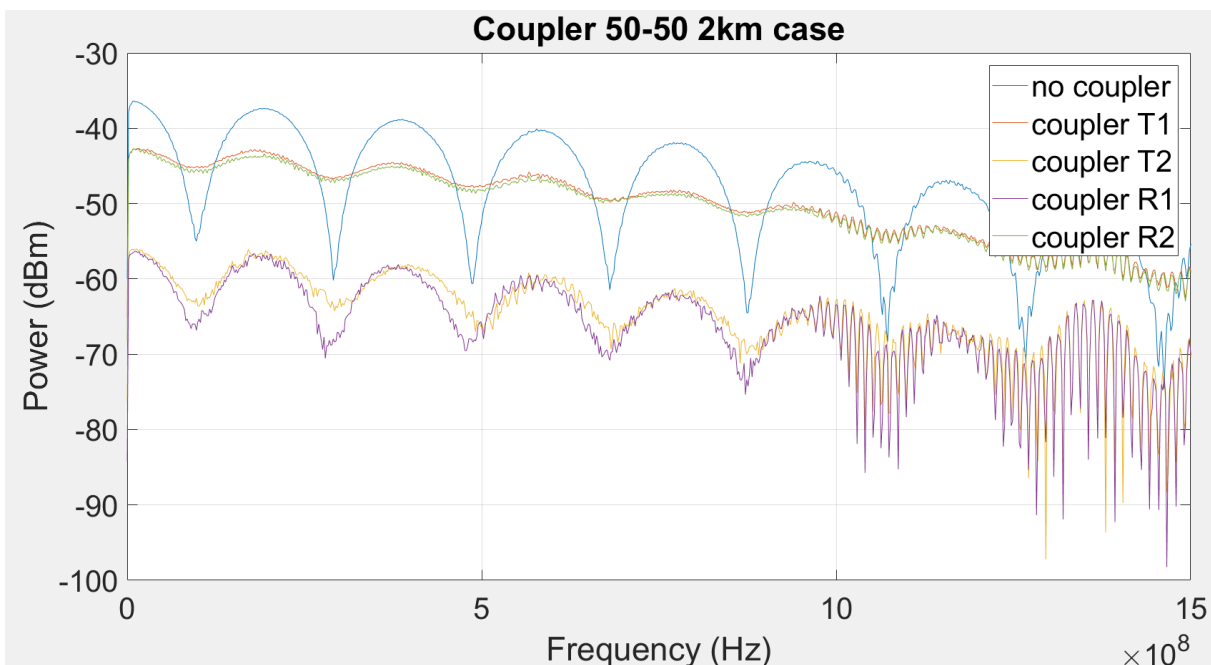
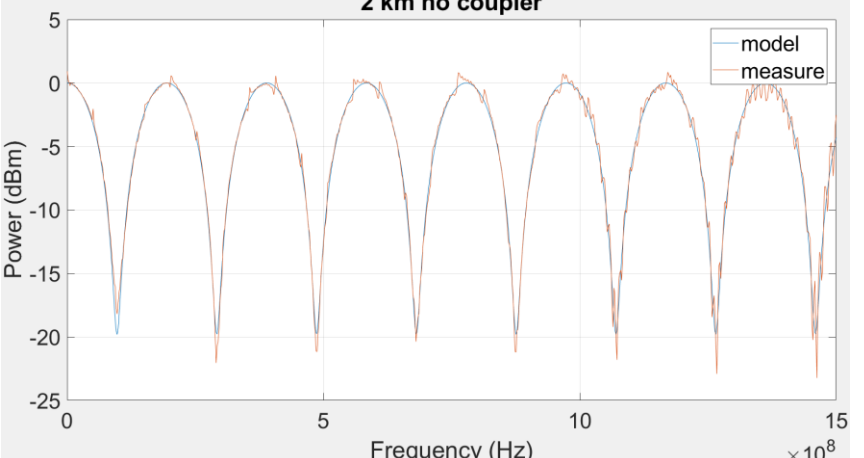
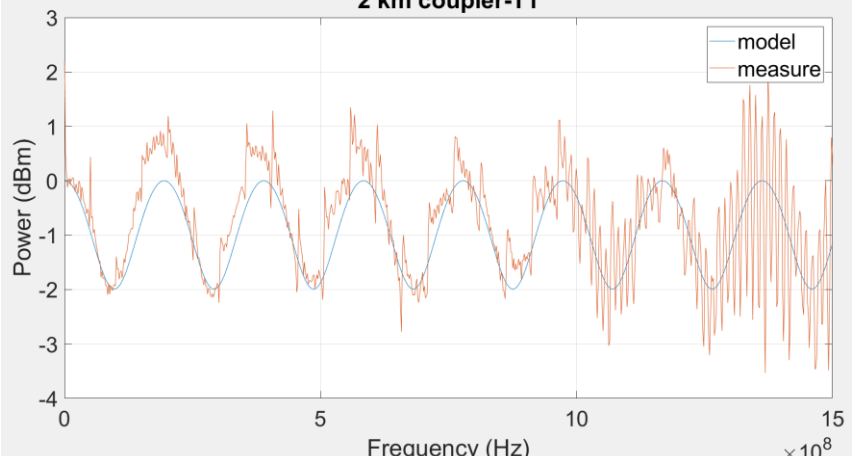
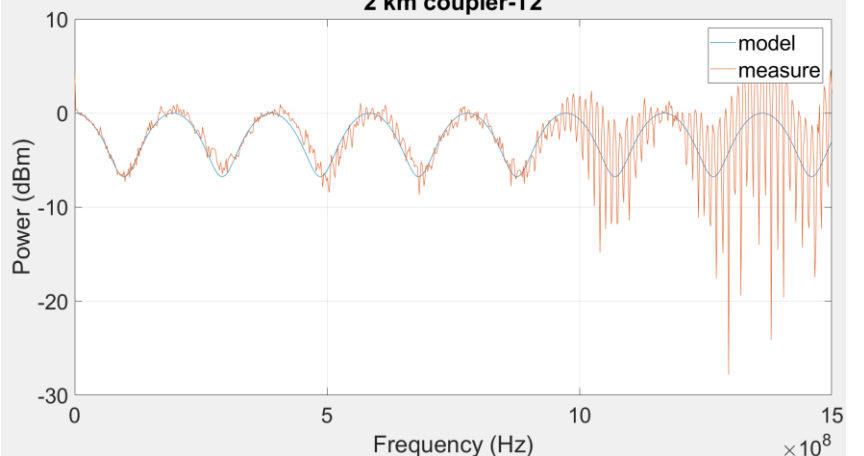
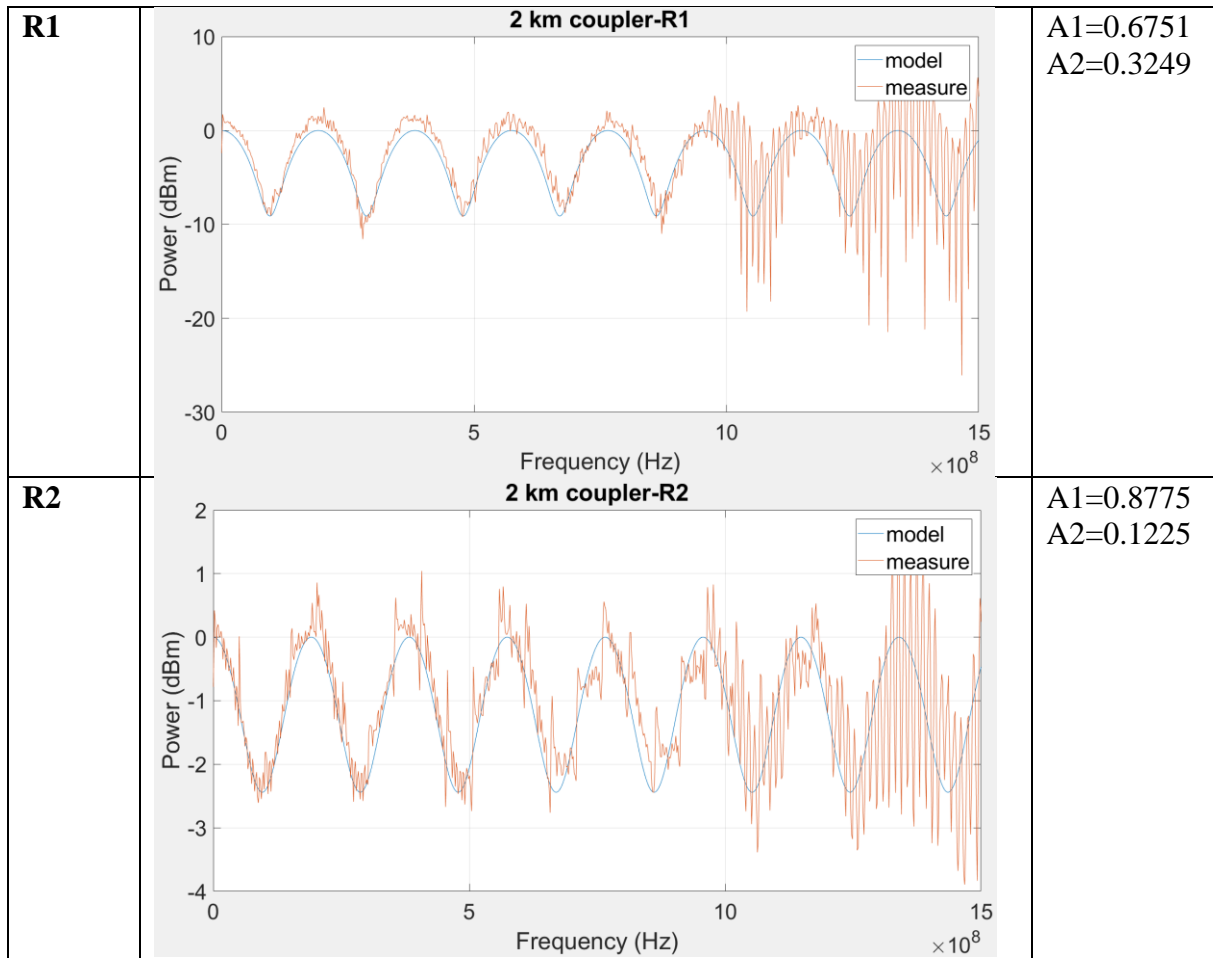


Figure 22: Non-normalized measure 2 km case.

Then the 4 different configurations are analysed:

case	graph	Power coefficients
No coupler		<p>A1=0.5511 A2=0.4489</p>
T1		<p>A1=0.8976 A2=0.1024</p>
T2		<p>A1=0.7296 A2=0.2704</p>



1.6.2) COUPLER 90-10

In the same way as before we first present the normalized and denormalized measurements:

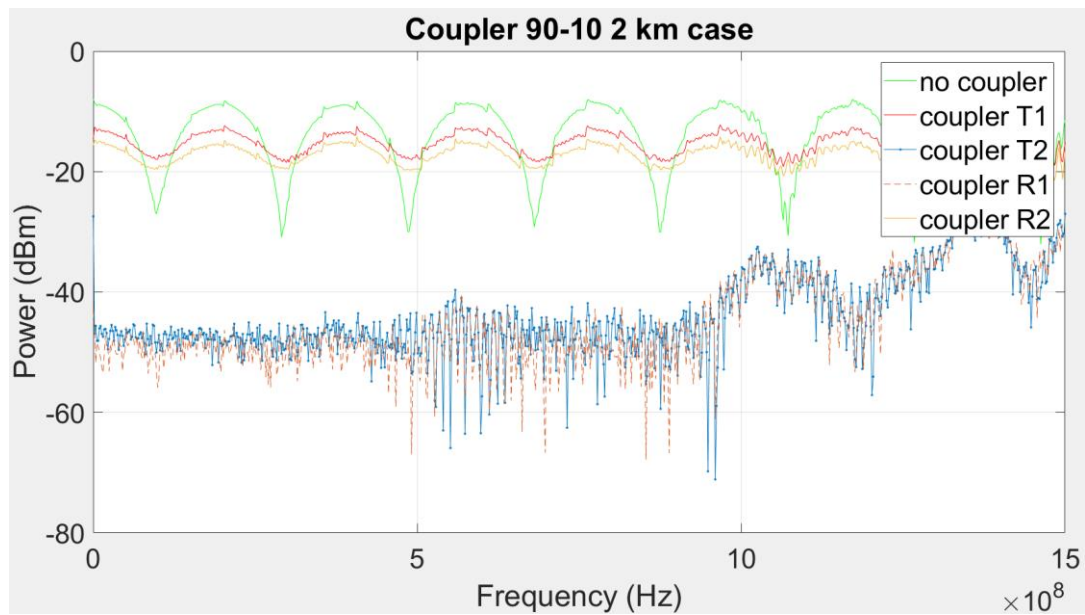


Figure 23: normalized measure 2 km case.

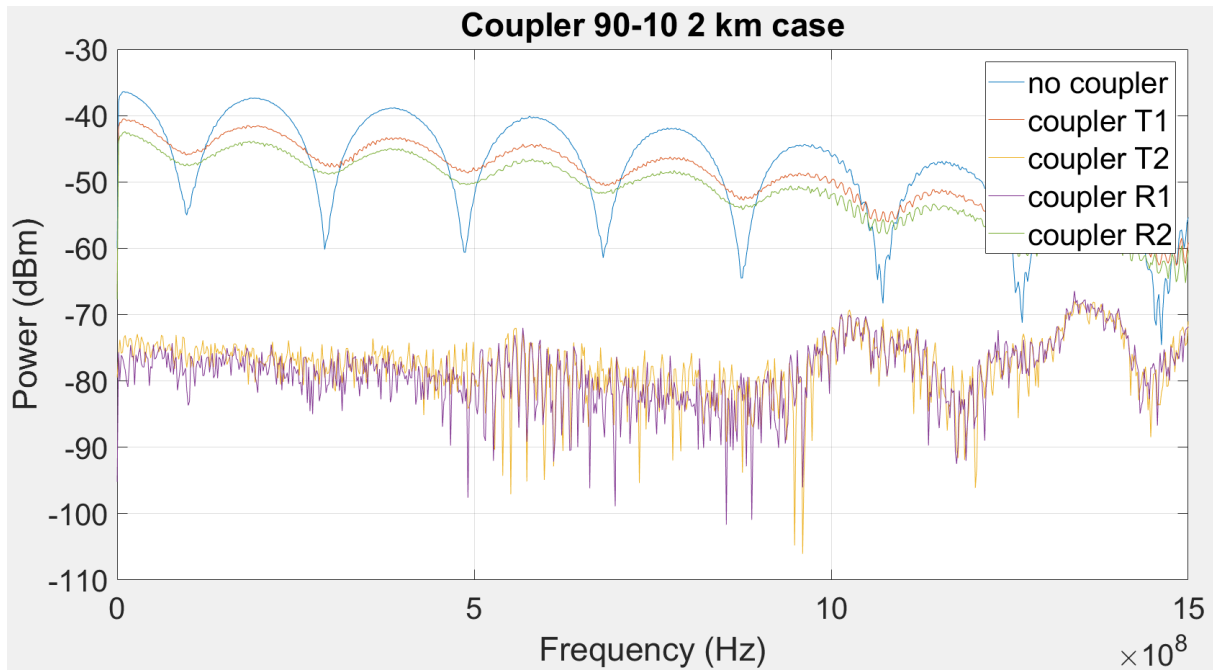
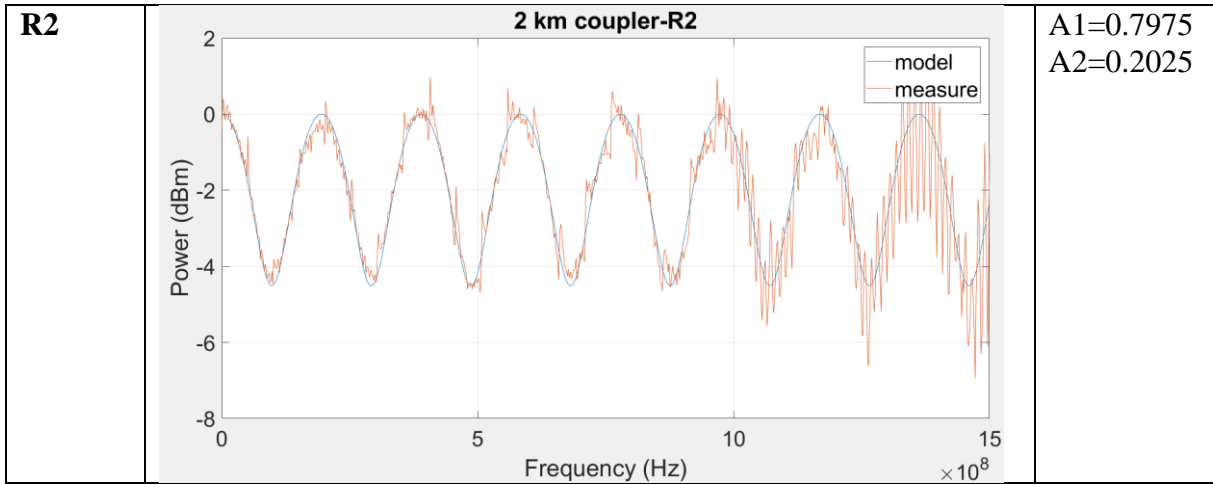


Figure 24: Non-normalized measure 2 km case.

Now we proceed with the 4 different configurations of the coupler:

case	graph	Power weights
No coupler	<p>The graph shows Power (dBm) on the y-axis (ranging from -25 to 5) against Frequency (Hz) on the x-axis (ranging from 0 to 15 $\times 10^8$). Two data series are shown: 'model' (blue) and 'measure' (orange). Both series show a clear periodic oscillation between approximately -20 dBm and 0 dBm.</p>	<p>A1=0.5511 A2=0.4489</p>

T1	<p>2 km coupler-T1</p>	<p>A1=0.7884 A2=0.2116</p>
T2	<p>2 km coupler-T2</p>	<p>A1=0.9375 A2=0.0625</p>
R1	<p>2 km coupler-R1</p>	<p>A1=0.9375 A2=0.0625</p>



1.6.3) COUPLER 99-01

Normalized and non-normalized measurements:

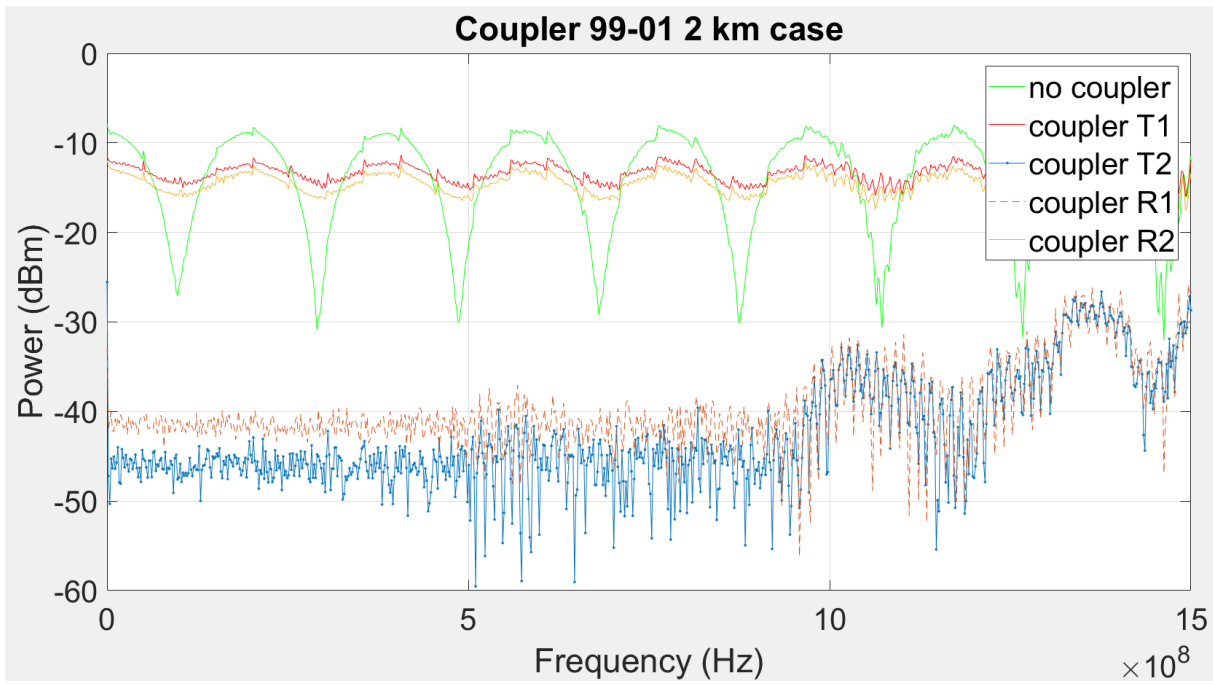


Figure 25: normalized measure 2 km case.

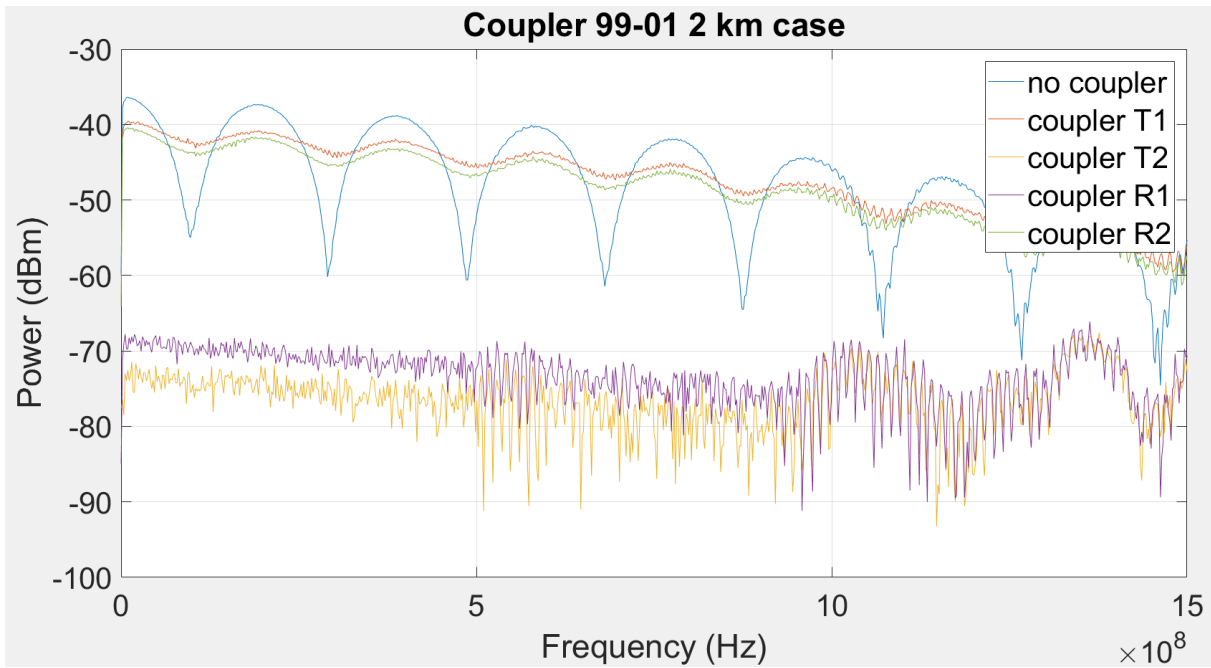


Figure 26: Non-normalized measure 2 km case.

Analysis of the different configurations:

case	graph	Power weights
No coupler		A1=0.5511 A2=0.4489
T1		A1=0.8844 A2=0.1156

T2	<p style="text-align: center;">2 km coupler-T2</p>	A1=0.96 A2=0.04
R1	<p style="text-align: center;">2 km coupler-R1</p>	A1=0.96 A2=0.04
R2	<p style="text-align: center;">2 km coupler-R2</p>	A1=0.8556 A2=0.1444

1.6.4) MEASURE COMPARISON

In order to compare the different couplers we have collected all the data inside a tab in order to see the different.

comparison between different coupler 2 km case				
		50-50	90-10	99-01
T1	A1	0,8976	0,7884	0,8844
	A2	0,1024	0,2116	0,1156
T2	A1	0,7296	0,9375	0,96
	A2	0,2704	0,0625	0,04
R1	A1	0,6751	0,9375	0,96
	A2	0,3249	0,0625	0,04
R2	A1	0,8775	0,7925	0,8556
	A2	0,1225	0,2025	0,1444

Tab 5: the tab shows a comparison for the power splitting coefficients with the three different couplers tested.

1.7) CONCLUSION ON THE TWO MEASUREMENTS SET

After the two complete analysis of 300 m and 2 km SSMF we can conclude that the coupler act somehow like a mode filtering. In all the test realized so far, we have supposed that the principal mode LP01 is the dominant one so the coefficient of A1 will always bigger than A2. This assumption will be demonstrated in the following sections.

After the experiment carried out, we can conclude that, all the couplers somehow filter the LP11 mode, anyway our final scope is to realize a predistortion using the feedback branch so even the output power level becomes important.

Both in 300 m and 2 km we can appreciate that the feedback path, corresponding to T2 or R1 configuration, has different power level in function of which coupler we are considering. In order to realize a feedback predistortion, we need sufficient power on the T2 or R1 configuration, so in this case the most suitable solution will be to implement the coupler 50-50 in our system in order to have enough power on the feedback path.

1.8) 5 μm TEST

In order to demonstrate that the most dominant mode is LP01 as we have supposed, and also to make a comparison with the initial solution already proposed in the literature, where a small strand of 5 μm SMF is placed at the input section of SSMF. So the system can be represented as follow:

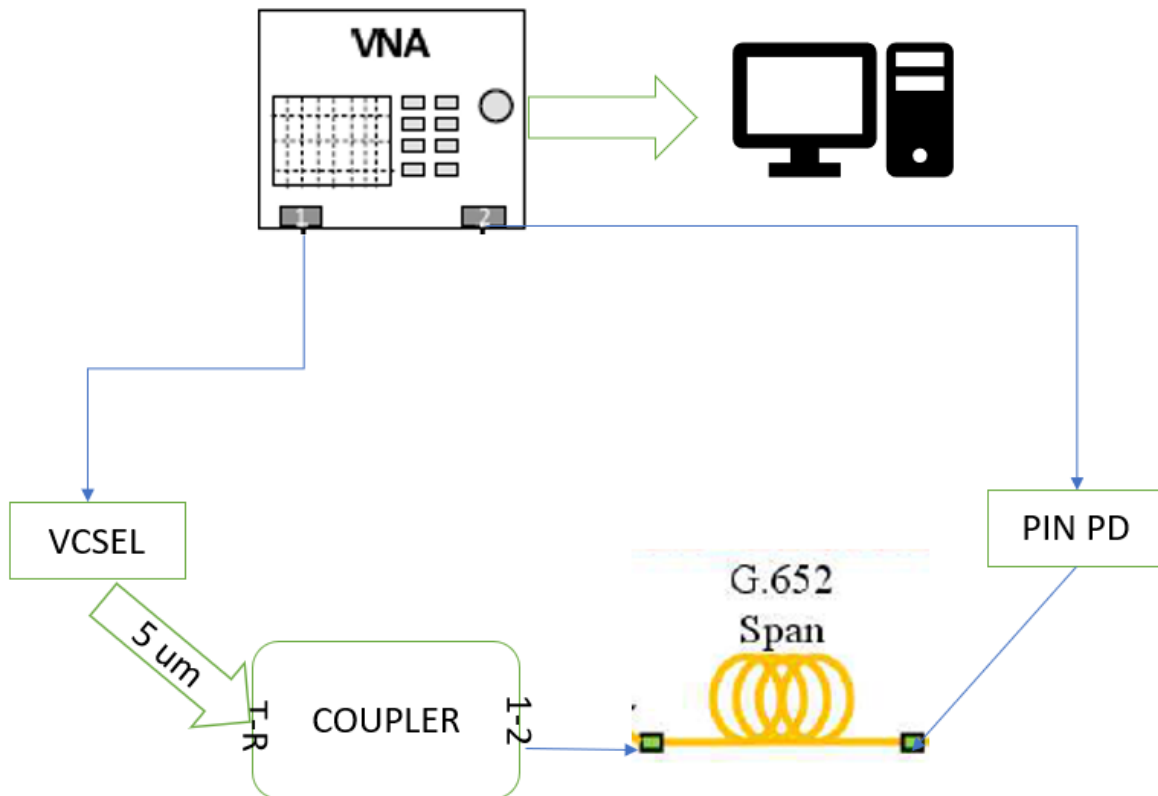
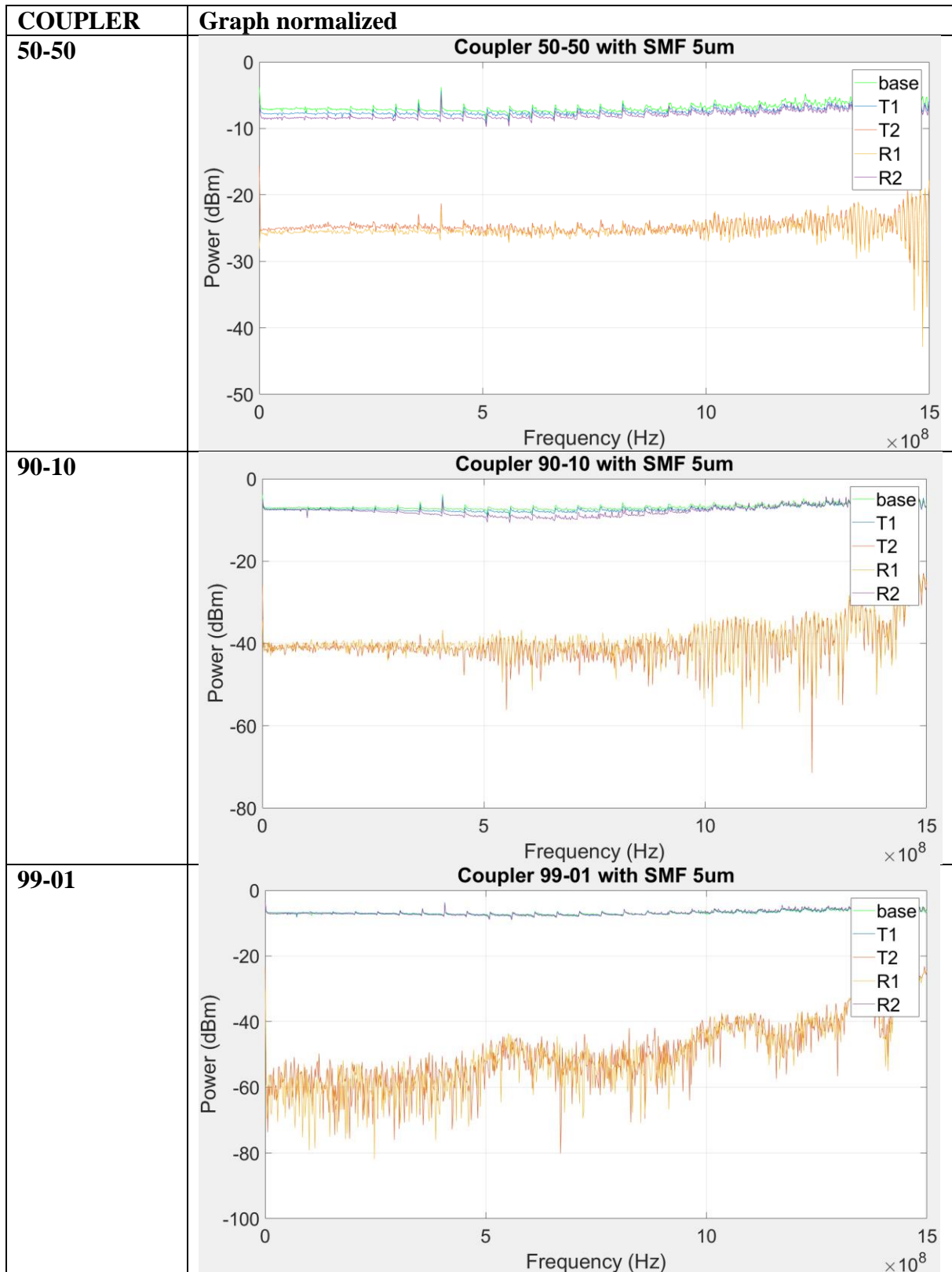
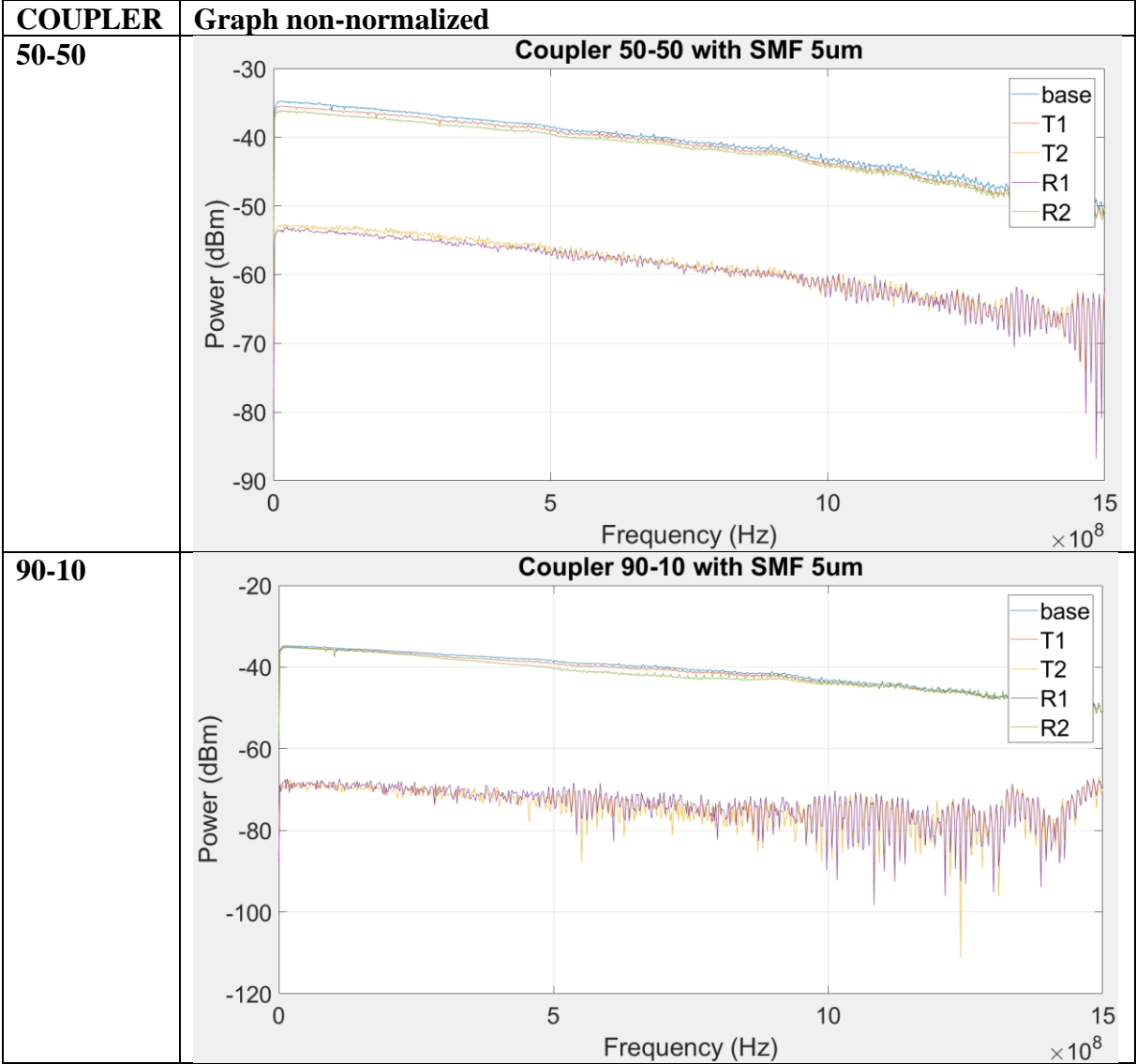


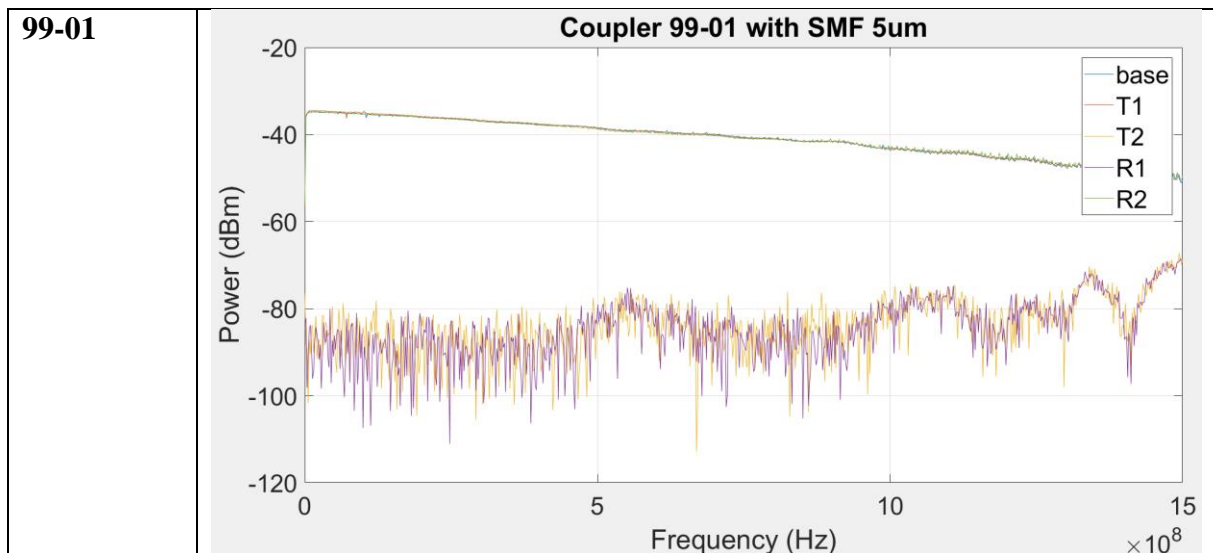
Figure 26: schematic of the tested link with SMF 5 μm .

we have already analysed the effect of 5 μm from a theoretical point of view, now we modify the previous scheme in order to realize a further analysis.

In the following tabs it is presented a comparison between the three different couplers with this particular configuration:







We do not show the results of the analysis of the four configurations of each coupler since the starting 5 μm SMF basically filter out all the LP11 mode so all the four configuration presents a flat behaviour, demonstrating the presence of LP01 only.

1.8.1) CONSIDERATION ON 5 μm SMF

A further experiment has been carried out in order to understand a strange behaviour we have encountered during the measurements. Basically, a measurement of the power was carried out at the laser output section and on the two output paths going out from the coupler, for example T1 and T2. We should expect that the collected power on the two paths is the same as the output laser but actually what we measure was 3 dB lower with respect to what we expected.

In order to better understand this behaviour, we have repeated the test inserting the 5 μm SMF between the laser and the SSMF fiber and repeat the measurements of power.

A first measure is taken at the input section of the coupler so just after the 5 μm SMF fiber and a second set of measure has been carried out at the two output of the coupler, T1 and T2.

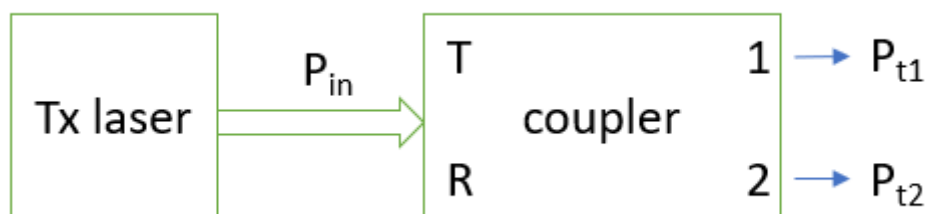


Figure 27: schematic of the first measure

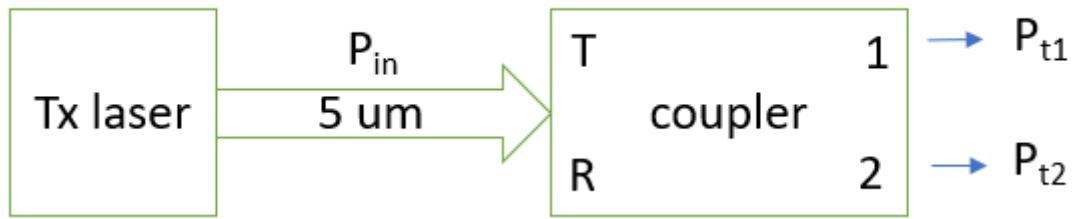


Figure 28: schematic of the second measure.

We have transmitted -8 dBm from the laser and the measure at the input of the coupler was -8.34 dBm.

Then the second measure was carried out with the following results:

P at T1: -8.93 dBm \rightarrow 127.8 uW

P at T2: -17.3 dBm \rightarrow 18.48 uW

If now we sum together the linear power and we reconverts it in dBm we found -8.349 dBm. In this case we do not have the 3 dB losses observed in the first case.

In conclusion we can assert that the loss is given by the LP11 mode only, that somehow convert into radiant mode, causing the 3 dB loss we have observed in the first case.

This experiment also demonstrate that the most dominant mode is the LP01 so the assumption we have taken in all the previous measure of assuming A1 always greater than A2 it is valid.

The limit case of power weights is represented by the case with no coupler where we have half power coming from LP01 and half power coming from LP11.

1.9) CONCLUSION

In this chapter we first put into evidence the possible application of this new solution for low-cost Radio-Over-Fiber system. Initially, a study of the state of art of this technology has been performed to show the technical solution implemented nowadays. The analysis performed on the differ couplers shows that can behave somehow like a mode-filter. Our final goal is to realize a predistortion system that exploits the feedback path, so even the power going out from this via assume an important role. For our scope, the best solution is the coupler 50-50 that present 10-15 dB more, respect to the 90-10 or 99-01, from the feedback path.

In the next chapter we will focus on the actual predistortion algorithm realized from this architecture and how the performance can be improved using this technical solution.

CHAPTER 2 DIGITAL PREDISTORTION

2.1) OVERVIEW ON PREDISTORTION

The scope of this dissertation is to explain theoretically and experimentally the benefit coming from digital predistortion of the link itself. The idea is to enhance the linearity of short and medium link for the Mobile Front Haul links already present in the mobile communication system. As seen before it will be used a VCSEL operating at 850 nm and the standard single mode fiber SSMF, in order to maintain a low-cost and low-consumption solution for the RoF link.

In this dissertation the memory polynomial (MP) is used together with Indirect Learning Architecture (ILA). The performance improvement is measure through some significative quantities like Adjacent Channel Power Ratio (ACPR), Normalized Mean Square Error (NMSE) and Error Vector Magnitude (EVM).

The Radio over Fiber technology can be exploited for long range and short-range communication, anyway the focus of this work is for short range link. In this kind of link, the main part of the non-linearities comes from the laser source and the photodiode, placed at the receiver. All the other non-linearities can be neglected for the shake of simplicity, since they do not affect the link in a significative way [6].

The effect of the non-linearity leads to a distortion in-band and out of band, this damage the link quality and raise the interference among the channels.

There are different techniques for predistortion that will be explained in the next sections, anyway among the different techniques we focus on Digital Predistortion (DPD). The basic idea behind the DPD is to adopt a digital pre-distorter able to recreate an opposite non-linear characteristic of the RoF link.

This way the cascade pre-distorter + RoF link has a linear behaviour. Note that the next graph is referred to a PA, not the full RoF link, anyway the idea of digital predistortion remain the same and can be appreciated in the following figures:

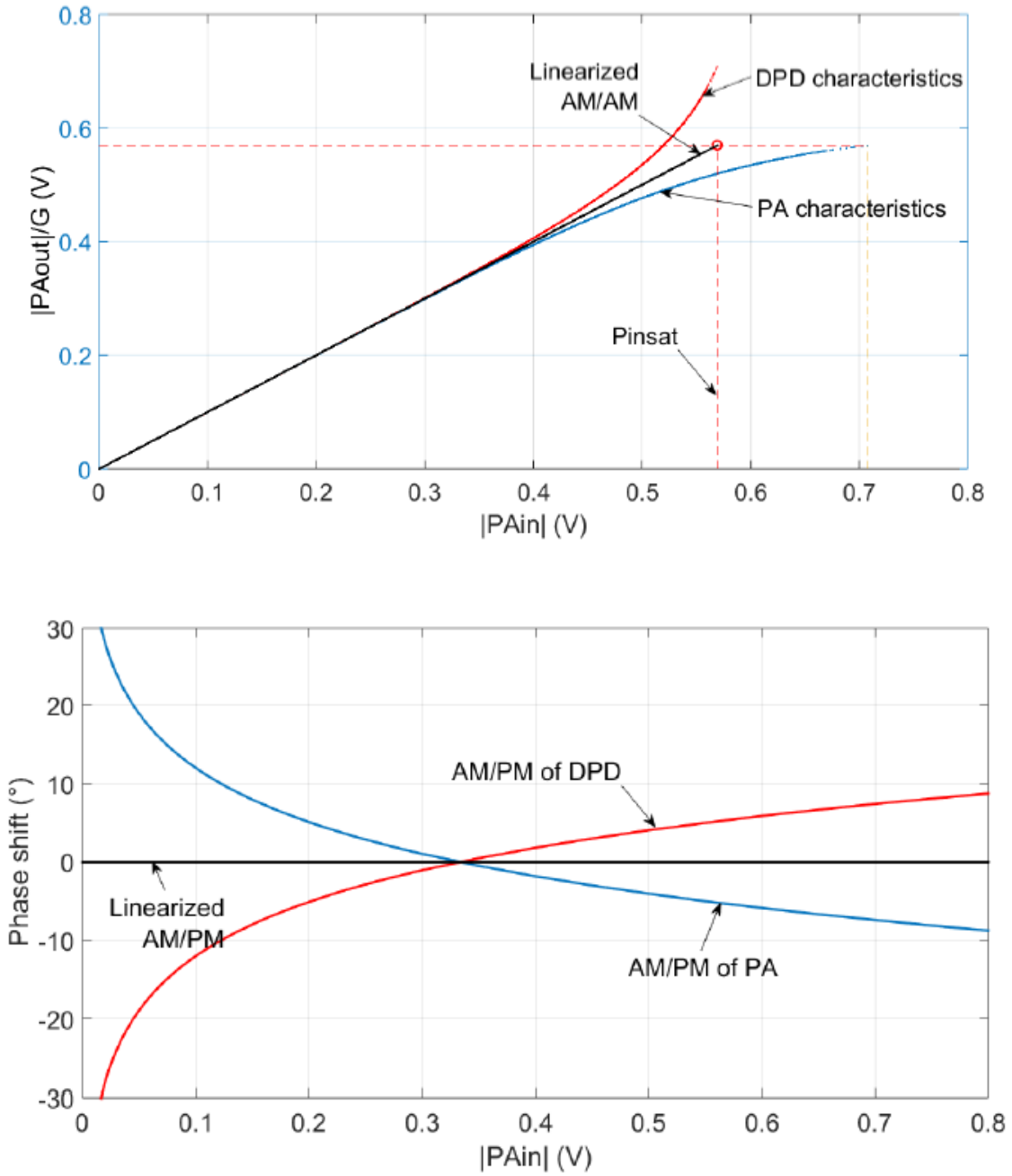


Figure 29: AM/AM and AM/PM characteristics of PA and DPD [16].

In the context of this dissertation the DPD is applied for an LTE application in order to increase the linear behaviour. In general, DPD is applied to the PA that become strongly non-linear with wideband, high envelope signals like those of LTE. In this particular case, the DPD algorithm, is applied to the whole RoF link, including transmitting laser, PA and PIN receiver.

The VCSEL laser chosen for this work as already seen is low cost and low consumption but has a serious problem because of its small dynamic. In fact, LTE signal presents signal with a high value of Peak-to-Average Power Ratio (PAPR) and this create a problem with the small

dynamic of the laser since the peak of the signal can be so high with respect to the mean value, that can be subjected to strong non-linearity.

In order to characterize the nonlinear model, we use memory polynomial since a memoryless model would not be enough accurate to describe the electro-optic conversion. The MP model will be further investigated in the next section and represents a special case of Volterra series.

The DPD model identification used is Indirect Learning Architecture and it is structured like the scheme presented in figure 30.

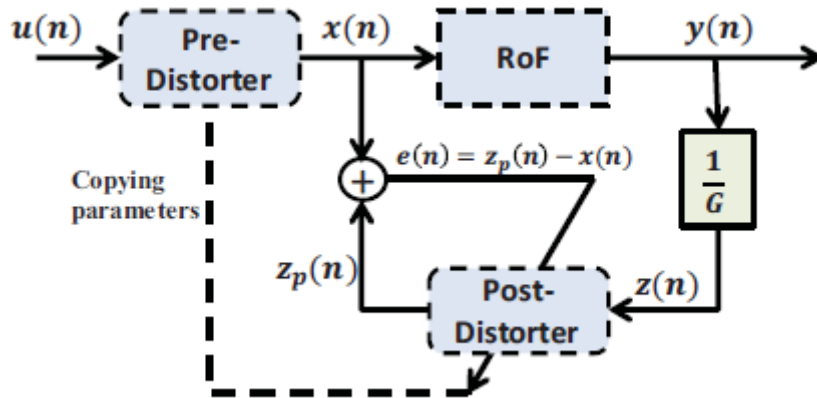


Figure 30: ILA architecture model.[6]

The MP is applied as follow:

$$x(n) = \sum_{k=1}^K \sum_{q=0}^Q a_{kq} * u(n - q) * |u(n - q)|^{k-1}$$

$$z_p(n) = \sum_{l=0}^{L-1} \sum_{m=0}^M \gamma_{lm} * z(n - m) * |z(n - m)|^l$$

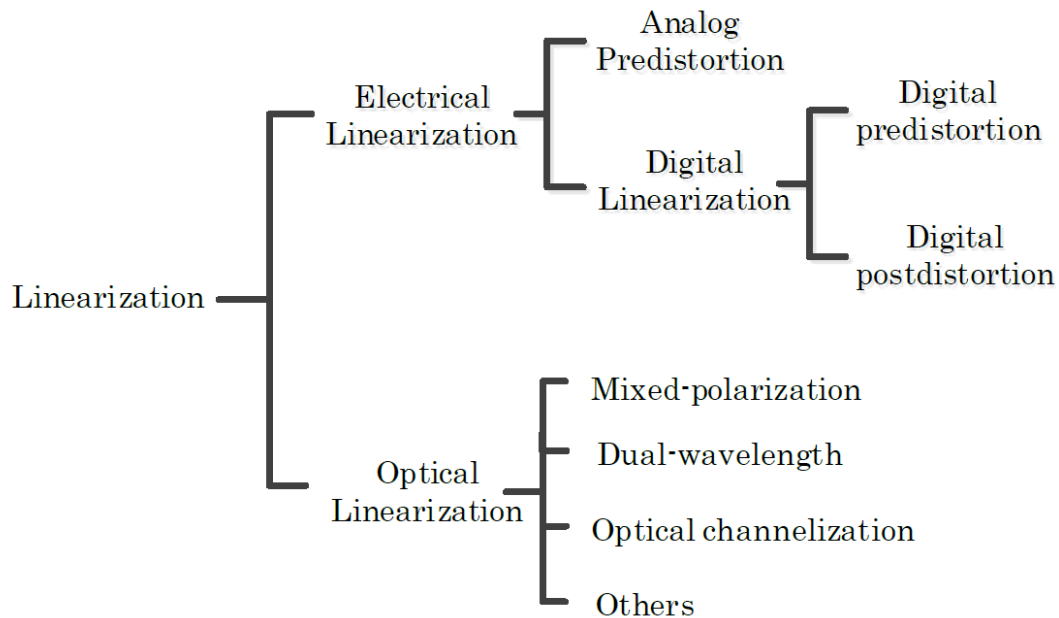
DPD model is based on the estimation of the coefficients presents in those two formulas; anyway, in ILA post-inverse can be used as pre-inverse and this permits to realize a linear estimation of the coefficients. Obviously, the training phase, where the coefficients are estimated, can be done offline it the system does not change in time.

In this architecture the first evaluation is for the post distorter coefficients, then the pre-distorter is updated. In order to complete the overview, we focus on the figure of merit that are exploited to evaluate the performance improvement:

- $NMSE_{dB} = 10 \log_{10} \left(\frac{\sum_{n=1}^N |x(n) - z_p(n)|^2}{\sum_{n=1}^N |x(n)|^2} \right)$ the NMSE is evaluated between the estimated post distorter output $z_p(n)$ and the pre-distorter output $x(n)$. N represents the length of the signal.
- $ACPR_{dB} = 10 \log_{10} \left(\frac{\int_{adjacentBand_{low}}^{adjacentBand_{up}} S(f) df}{\int_{usefulBand_{low}}^{usefulBand_{up}} S(f) df} \right)$ in this case S(f) represents the power spectral density of the output signal $y(n)$.
- $EVM_{dB} = \sqrt{\frac{\sum_{k=0}^N (I_k - \bar{I}_k)^2 + (Q_k - \bar{Q}_k)^2}{\sum_{k=0}^N I_k^2 + Q_k^2}}$ this equation operated directly on the constellation, in fact I and Q represents the transmitted component, instead \bar{I} and \bar{Q} represent the received components respectively of the in-phase and quadrature via. N represents the number of samples and k is the index of the sum operator.

2.1.1) LINEARIZATION METHODS

There are different linearization techniques available for our purpose, they can be classified as the following scheme:



They have different characteristics but the same final purpose, let's look more in detail the different techniques [7]:

- **Electrical linearization:** it can be split in analog pre-distortion and digital linearization that will be discussed next. For the analog case, the idea is to create a predistortion circuit that suppresses the intermodulation products that are particularly dangerous, since they fall close to the useful bandwidth. In general, the intermodulation products of third order (IMD3), are in antiphase with respect to the RF signal so, the analog predistortion circuit, generates IMD3 components in phase with the signal [7] in order to cancel out the original IMD3. Usually to achieve a broadband linearization, Schottky diodes are implemented since their ability to generate all order nonlinearities.
- **Optical linearization:** it can be differentiated into mixed-polarization, dual wavelength and optical channelization [7]. This technique is able to cancel out both second and third order nonlinearities. The linearization bandwidth is only limited by the bandwidth of the optical modulator, anyway we do not enter inside this technological solution since it is out of the scope of this dissertation.
- **Digital linearization:** the goal is always to suppress the IMD3 generated by RF power amplifiers. This technique exploits the analog-to-digital converter (ADC) to sample the analog signal and realizing digital signal processing on the samples. For this reason, the actual band that can be linearized, is limited to 100 MHz [7], due to the limits in the sampling frequency of the ADC. Actually, it is possible to achieve greater bandwidth but the DSP, using for instance the Lagrange procedure, require complex calculation and a big power consumption. The principle of digital predistortion techniques is that the pre-distorter generates an inverse nonlinear characteristic in order to compensate the RoF transmission. Anyway, when broadband signals are transmitted over RoF system the memory effects start to be not negligible.

In general, Volterra series is adopted to estimate the behaviour of the RoF link and in general all non-linear dynamic systems. In practical cases some other techniques will be implemented because of the huge calculation complexity of Volterra analysis.

The most adopted solution is the memory polynomial, as the one we use for our dissertation, that allows to reduce a lot the computational complexity, reaching a good accuracy level.

An alternative is the post-linearization but since the nonlinearity information of RoF transmission is blind at receiver side, this technique has to use a recursive algorithm in order to find the optimal coefficients of the memory polynomial.

After this overview on the different predistortion techniques, the conclusion is that analog predistortion techniques can be very broadband and can be used to suppress third order nonlinear distortion. The optical linearization is more complex but is able to suppress both the second and third order non-linear distortion. This technique is ultra-broadband but, it is limited by the modulation bandwidth of the modulator. Digital predistortion linearization has the limit of bandwidth, if compared with the other techniques, but presents the best performance and has big margin of improvements [7].

2.2) BEHAVIORAL MODELLING OF ROF LINK

A fundamental aspect for exploiting the predistortion is a simple and fast way to characterize the radio-over-fiber link behaviour, including both non-linearity and memory effects. The reason of this analysis is due to the fact that, the RoF system, can be limited by the nonlinear distortion of the optical link itself, and this is due to the lasers and photodiodes, especially in a multi-user scenario. Furthermore, in general, the mobile standard, like LTE, exploit Orthogonal Frequency Division Multiplexing (OFDM) that are vulnerable to the link non-linear distortions because of their PAPR in their envelope.

Nonlinear system can be classified as memoryless or dynamic, anyway if we deal with wideband OFDM signals a memoryless model is not enough to characterize the link and the electro-optic conversion so it is fundamental to take into account the memory effects.[8]

Volterra is the most general and powerful tool that can be exploited to characterize a non-linear dynamic system but is very complex and the number of coefficients to be evaluated is huge. The complexity become even heavier in the case of RoF driven by wideband signals because of the Volterra kernels order that let the complexity explodes. For this reason, a simplification of this model is necessary, for instance the memory polynomial.

In general, the modelling of the system can be approached in different way [8]:

- **Physics-based modelling:** it is based on the physics of the devices but actually a lot of physical parameters of the laser are unknown and other parameters can be measured but the operation it's a complex task.

- **Behavioural modelling:** this technique is a black-box approach where, the only parameters necessary, are the input and output characteristic of the link. With this approach, the RoF link non linearities and memory effects can be obtained using some optimization algorithm.

2.2.1) MODEL ARCHITECTURE

As we have already mentioned there are two possible architecture that can be exploited for our purpose:

- **Indirect Learning Architecture (ILA):** post-inverse of RoF is first identified and then used as pre-distorter.
- **Direct Learning Architecture (DLA):** a model for the RoF is first identified then the pre-distorter is obtained.

In both cases, the best performances are achieved by an iterative procedure and as usual the improvement is presented in term of ACPR, EVM and NMSE.

Power amplifiers are one of the most important nonlinearity sources and exhibits non-linear characteristics when driven towards the high efficiency saturation region. The non-linear behaviour of PAs is able to distort the transmitted signal, both in band and out of band, causing a worsening of the figure of merits. The issues of the Pas, are even augmented by the employing of varying-envelope waveforms like OFDM that shows a high PAPR; those effects can be appreciate in the figure 31 as follow:

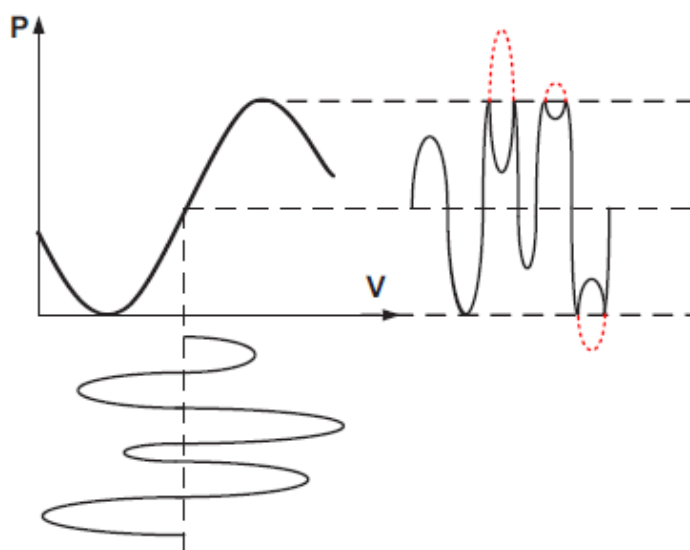


Figure 31: example of a varying envelope signal applied to a PA. [11]

There are a lot of techniques for linearize this behaviour, as we have seen, but digital predistortion has gained credits since it is an effective and low-cost method. The pre-distorter generates an inverse characteristic with respect to the RoF link so that the cascade pre-distorter + PA shows a linear behaviour with a constant gain; this means that the output is an amplified version of the input itself. Both solution DLA and ILA needs an iterative approach in order to reach the best performances.

2.2.2) NL SYSTEMS

Volterra series is the most general methods to study those kinds of systems that shows nonlinearity and memory effects. It can be formulated as follow, considering $y(n)$ as the system output and $x(n)$ as the input [12].

$$y(n) = \sum_{k=0}^K y_{2k+1}(n)$$

Where:

$$y_{2k+1}(n) = \sum_{l_1=0}^L \sum_{l_{k+1}=l_k}^L \dots \sum_{l_{2k+1}=l_{2k}}^L a_{l_1, l_2, \dots, l_{2k+1}} \prod_{m=1}^{k+1} x(n-l_m) \prod_{m=k+2}^{2k+1} x^*(n-l_m)$$

$a_{l_1, l_2, \dots, l_{2k+1}}$ denotes the $(2k+1)$ -th order Volterra kernel and L it's the memory depth. As previously mentioned, the main issue of this method is on the computational complexity for the identification of Volterra kernels.

For this reason, in practical implementation some other models are implemented, in order to maintain the complexity under an acceptable level. Among the different methods, the most employed is the Memory Polynomial, that represents a simplification of Volterra in which only the diagonal terms are taken into account. In this case $l_1=l_2=\dots=l_{2k+1}=l$.

$$y(n) = \sum_{k=0}^{K-1} \sum_{l=0}^L a_{kl} * \Phi_{kl}[x(n)]$$

Where $\Phi_{kl}[x(n)] = x(n-l) * |x(n-l)|^k$

K represents the maximum order of non-linearities, L is the memory depth, so the total number of components is $K*(L+1)$.

It can be expressed even in matrix form in a very simple way $\bar{y} = \bar{X}\bar{a}$, where y represents the vector of the modelled signal, a represents the vector of coefficients and X is the matrix, formed by the basis functions.

This method is a good trade-off between complexity of calculation and accuracy of modelling. The coefficients a_{kl} can be estimated using different methods, one of the most used is least square algorithm [12]:

$$\hat{a} = (X^H * X)^{-1} * X^H y$$

2.2.3) DIRECT LEARNING ARCHITECTURE

The focus of our attention is put now on DLA, where the identification of PD is realized in two steps. The first step is the pre-identification of nonlinear model of the PA because is the main source of NL, then the second step the model of PA is used for the estimation of the PD itself. The structure can be schematized as follow:

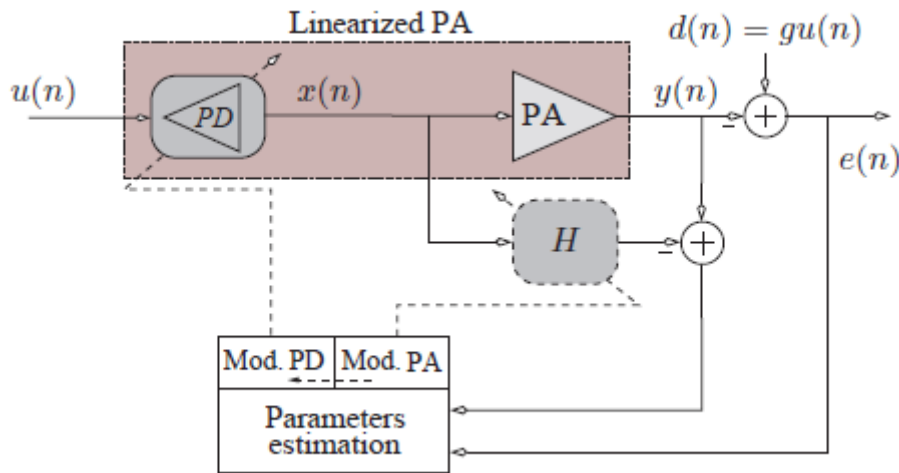


Figure 32: DLA architecture [12]

Actually, there are two different ways for the identifications of the PD [12]:

- **DLA based on analytical model:** in this procedure an analytical model is adopted to evaluate the output of the pre-distorter using MP model for power amplifier. So, $x(n)$ can be calculated as follow:

$$x(n) = \frac{1}{\sum_{k=0}^{K-1} a_{k0} * |x(n)|^k} * \left(y(n) - \sum_{k=0}^{K-1} \sum_{l=0}^L a_{kl} * \Phi_{kl}[x(n)] \right)$$

An ideal PD-PA shows an output $y(n)=g*u(n)$, where g represents the small signal gain of the PA. The main problem of this approach is that, in order to calculate $x(n)$ it's needed the value of $|x(n)|$. To solve this problem the $u(n)$ is used to calculate an approximate version of $|x(n)|$.

- **DLA based on non-linear filter architecture:** in this case, an adaptive algorithm is adopted for the evaluation of PD parameters of the power amplifier. The memory polynomial is used.

$$x(n) = \sum_{p=0}^{P-1} \sum_{m=0}^M w_{pm} * \Phi_{pm}[u(n)]$$

Where the w represents the complex coefficients of the pre-distorter.

The output of the pre-distorter is then fed into the power amplifier, and the goal is to obtain an output $y(n)$ as close as possible to the ideal output $d(n)=g*u(n)$. The error is identified as $e(n)=d(n)-y(n)$.

There exist 2 different method for the evaluation of the coefficients w :

- I. **Nonlinear filtered-x LMS algorithm:** in this case the coefficients are obtained by minimizing the mean square error function:

$$E\{|e(n)|^2\} = E\{|d(n) - y(n)|^2\}$$

The weight update is based on a gradient method:

$$w(n + 1) = w(n) - \frac{1}{2} \mu \nabla(n)$$

Where μ represents the step size and $\nabla(n)$ represents the instantaneous estimate of the gradient.

For the shake of simplicity, we omit all the intermediate step that are presents in [6], and report just the final results.

$$w(n + 1) = w(n) - \mu e(n) * \sum_{k=0}^K \sum_{l=0}^L \frac{k + 2}{2} a_{kl} * |x(n - l)|^k * u(n - l)$$

- II. **Nonlinear filtered-x RLS algorithm:** in this case the cost function to be minimized is composed by an exponentially weighted sum of squares errors:

$$\delta(n) = \sum_{i=1}^n \lambda^{n-1} |e(i)|^2$$

In which λ represents the exponential forgetting factor that can have a value between 0 and 1. In order to obtain the minimum of the function, a derivative

operation is realized. As before all the intermediate steps are omitted but are presents in [6].

The final result is:

$$w(n + 1) = w(n) + \mu e * (n)k(n)$$

Where k(n) is

$$k(n) = \frac{\lambda^{-1}P(n - 1)\varphi^*(n)}{1 + \lambda^{-1}\varphi^H(n) * P(n - 1)\varphi(n)}$$

Another important aspect to be consider is that in case of additive white gaussian noise (AWGN) the DLA architecture is more robust compared with ILA.

2.2.4) INDIRECT LEARNING ARCHITECTURE

This case represents the one adopted as our final solution and can be schematized as follow:

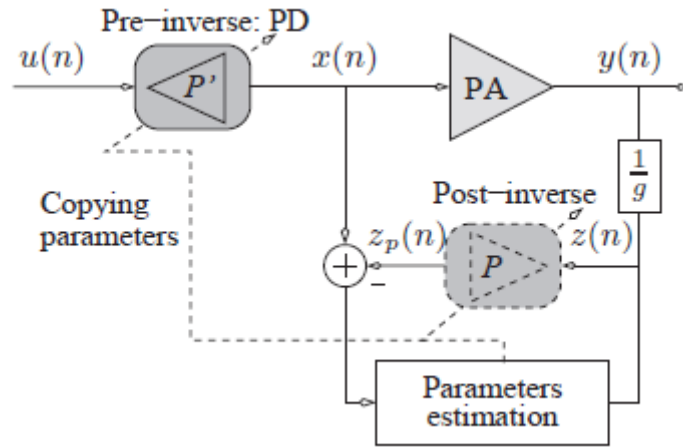


Figure 33: ILA architecture [12].

In this case the identification is realized in a single step. A post-inverse of the PA is first extracted and then used as pre-distorter [12]:

$$z_p(n) = \sum_{p=0}^{P-1} \sum_{m=0}^M c_{pm} * \Phi_{pm}[z(n)]$$

Where the variable $z(n)=y(n)/G$ is used as the input of the post-inverter.

As the previous solution needs an iterative procedure and after three or four iterations it converge to its final solution and ideally, we should have $z_p(n)=x(n)$.

As we have already seen, it is possible to formulate the problem in matrix form as follow:
 $z_p = Zc$.

Where Z is the matrix of the basis function, c the vector of coefficients we want to estimate and z_p the signal going out from the post-distorter. The estimation procedure can be done in different ways, in this dissertation the least square solution will be implemented:

$$c = (Z^H Z)^{-1} Z^H z_p$$

2.3) MODELLING OF MEMORY EFFECTS

For wideband, high varying envelope signals a memoryless model is not enough to fully describe the RoF link. Memory needs to be taken into account, in order to have an accurate design of the system.

As already mentioned, the RF power amplifiers in a wideband scenario are susceptible to the in-band and out of band distortion, causing a spectral regrowth. In the radio standard, there are some regulation on the emission out of band, in order not to disturb other systems; for this reason, it is important to find a countermeasure to this unwanted behaviour.

Current DPD implementation adopt memoryless techniques to compensate the impairments, and the instantaneous behaviour is presented by the AM/AM and AM/PM graphs. In order to exploit the potential of DPD, memory effects have to be considered since they become significant for wideband varying envelope signals [10]. The origin of these effects is due to transport delay, rapid thermal time constant and components biasing circuits that depends on the signal envelope itself. Those effects become more significant as the bandwidth increase.

In general, the memory effects of an RF transmitter are caused by thermal and electrical dispersion effects. If we consider a wideband transmitter electrical memory effects become the more significant since the thermal time constant is too large compared to the inverse of the bandwidth of the signal.

Source of electrical memory effects for the PA [10]:

- Trapping effect
- Impact ionization
- Frequency response of the PA around the central frequency f_0
- Matching condition at harmonic frequencies

- Impedance matching condition at the envelope frequency

The most significant cause of memory is the electrical memory effect generated by the variation of circuit components impedances in function of different signal modulation frequency. For wideband signal, the impedance variation can be so large that the other memory effect can be neglected and produce both long term and short terms memory effects.

The thermal effects are caused by electro-thermal couplings and increase the temperature of the transistor, modifying some electrical parameter.

The last two sources generate extra odd order intermodulation product which are very close to the main channel.

2.3.1) MEMORY STRUCTURES

We consider a basic structure of digital pre-distorter as schematized in the following figure:

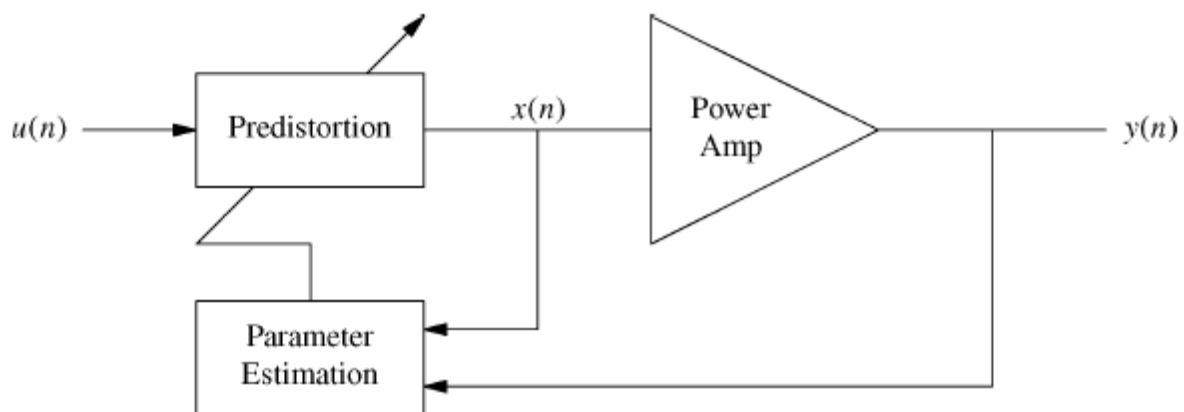


Figure 34: basic pre-distorter schematic [13].

The scope of this section is an overview on different methods for taking into account memory effects. The most general methods, study the memory effects using an M-tap memory, described though a Volterra series, that as already seen, consist in a sum of multidimensional convolutions and can be formalized as follow [13]:

$$y(n) = \sum_{k=1}^K y_k(n)$$

Where:

$$y_k(n) = \sum_{m_1=0}^{M-1} \sum_{m_2=0}^{M-1} \dots \sum_{m_k=0}^{M-1} h(m_1, m_2, \dots, m_k) \prod_{l=1}^K x(n - m_l)$$

The $y_k(n)$ represents the convolution of the input with the Volterra kernel h_k having memory length M . In order to better exploit this formulation, is useful to rewrite it in an alternative form using diagonal index variables.

$$n_l = m_l + 1 - m_l \quad l = 1, 2, 3, \dots, k - 1$$

So, we obtain:

$$y_k(n) = \sum_{n_1=-M+1}^{M-1} \sum_{n_2=-M+1}^{M-1} \dots \sum_{n_{k-1}=-M+1}^{M-1} g^{(k)}_{n_1, n_2, \dots, n_{k-1}}(n) * [x(n) \prod_{l=1}^{K-1} x(n - n_l)]$$

Where $*$ is a mono-dimensional convolution:

$$g^{(k)}_{n_1, n_2, \dots, n_{k-1}}(n) = h_k(n, n + n_1, \dots, n + n_{k-1})$$

In this alternative form the Volterra kernel h_k can be expressed as a summation of linear filter outputs, in which the output of each filter is the product of k differentially delayed input signals $x(n) \prod_{l=1}^{K-1} x(n - n_l)$

Another important simplification introduced in the alternative Volterra form, is to consider the kernels symmetric, in order to reduce the complexity of this equation.

The Volterra formulation can be adjusted in the case of signals having bandwidth small with respect to the carrier frequency. In this case the signal can be expressed using its envelope as follow:

$$x(n) = \text{Re}\{e^{j\omega_0 n} \bar{x}(n)\}$$

Then this notation is put into the previous formulation as follow:

$$[e^{j\omega_0 n} \bar{x}(n) + e^{-j\omega_0 n} \bar{x}(n)^*] * \prod_{l=1}^{k-1} [e^{j\omega_0 n} \bar{x}(n - n_l) + e^{-j\omega_0 n} \bar{x}(n - n_l)^*]$$

Our interest goes to the components close to the f_0 , so only the k odd components will be considered. For example, if we consider $k=3$, the terms to be taken into account are the listed ones plus their complex conjugate:

$$\tilde{x}(n)\tilde{x}(n - n_1)\tilde{x}^*(n - n_2)$$

$$\tilde{x}(n)\tilde{x}^*(n - n_1)\tilde{x}(n - n_2)$$

$$\tilde{x}^*(n)\tilde{x}(n - n_1)\tilde{x}(n - n_2)$$

In the same way for $k=5$ we have [13]:

$$\tilde{x}(n)\tilde{x}(n - n_1)\tilde{x}(n - n_2)\tilde{x}^*(n - n_3)\tilde{x}^*(n - n_4)$$

$$\tilde{x}(n)\tilde{x}(n - n_1)\tilde{x}^*(n - n_2)\tilde{x}(n - n_3)\tilde{x}^*(n - n_4)$$

$$\tilde{x}(n)\tilde{x}^*(n - n_1)\tilde{x}(n - n_2)\tilde{x}(n - n_3)\tilde{x}^*(n - n_4)$$

$$\tilde{x}^*(n)\tilde{x}(n - n_1)\tilde{x}(n - n_2)\tilde{x}(n - n_3)\tilde{x}^*(n - n_4)$$

$$\tilde{x}(n)\tilde{x}(n - n_1)\tilde{x}^*(n - n_2)\tilde{x}^*(n - n_3)\tilde{x}(n - n_4)$$

$$\tilde{x}(n)\tilde{x}^*(n - n_1)\tilde{x}(n - n_2)\tilde{x}^*(n - n_3)\tilde{x}(n - n_4)$$

$$\tilde{x}^*(n)\tilde{x}(n - n_1)\tilde{x}(n - n_2)\tilde{x}^*(n - n_3)\tilde{x}(n - n_4)$$

$$\tilde{x}(n)\tilde{x}^*(n - n_1)\tilde{x}^*(n - n_2)\tilde{x}(n - n_3)\tilde{x}(n - n_4)$$

$$\tilde{x}^*(n)\tilde{x}(n - n_1)\tilde{x}^*(n - n_2)\tilde{x}(n - n_3)\tilde{x}(n - n_4)$$

$$\tilde{x}^*(n)\tilde{x}^*(n - n_1)\tilde{x}(n - n_2)\tilde{x}(n - n_3)\tilde{x}(n - n_4)$$

This is the most general and complete methods but actually, in practical case, can results to a huge burden of calculation, so it is preferred to use some simplified notations derived from this general theory.

2.3.2) WIENER MODEL

The Wiener model is a simplification of Volterra, in order to decrease the burden of calculation. This model can be schematized as follow:



Figure 35: schematic of Wiener model [13].

It consists in a linear filter and a memoryless nonlinear block. The idea behind, is to exploit the first block to characterize the memory effects, and the second for the nonlinearities.

The first block is a linear autoregressive moving average filter that model the memory effects. The second block is a conventional Bessel series model that characterize the memoryless nonlinearity [10,13].

The Volterra kernel becomes:

$$h_k(m_1, m_2, \dots, m_k) = a_k h(m_1) \dots h(m_k) \quad k = 1, 2, 3 \dots K$$

a_k are the polynomial coefficients related to the nonlinearity.

Finally, the output of the Wiener model can be formalized as follow:

$$y_W(n) = \sum_{k=1}^K a_k \left[\sum_{m=0}^{M-1} h(m)x(n-m) \right]^k$$

This model is powerful since it is one of the simplest ways to combine nonlinearities and memory effects but, actually, its effectiveness for PA modelling is limited. The main issue is the dependence of the output on the coefficients $h(m)$ is non-linear and this makes the estimation complex.

2.3.3) MEMORY POLYNOMIAL

The idea behind the memory polynomial is a generalization of the Hammerstein model in which, it is chosen different filters for each different order k . This model is particularly important for this dissertation since it is the method adopted in our analysis, with the possibility to extend it in the general memory polynomial, a more complete and accurate analysis, but also more complex from a calculation point of view [13].

So, combining the different filter and power series, we can formulate the generalized Hammerstein model as follow:

$$y_{GH}(n) = \sum_{k=1}^K \sum_{m=0}^{M-1} a_{km} x^k(n-m)$$

In the narrowband case we can formulate it in the classical form as already seen:

$$y_{MP} = \sum_{k=0}^K \sum_{m=0}^{M-1} a_{km} x(n-m) |x(n-m)|^k$$

This method represents the best trade-off between accuracy and complexity, and it is a very powerful tool for the design of RF power amplifier.

2.3.4) GENERALIZED MEMORY POLYNOMIAL

This method is more complete than the classical memory polynomial since introduces also the cross terms. It represents basically the link between Volterra and MP; the complexity increase respect to the memory polynomial, but it is not as heavy as Volterra and can handle stronger nonlinearities than MP [13].

The formulation of the GMP is quite similar to the MP but, include also the cross terms as follow:

$$\begin{aligned}
 y_{GMP} = & \sum_{k=0}^{Ka-1} \sum_{l=0}^{La-1} a_{kl} x(n-l) |x(n-l)|^k \\
 & + \sum_{k=1}^{Kb} \sum_{l=0}^{Lb-1} \sum_{m=1}^{Mb} b_{klm} x(n-l) |x(n-l-m)|^k \\
 & + \sum_{k=1}^{Kc} \sum_{l=0}^{Lc-1} \sum_{m=1}^{Mc} c_{klm} x(n-l) |x(n-l+m)|^k
 \end{aligned}$$

In this formulation we can denote three terms. The first one is the aligned signal and the envelope, corresponding to the one of the classical memory polynomial.

The second term represents the signal and the lagging envelope, while the third term represents the signal and the leading envelope.

The big advantage is that the coefficients are in linear form so they can be simply estimated using for instance the least-square algorithm. This means that the computational burden is taken under control.

2.3.5) COMPUTATIONAL COMPLEXITY

The models just analysed has different level of complexity and accuracy. More sophisticated models are more effective in terms of reducing the spectral regrowth but the price to pay is in term of computational complexity. As general rule of thumb the performance increase as the number of coefficients in the model increase up to a certain limit, where a steady situation is reached.

2.4) ESTIMATION ALGORITHMS

The estimation of the model coefficients is one of the most delicate and important steps in the predistortion analysis. In general, the most employed are the least-square type algorithm for the

estimation procedure. There are a lot of this least-square methods but have the same concept behind [13].

The easiest way to handle this problem is to collect the coefficients a_{kl} , b_{klm} , c_{klm} into one vector having size $J \times 1$, called w .

Every component in w , is associated with a signal sampled over some period $n=1,2\dots N$, and all the values are collected into a vector.

For instance, if we consider the coefficients a_{31} is associated to the signal $x(n-1)|x(n-1)|^3$ and its time samples generates a vector $N \times 1$.

The same kind of analysis is repeated for all J elements of the coefficients vector and assembled into one matrix X having dimensions $N \times J$.

At this point the problem can be formulated in matrix form as follow:

$$\bar{y} = \bar{X}\bar{w}$$

Where y is a $N \times 1$ vector that basically represents the estimate of the output vector y .

In case of inverse modelling method, the same formulation is employed but x and y are swiped as follow:

$$\bar{x} = \bar{Y}\bar{w}$$

The estimation procedure is never perfect, and an error vector must be considered for the sake of completeness. The error vector is defined as follow:

$$e(n) = x_{\text{REAL SIGNAL}}(n) - x(n)$$

Or in analogue way in matrix form

$$e = x - \bar{x}$$

Now the goal is to minimize the $\|e\|^2$ so using least-square algorithm the coefficients vector can be formulate as follow:

$$w = (Y^H Y)^{-1} Y^H x$$

The evaluation of the w vector can be easily done in matlab and the complexity is $O(J^2)/\text{sample}$ where J is the dimension of the coefficients w .

In the inverse matrix evaluation $(Y^HY)^{-1}$, having dimensions $J \times J$, there are some problems to deal with for the conditioning of the matrix. In fact, considering a simple case of MP, the chosen of coefficients K and M related to the non-linearity order and memory order become a fundamental step, since it influences the dimension of the matrix Y . If, for instance, we choose K and M values larger than what they should, the matrix will be ill-conditioned, and the algorithm stop to work. This problem puts the attention on the sizing of the MP, in order to fully exploit this algorithm.

In the field of numerical analysis, the condition number measures how much the output value of the function can change for a small change in the input.

The condition number is used to measure how sensitive a function is to changes or error in the input and how is the results output. In general, a problem with a low condition number is said to be well-conditioned, instead if condition number is high it is said to be ill-conditioned. From a non-mathematical point of view an ill-conditioned problem is characterized by a large change in the output for a small change in the input. This means that the correct solution is very hard to find.

In order to reach a more stable situation, a variant of the algorithm is adopted to partially update w from the precedent estimation procedure, and this induce continuity in the estimation process.

This process is called damped Newton algorithm and it can be formulated as follow [13]:

$$w_{p+1} = w_p + \mu(Y^HY)^{-1}YH_e$$

In this formula μ represents the relaxation constant. It is easy to understand that if $\mu = 1$ and $w_0=0$, the algorithm converges to the least-square algorithm.

In the case of $\mu < 1$ there is a limit on how w can change between two subsequent iterations, so memory is induced in the process. This solution is more robust and generally drive the solution that minimize the average error.

There are some other methods, for instance the stochastic gradients algorithms like least mean-square algorithm that reduce the complexity in the problem having $O(J)/sample$. Anyway, in general predistortion application, high order NL terms are always small and this drives to an ill-conditioned situation. Those kinds of algorithms are simpler but has slow convergence and usually are not employed in practical case.

Another popular algorithm is the recursive least-squares algorithm, but the complexity is $(J^2)/sample$. Some variation of this algorithm exists in order to reduce the complexity but as before presents the problem of ill-conditioned matrix.

2.5) MATLAB MODEL

For the realization of a model such as ILA applying memory polynomial, a Matlab program has been developed. The final goal of the designed system is to adjust the input signal, in order to increase the linear behaviour. The idea, is to characterize the RoF link into the simulation, evaluating the post-distorter coefficients and then copying it on the pre-distorter side. This way the cascade of pre-distorter + RoF link assume a linear behaviour as will be observed through AM/AM and AM/PM curves.

The program can be disassembled into a cascade of blocks, each one performs an operation that at the end, produce the final result of improving the linearity of the system. An LTE signal at the 800s MHz operating band, having a band of 20 MHz, will be used for the characterization since it represents a common applicative situation, for instance as a mobile front haul in the 4G infrastructure.

In this first simulation on matlab, the input and output signal measurements are imported from a previous set of measures from the Esiee Paris University.

Now the focus is on the blocks of the matlab program:

1. **Front run:** define the path into the PC for the program and sets some variables for the spectral evaluation of the signals.
2. **Get stimulus:** in this section of the program are defined the sampling frequency, the bandwidth, and the offset. Then the input and output data of the LTE signal measurements are imported and, a plot of the input signal is created to check if everything is working properly.
3. **Get PA model and setup:** in this section the wiener model is loaded and a first AM/AM, AM/PM representation of the input and output signal is plotted as follow:

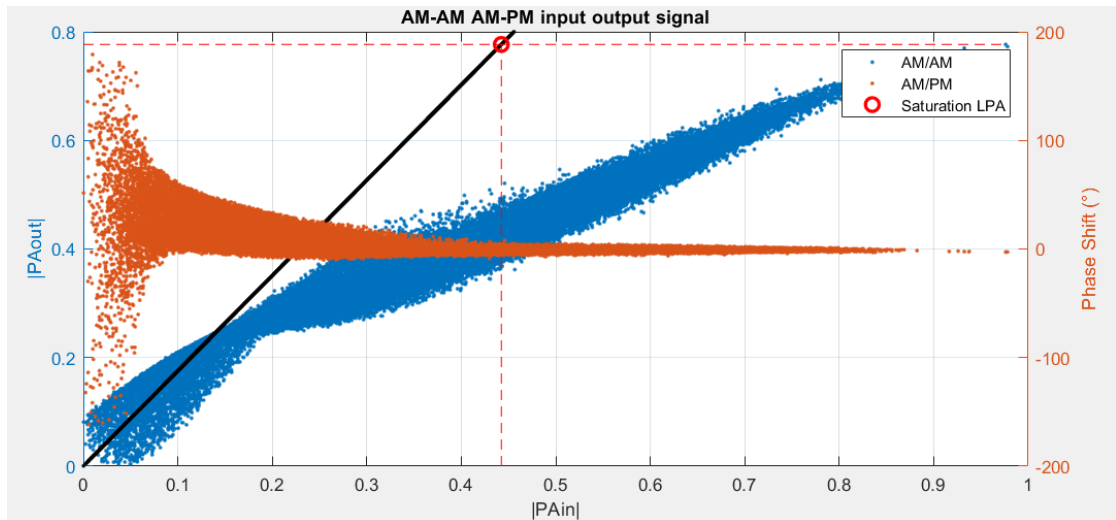


Figure 36: AM/AM AM/PM plots of input and output signal imported in the matlab environment.

4. **Set Feedback path Noise:** in this section is defined the SNR value and a string that can be 'on' or 'off' in order to enable or disable the presence of noise in the system.
5. **Initial ACPR:** in this section are evaluated the ACPR in an out, and the power spectral density in and out using a function called `acpr`.

The ACPRin and out are structure having 6 fields inside:

- Bandwidth.
 - Offset.
 - U1: it is the ACPR in the first upper adjacent window.
 - L1: the same as before for the first lower adjacent channel.
 - U2: it is the ACPR in the second upper adjacent channel.
 - L2: the same as before for the second lower adjacent channel.
6. **Defining pre-distorter structure:** in this section it is created the structure of the pre-distorter itself and a structure PD is created defining the number of branches, number of stage and number of iterations.
 7. **Model of branch 1:** In our structure we only have one branch and one stage to define. It is an important aspect to set properly the coefficients for the nonlinearity order and memory order. Note that the program is configured to be extended to the generalized memory polynomial but, in our work, only the memory polynomial will be considered.

The function `nbcoeffgmp` inside this section, is just for counting the number of coefficients. For example, if we consider k from 0 to 5 and Q from 0 to 1, the number of coefficients will be 12. The initial situation is with all the coefficients equal to zero

except the first that is set to 1. At each iteration, the coefficients will be estimated and updated.

8. **System iteration parameters:** in this section are defined some parameters of working of the system as the step, that represents the number of samples for each iteration, and the structure stimulus containing Pain, Fs and the ACPR is instantiated.
9. **Algorithm settings:** in this section there are only some working setting as the mu coefficients for the damped newton algorithm.
10. **Actual DPD processing:** this part is the core of the code and it will be analysed with particular attention.

The most important part of the code is hidden inside the function `dpdTest`:

```
function SystIter = dpdsbd(Stimulus, PA, ACPRout, ...  
    Algorithm, PD, Noise, SpectrumObject, PAout)
```

The input arguments are:

- Structure Stimulus, having inside Wf (waveform), sampling frequency and a structure ACPR having the fields band and offset inside.
- Structure PA, it is a large structure with a lot of fields inside, among them the most important are Model and G (linear gain).
- ACPRout, this field is used as reference to evaluate the improvement in the ACPR with respect to the starting situation.
- Algorithm: this structure contains some working parameters like the number of iterations, etc...
- PD, it is the pre-distorter model.
- Noise, containing the SNR value and the enable string.
- SpectrumObject, containing some parameters for the spectral evaluation.

The output is a structure `systIter` with a lot of field inside, that will be our output of the system and will be used for the improvement analysis.

This function is very big and complex and can be split in blocks for the shake of simplicity:

a) **Post distorter setting:**

In this section some variables are instantiated from the variable passed in the function `systIter`, in order to manipulate them in the next sections.

b) Central core:

Here the procedure starts initializing the nested loop. The input signal is assigned to the u and x is evaluated through the memory polynomial method.

Then an AM/AM, AM/PM representation, considering u as input and x as output, is plotted. Now, the attention is focus on the gmp function:

2.5.1) GMP FUNCTION

```
function y = gmp(x, Model)
```

This function is a matlab formulation of the previous dissertation about the memory polynomial and generalized memory polynomial. The model is divided into three separate sections:

- I. Memory polynomial.
- II. Signal and lagging envelope term.
- III. Signal and leading envelope term.

Note that inside Model, there is a field called Symmetric that in our case is set to 'on'. This means that the second and third sections regarding respectively the lagging and leading envelope part share the same coefficients in the GMP model.

```
A1=[];  
for k=1:length(Kav)  
    for l=1:length(Lav)  
        cv=zeros(Lav(l),1) ; x(1:end-Lav(l));  
        A1= [A1 cv.*(abs(cv).^ (Kav(k)))]; %#ok<*AGROW>  
    end  
end
```

Here there is a small fragment of the code that shows how the model is built, composed by a sum of various terms inside its range of nonlinearity and memory.

The matrix A1 generated at the end of the procedure has the same number of rows as the length of the input stream and the number of columns corresponds to the number of coefficients in the model, 12 in this specific case.

In order to extend this formulation for the generalized MP, the same analysis on the leading and lagging envelop has to be done, at the end the modelled y will be built as follow:

```
A=[A1 A2 A3];  
  
y=A*av;
```

2.5.2) SIMULATION OF RoF SYSTEM

At this point, we have found out the x using the MP model on the input u , so we proceed evaluating y through the wiener function.

```
y=wiener(x, PA.Model);
```

This function simply extracts the FIR coefficients from the model loaded at section 3 and the input signal. Inside this function there are the filtering and the saleh procedure. Y is just evaluated using the filter function in matlab, where h represents the numerator coefficients, l the denominator coefficients and x is the input signal. The function saleh add the memoryless nonlinearity to the model, so basically takes as input the y just evaluated and add the NL, using the coefficients presents in the same structure from where the coefficients of the FIR were extracted. This way we can simulate the presence of a RoF link in our simulation environment. The RoF link that simulate the cascade amplifier + optical link presents a characteristic as follow:

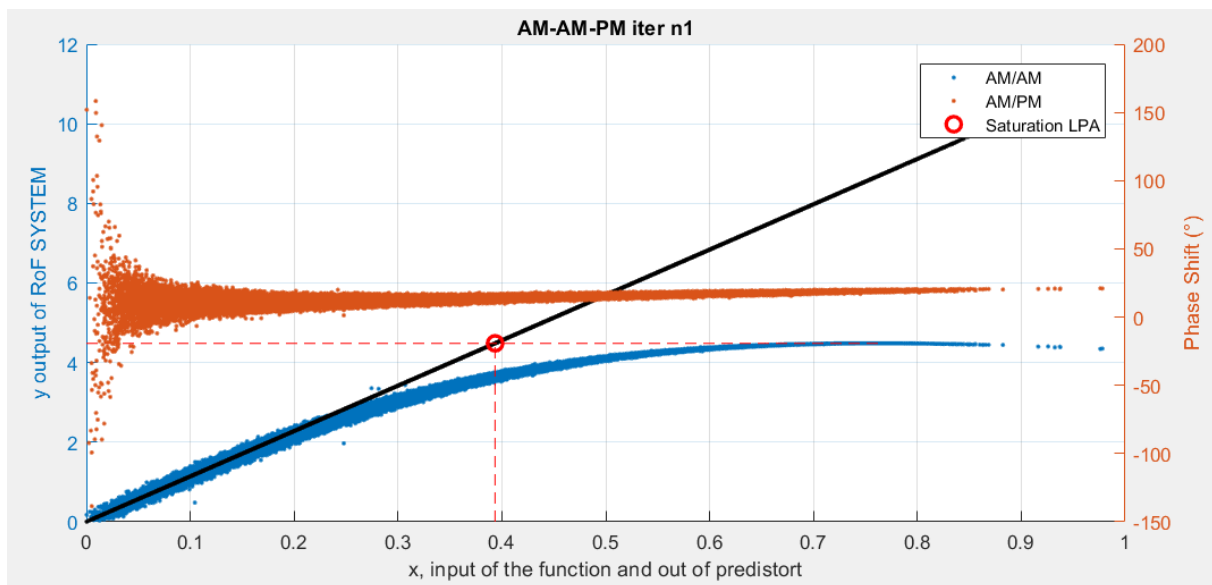


Figure 37:AM/AM AM/PM graph of the RoF simulated link introducing the NL and memory effects.

Once we have generated the y signal, the classical ILA procedure starts so, a signal z is generated dividing the signal y for the gain of the link $\rightarrow z=y/G$

At this point the AWGN noise is added to the z signal, if inside the structure noise, is present the enable in 'on' configuration.

Once the y and z are found the system is complete and the procedure can start. The system put into analysis correspond to the ILA structure as already seen:

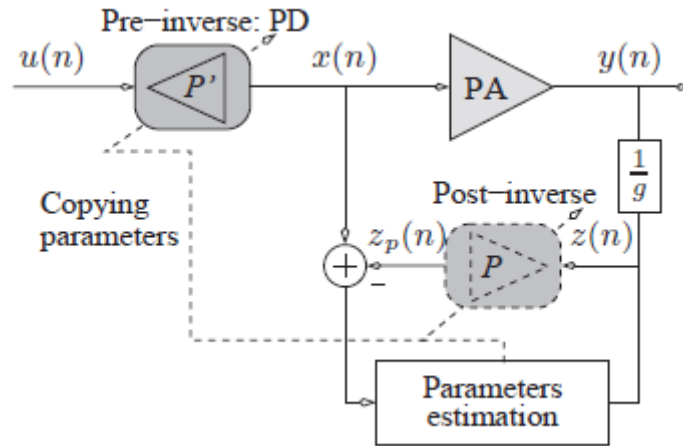


Figure 38: ILA structure adopted in the procedure [12].

As we can see in the code, the signal y is obtained normalizing with respect to the channel gain to obtain z , that is the input of the post-distorter. In order to check how the system is working, an AM/AM, AM/PM representation is plotted.

2.5.3) POST AND PREDISTORTER OPERATION

At this point the procedure already seen, the algorithm starts with the evaluation of the post-distorter and its coefficients are then copied into the pre-distorter. The system converges to the situation where x is equal to z_p . The signal z_p is generated using the `gmp` function, with the signal z as input.

The first operation realized by this section of code, is the evaluation of NMSE using the signals x and z_p , representing respectively the outputs of the pre, and post distorters. The value obtained is set as a field of the `sysIter` structure, that at the end will be the output of the `dpdTest` function.

Once NMSE is evaluated, a structure `Data` is created with z , representing the input data and the x as output. This is realized because the parameters estimation is realized with those signals. Then the function `gmpidentifier` is called, to evaluate the coefficients of the memory polynomial, but as the `gmp` function, can be extended to the GMP model. An important aspect to handle is the sizing of the MP, since a wrong coefficients configuration will cause an ill-conditioned matrix and the procedure does not work. The output of this function is the coefficients vector, evaluated using the least-square algorithm. Once the coefficients have been evaluated, they are copied into the pre-distorter model, then the damped newton procedure starts in order to introduce some continuities in the coefficients vector.

At each iteration, some AM/AM AM/PM graph are extracted to check the evolution of the procedure. For each iteration, the results obtained are placed inside the systIter(n) structure, to track the progression of the algorithm.

2.5.4) DATA POST-PROCESSING FIGURE

At this point in the program a graphical representation of the spectra, ACPR and NMSE is realized, in order to check how the performance has changed during the iterations. For the convergence we have choose four iterations since, usually, this kind of system takes three iteration for its stabilization.

For example, in the case of SNR=25 dB the results we reach after four iterations are as follow:

- **Initial**

AM/AM-AM/PM:

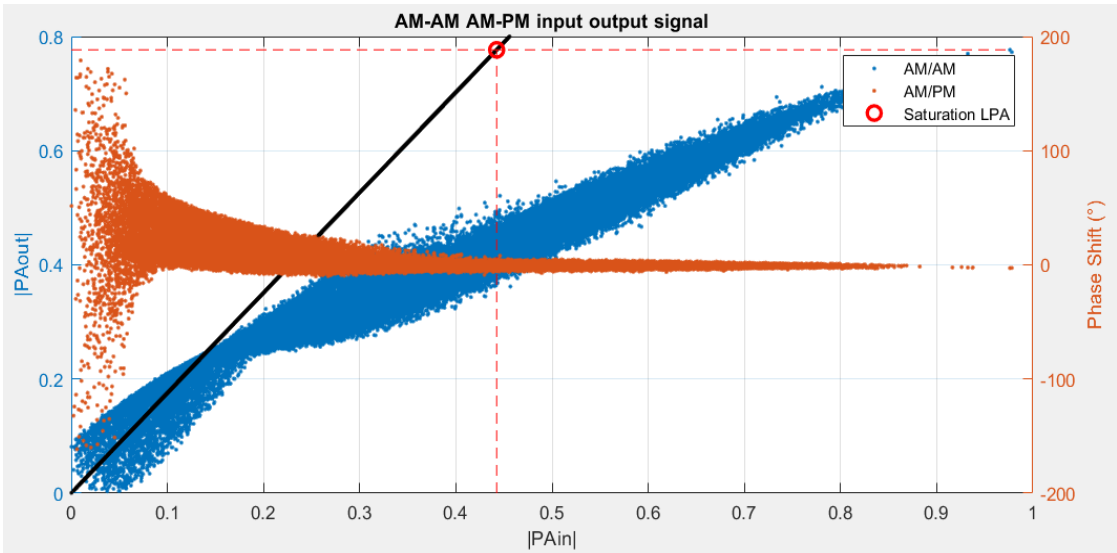


Figure 39: starting AM/AM AM/PM graph.

- **Final**

AM/AM-AM/PM:

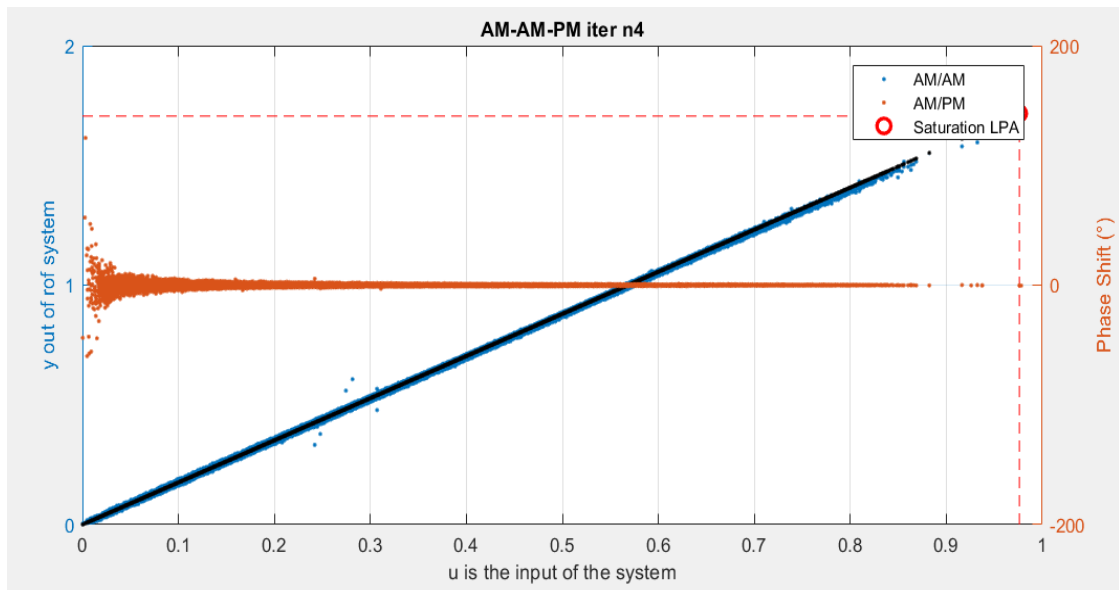


Figure 40: AM/AM AM/PM of the linearized system.

- **Spectra evolution:**

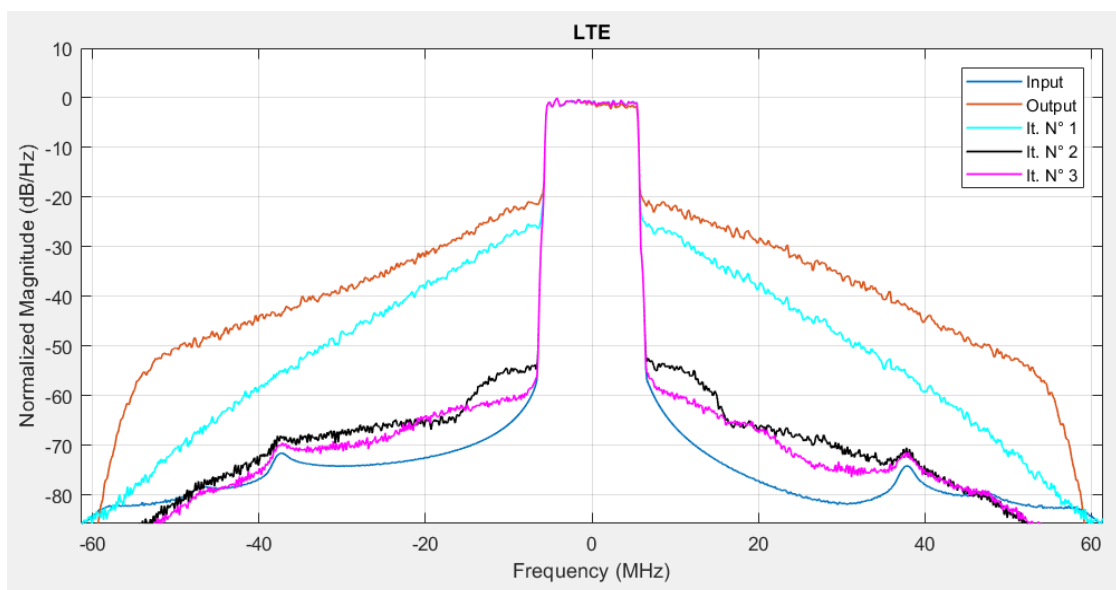


Figure 41: spectra evolution iteration per iteration.

- **ACPR evolution:**

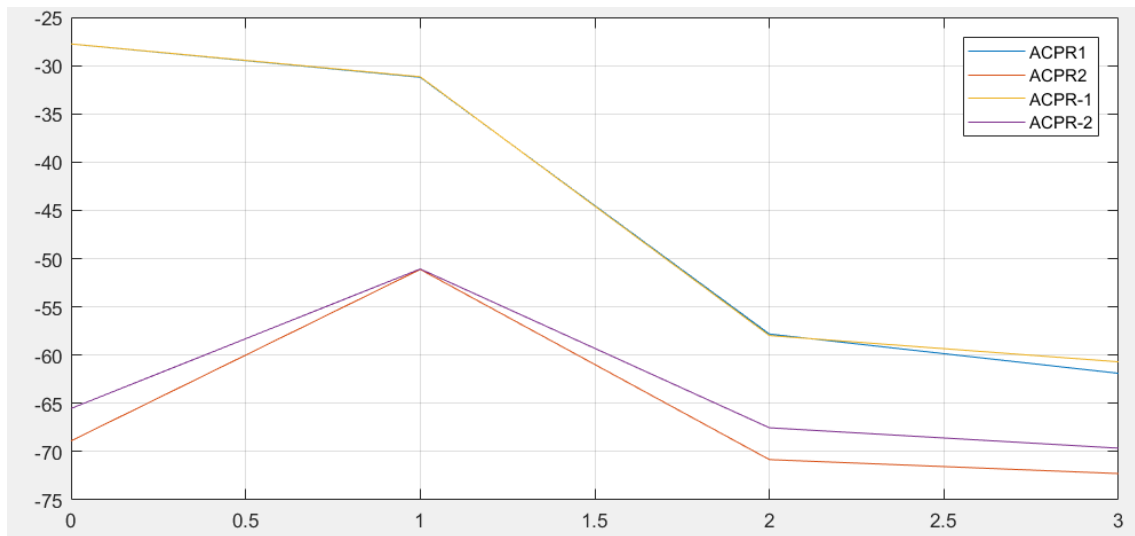


Figure 42: ACPR improvement.

- **NMSE evolution:**

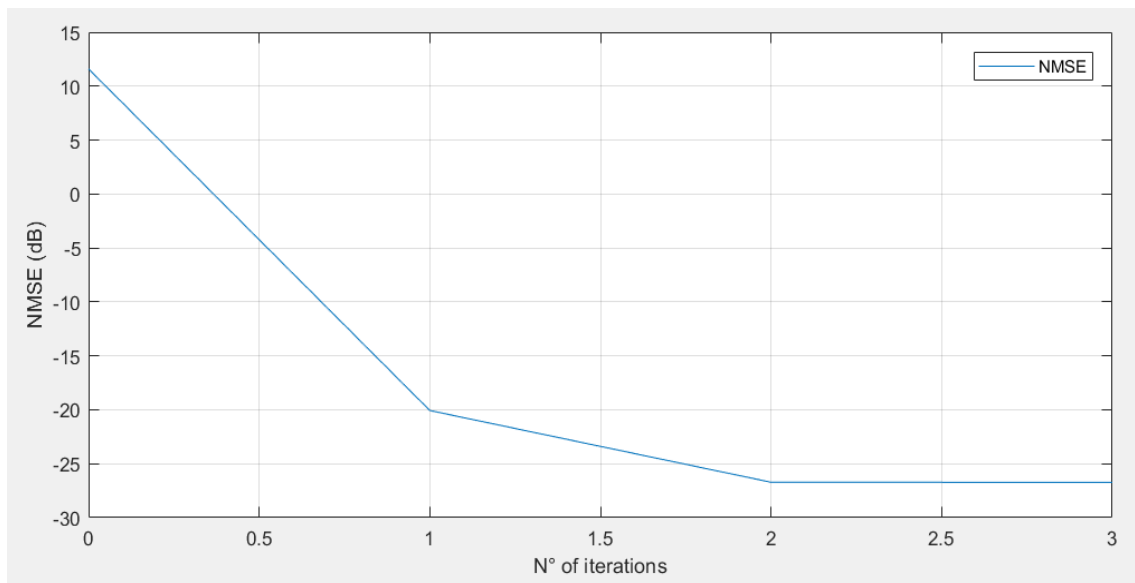


Figure 43: NMSE progression.

CHAPTER 3: REALIZATION OF THE FINAL SYSTEM

The final goal of this dissertation is the realization of a feedback loop, implementing the predistortion algorithm just analysed. In the first chapter we have focus our attention on the filtering capability of the coupler 50-50,90-10 and 99-01. The most suitable solution is represented by the coupler 50-50 because, in the feedback path, have a sufficient amount of power, to exploit the predistortion algorithm. The other two configurations have less power on the feedback via and this, can raise some problems during the algorithm. In the second chapter, we applied predistortion to a fixed input and output sequence that has just been imported on matlab but, for our final application, we want to realize a system working on a generic LTE signal. In order to realize this, we have merged the previous matlab program with another one that produces sequence of LTE frame randomly generated. The improvements will be measured, as usual, by the EVM, NMSE, ACPR and spectral regrowth reduction.

3.1) LTE FRAME GENERATOR

The program that generates the LTE frame has been developed by Francesco Pizzuti and has been merged with the predistortion program so, we do not use the imported signal anymore. In order to realize it, a deep study of the LTE standard has been realized in order to recreate the same kind of frame of a real network.

Principal features introduced by LTE [15]:

- OFDM/OFMDA for downlink
- SC-FDMA (single carrier FDMA) for uplink
- MIMO (multiple input- multiple output)
- CA (carrier aggregation): it allows to concatenate different bands, to obtain a flexible band allocation system.
- Improvement of spectral efficiency and network efficiency.
- Reduction of power consumption by terminal
- Improved mobility

It operates in different bandwidths:

- 800 MHz
- 900 MHz
- 1800 MHz

- 2600 MHz

LTE standard has to satisfy some requirements:

- Improvement in throughput for Downlink (more than 3 Gbit/s) and for Uplink (more than 500 Mbit/s)
- Flexible bandwidth allocation → 1,4 / 3 / 5 / 10 / 15 / 20 MHz
- Low latency (less than 5 ms)
- Mobility up to 500 Km/h

3.1.1) OFDM/OFDMA

The OFDM is a modulation format in which, all the subcarriers, are orthogonal each other and allow to communicate even for very bad channel conditions.

The data transmission suffers a lot by multipath fading in radio mobile channel since the RX will see a sequence of signals with different delay and attenuation.

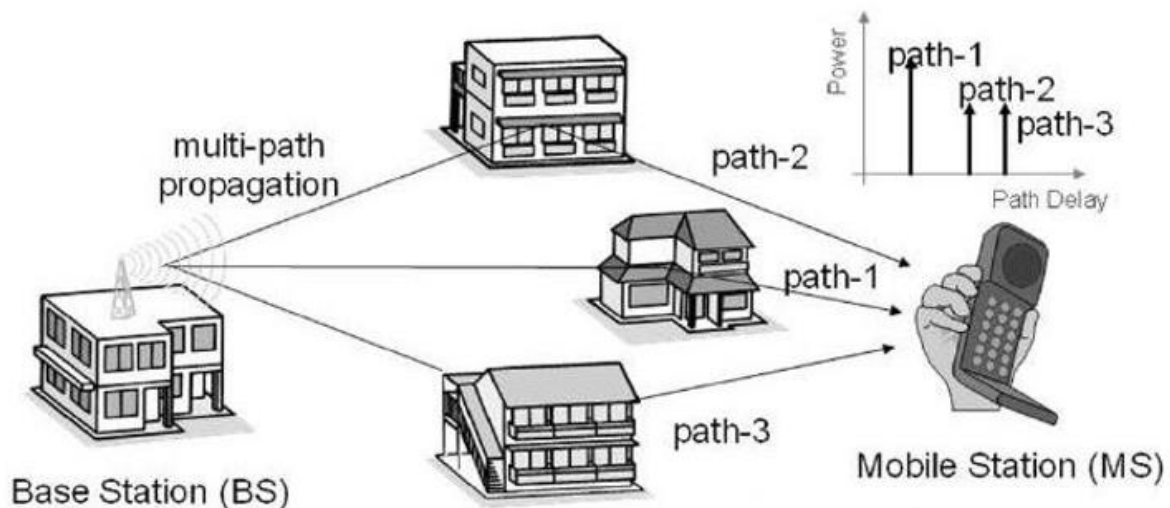


Figure 44: example of propagation in presence of multipath. [15]

The high-speed transmissions are limited by the Inter-symbol interference (ISI) but actually, this effect, can be neglected if the propagation delay is much lower than the duration of the transmitted symbols. Instead, if the duration of symbol is less than the maximal dispersion in the channel the performance deteriorates.

OFDM solve this problem splitting the flux of data into N parallel flux modulated onto different subcarrier separated by a Δf .

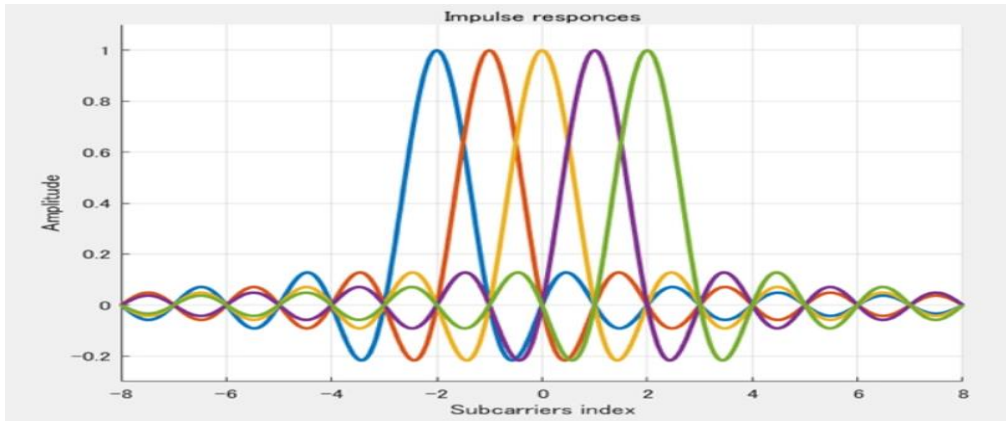


Figure 45: example of OFDM modulation format with orthogonal subcarrier.[15]

Each OFDM symbol is preceded by a cyclic prefix that is a replica of the final part of the symbol itself, and has the scope of reducing ISI at receiver.

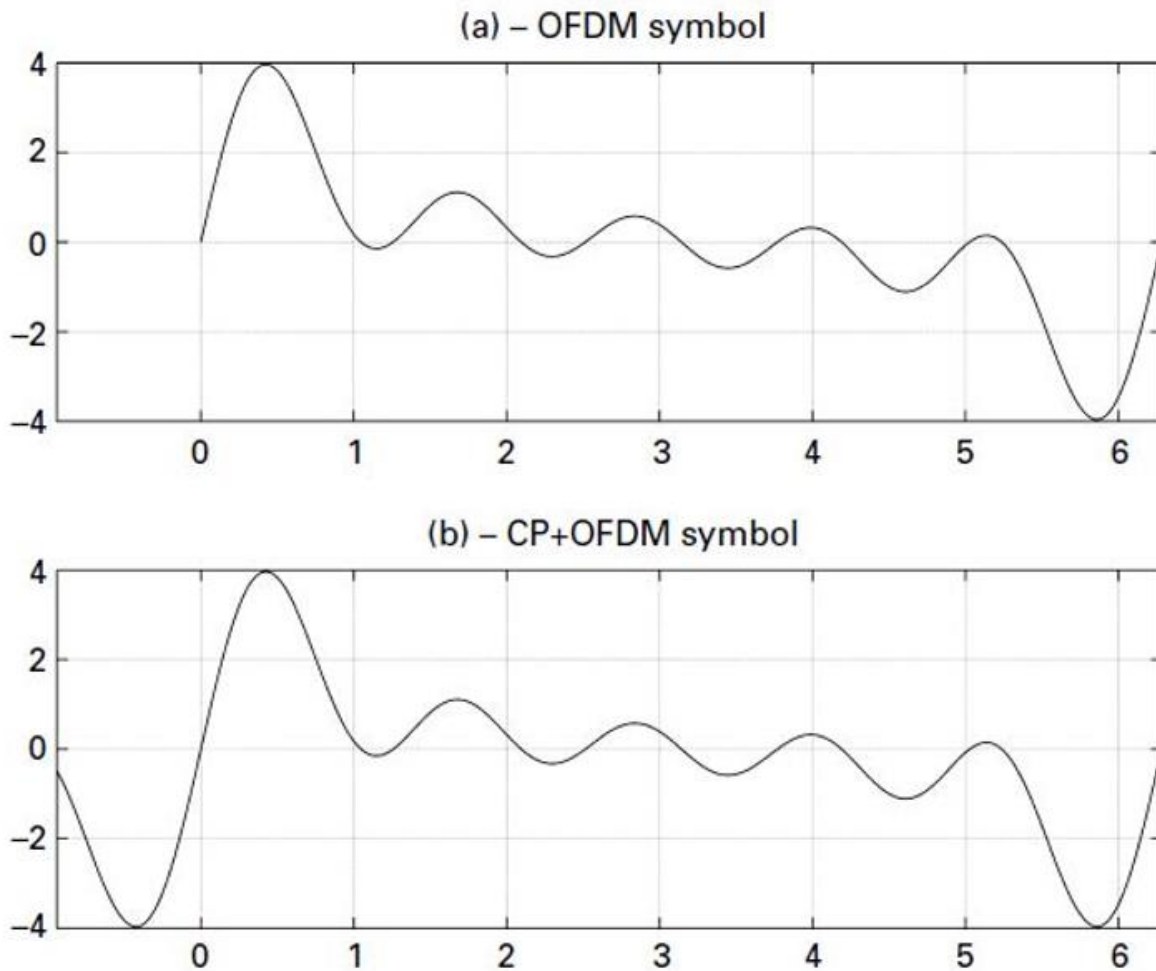


Figure 46: example of application of cyclic prefix [15].

OFDM is resilient to multipath and simplify the architecture of transmitter and receiver anyway it presents some important issue [15]:

- High PAPR requires an elevate dynamic range at amplifier and this reduce the efficiency of the PA itself.
- Instability in frequency since the orthogonality require high synchronization level between the local frequency at receiver and transmitter.

In downlink the OFDMA is adopted and represents just an application of OFDM for a multiple access system. as follow.

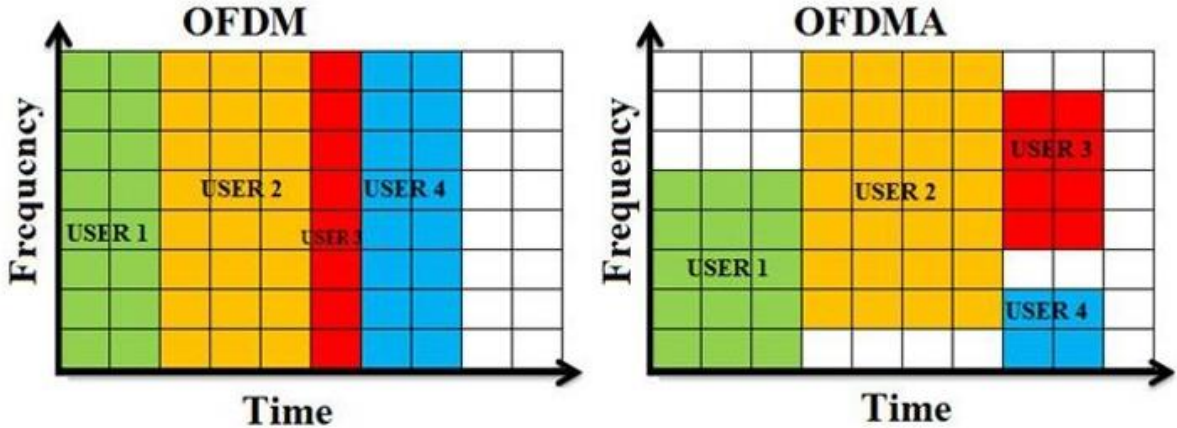


Figure 47: difference between OFDM and OFDMA [15].

In OFDMA each user is assigned to a subset of carrier for a certain amount of time, so it represents a combination of OFDM modulation and TDMA multiple access.

3.1.2) FRAME FORMAT

There exist different formats of frame:

1. FDD (freq. division duplex), the most used
2. TDD (time division duplex)
3. LAA (licensed assisted access)

Example of type 1 frame:

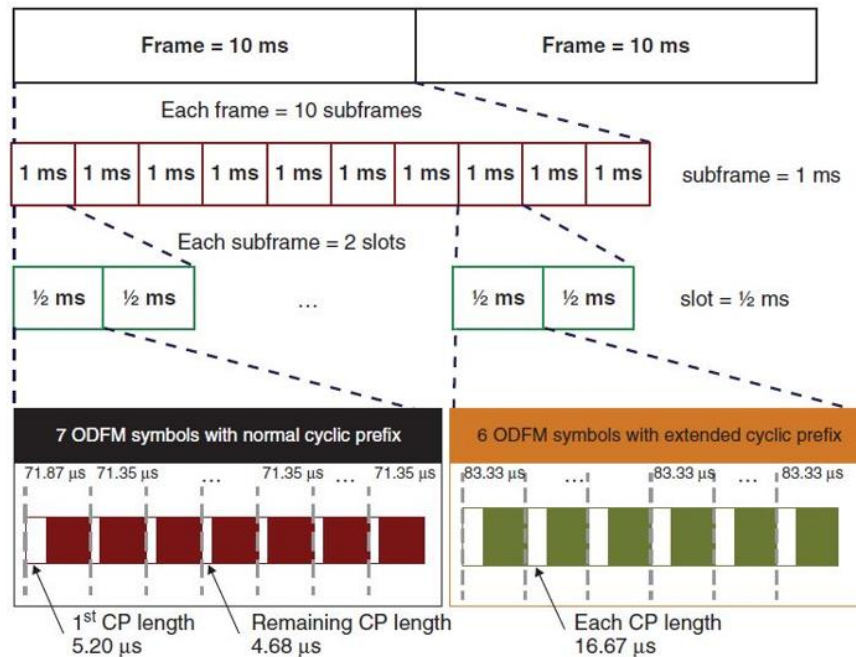


Figure 48: LTE frame structure of type 1.[15]

3.1.3) ALLOCATION BANDWIDTH

The allocation is flexible:

- 1,4 MHz: 12 sub.c. x 6 RB (resource block, that presents the smallest amount of resources that the network can allocate) = 72 sub.c.
- 3 MHz: 12 x 15 RB = 180 sub.c
- 5 MHz: 12 x 25 = 300 sub.c.
- 10 MHz: 12 x 50 = 600 sub.c.
- 15 MHz: 12 x 75 = 900 sub.c
- 20 MHz: 12x 100 = 1200 sub.c

	Bandwidth (MHz)					
	1.4	3	5	10	15	20
Frame Duration	10 (ms)					
Subframe Duration	1 (ms)					
Sub-carrier Spacing	15 (KHz)					
N. of sub-carriers in Resource Blocks	12					
N. of slots for subframe	2					
Sampling Frequency (MHz)	1.92	3.84	7.68	15.36	23.04	30.72
FFT Size	128	256	512	1024	1536	2048
Occupied Sub-carriers + DC	72+1	180+1	300+1	600+1	900+1	1200+1
Guard Sub-carriers	52	105	211	423	635	847
N. of Resource Blocks	6	15	25	50	75	100
Transmission Bandwidth (MHz)	1.095	2.715	4.515	9.015	13.515	18.015
OFDM Symbol for slots	7 (normal cyclic prefix)					
Samples for slots	960	1920	3840	7680	11520	15360
Samples for frame	19200	38400	76800	153600	230400	307200
Length (normal CP)	5.21 (first symbol) / 4.69 (six following symbols)					
Length samples (normal CP), first symbol / six following symbols	10/9	20/18	40/36	80/72	120/108	160/144

Figure 49: this tab shows the characteristic of each bandwidth size in LTE. [15]

3.1.4) PHYSICAL CHANNEL

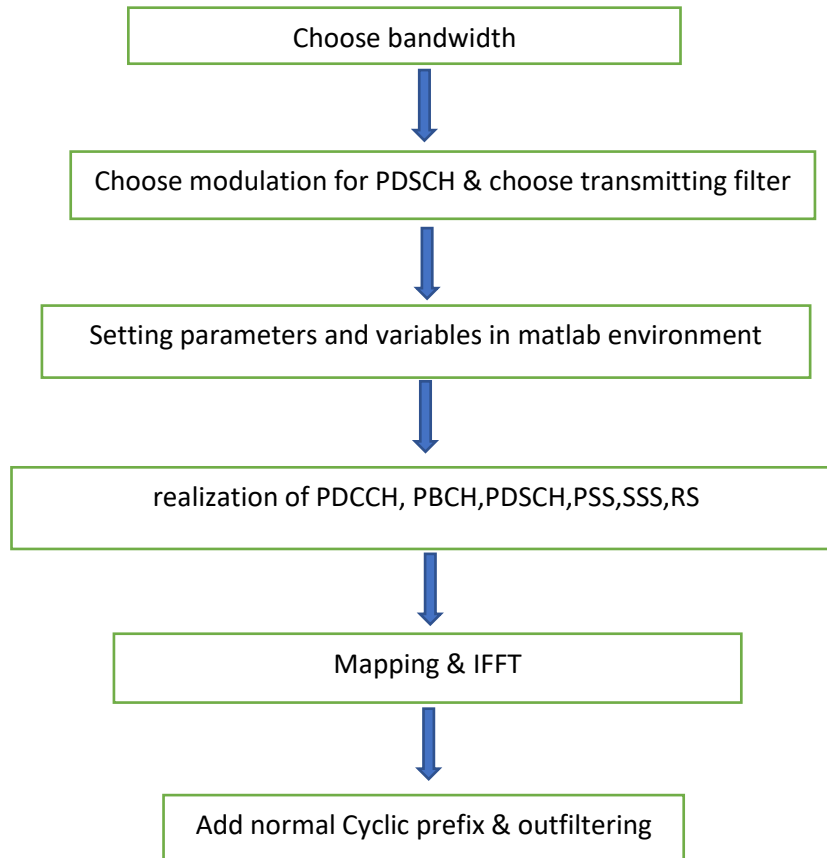
- **PDSCH** (physical downlink shared channel): used for data traffic, can support different modulations (QPSK,16QAM,64QAM,256QAM)
- **PBCH** (physical broadcast channel): sends info in broadcast to all the terminals in the network. Support QPSK and send info like the cell identification and the bandwidth.
- **PDCCH** (physical downlink control channel): it transports info about the frame format and modulation scheme used at receiver. Support QPSK.

3.1.5) PHYSICAL SIGNAL

- **Reference signals (RS):** it is a signal used by mobile terminal for the channel estimation procedure. These signals are mapped on a specific place into the time/frequency grid of the signal. The sequence transmitted is known at receiver.
- **Synchronization signal (SS):** the LTE standard has two synchronization signals used by terminals to obtain the cell identifier and the frame temporization.
PSS (primary synchronization signal) is used for a slot level synchronization.
SSS (secondary synchronization signal) is used for the frame synchronization.

3.2) TRANSMITTER LTE

The matlab program that generates the LTE frame, is composed by a transmitter and a receiver part. As regard the transmitting procedure we can split as follow:



At the beginning of the procedure the bandwidth is chosen among the set of BWs already presented, then the modulation format is chosen for the PDSCH channel.

At this point the physical channel and signal have to be realized using some matlab function created ad hoc, following the LTE standard.

PHYSICAL CHANNEL
[dataMod_PDSCH]=PDSCH(numBit,Nc,nRNTI,N-symb,n-slot,N-ID-cell,bit-for-symbol,Selecting-Modulation)
[dataMod-PDCH-simb-0, dataMod-PDCH-simb-1, dataMod-PDCH-simb-2, dataMod-PDCH-simb-3]=PBCH(N-ID-cell,Nc);
[dataMod-PDCCH]=PDCCH(N-rb,R-sc,n-slot,N-ID-cell,Nc)

PHYSICAL SIGNAL
[PSS]=Primary-Synchronization-Signal(Nid-2)
[SSS-sub-0, SSS-sub-5]=Secondary-Synchronization-Signal(Nid-1,Nid-2)
[RS]=Reference-Signal(N-rb,N-ID-cell,Nc)

At this point it's necessary to map those signals into a time/frequency grid as follow:

LTE - Mapping to resource elements

```
[ Resource_Grid ] =
Mapping(Selecting_Channel_bandwidth,N_symb,n_slot,dataMod_PDSCH,da
taMod_PDCCH,PSS,SSS_sub_0,SSS_sub_5,dataMod_PBCH_simb_0,dataMod_
PBCH_simb_1,dataMod_PBCH_simb_2,dataMod_PBCH_simb_3,RS );
```

The mapping function will allocate all the signals just seen in the following order, as the LTE standard requires:

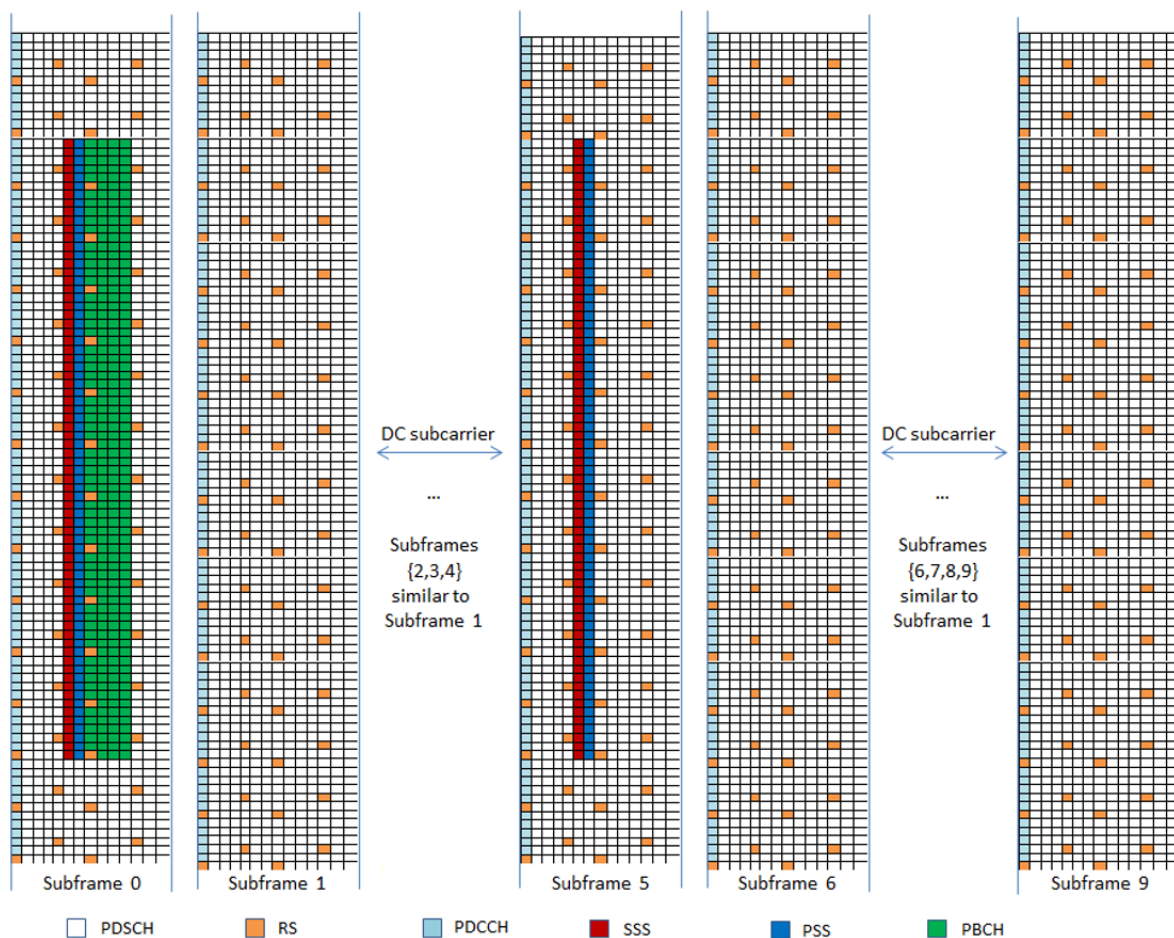


Figure 50: resource grid of LTE standard. [15]

At this point, to complete the transmitting sequence, it's necessary to realize an IFFT and then the cyclic prefix is added. Then a filtering operation is realized on the transmitting sequence.

LTE - Inverse fast Fourier transform and Normal cyclic prefix

```
[ LTE_Signal_Frequency, LTE_Signal_Time, LTE_Signal_Time_Serial,  
LTE_Signal_Time_Serial_CP, LTE_Signal_Frequency_Serial_CP ] =IFFT_CP(  
nFFTSize, N_symb, n_slot, Resource_Grid, f, dt, CP_1, CP_remaining,  
Occupied_Sub_carriers );
```

Filtraggio

```
[ LTE_Signal_Time_Serial_CP ] =  
Filter_TX(Selecting_Channel_bandwidth, LTE_Signal_Time_Serial_CP, Filtro_  
TX, fmax, CP_1, CP_remaining, nFFTSize, N_symb, n_slot );
```

At this point a frame of 10 ms is generated, coherently with the standard requirements. Two exact replicas of the frame are then concatenated to obtain three equal frames with random data inside. The reason of those three replicas is for the synchronization of the frame at receiver side.

3.3) RECEIVER LTE

The main goal of the receiving part is the evaluation of the EVM of the physical channel and signal, with particular attention towards the PDSCH.

As already seen in the first chapter the EVM can be expressed using a simple equation and its graphical representation can be interpreted as follow:

$$EVM_{RMS} = \sqrt{\frac{\frac{1}{N} \sum_{k=1}^N e_k}{\frac{1}{N} \sum_{k=1}^N (I_k^2 + Q_k^2)}}$$

$$e_k = (I_k - \tilde{I}_k)^2 + (Q_k - \tilde{Q}_k)^2$$

Where:

- e_k : average error.
- I_k : In-phase transmitted value.
- Q_k : In-quadrature transmitted value.
- \tilde{I}_k : In-phase received value.
- \tilde{Q}_k : In-quadrature received value.

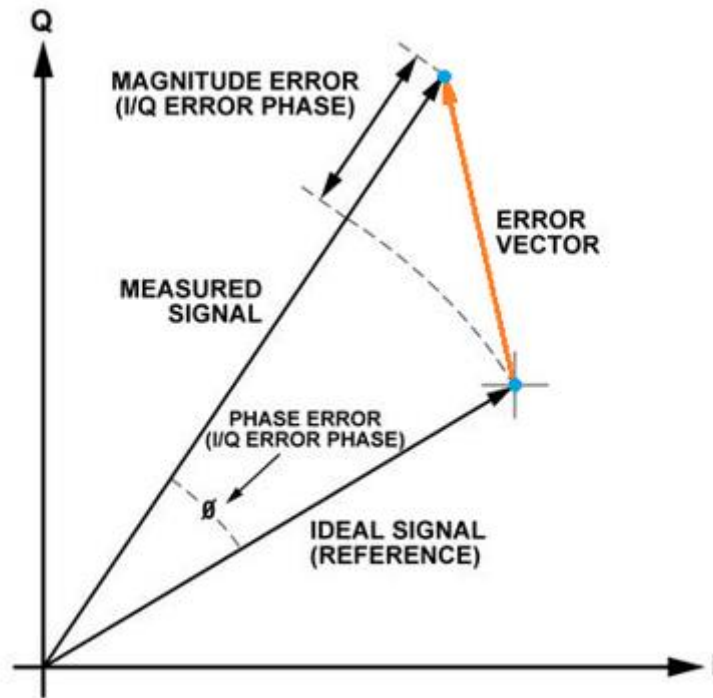


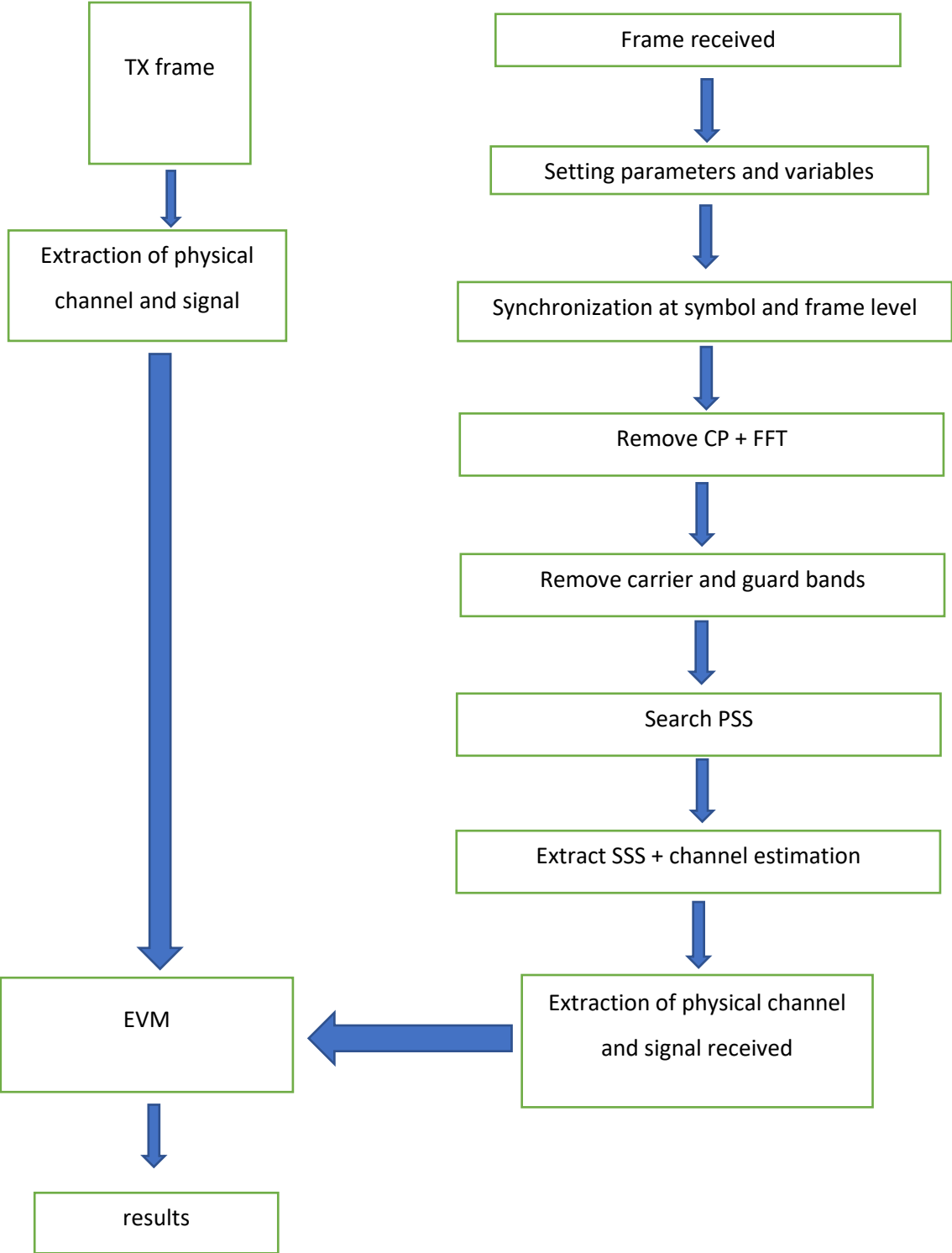
Figure 51: representation on the complex plane of EVM [15].

The LTE standards has some EVM requirements for the support of the different modulations of the PDSCH, as can be observed in the following tab:

Modulation scheme for PDSCH	Required EVM [%]
QPSK	18.5%
16QAM	13.5%
64QAM	8%
256QAM	3.5%

Tab 6: LTE requirements for each modulation format supported by PDSCH.

As already seen in the transmitter section, we can split the receiver in different blocks as follow:



3.3.1) RECEIVER SOFTWARE

As the transmitter, the functionalities of the receiver can be split in blocks function executed in sequence. At the beginning, it is necessary to select the file generated by the transmitter, specifying the bandwidth and modulation of the PDSCH; at this point the folder, containing the received file, has to be selected. Some parameters are initialized for the execution of the functions that will be executed.

At this point the real receiving procedure starts as follow:

- **Function for the synchronization on the OFDM symbol:**

LTE - Synchronization Symbol

```
[ pos_init, Rx_Sync_Symb, val_max] = Synchronization_Symbol (Rx, CP_1, CP_remaining, nFFTSize, Selecting_Channel_bandwidth)
```

- **Synchronization on the subframe:** based on the previous synchronization procedure, it takes two copies of the same frame. This procedure is the reason because we concatenate three frames in the transmitting sequence.

LTE - Synchronization Subframe

```
[ Rx_Sync_Subframe] = Synchronization_Subframe (Rx_Sync_Symb, n_slot, nFFTSize, N_symb, CP_1, CP_remaining)
```

- **Removal of the CP:**

LTE - Removing cyclic prefix

```
[ CP_size] = selezione_cp_size (Selecting_Channel_bandwidth)
```

```
%%%%%%%%%%%%%%%%%%%%%%%%%%%%%%%%%%%%%%%%%%%%%%%%%%%%%%%%%%%%%%%%%%%%%%%%  
for CP_remove = 1: CP_size  
    cp_out = CP_1-CP_remove  
    [ frame] = Removing_CP (Rx_Sync_Subframe, nFFTSize, N_symb, n_slot, CP_1, CP_remaining, cp_out)
```

- **Realization of FFT:**

LTE - Fast Fourier Transform (FFT)

```
[ RX_post_fft] = FFT (nFFTSize, frame)
```

- **Removal of guard band and carrier:**

LTE - Remove Guard Bands and Remove DC

[RX_Reordered] = Remove_GuardBands_and_DC (RX_post_fft, Occupied_Sub_carriers, nFFTSsize)

- **Correction of the rotation due to the removal of CP:**

LTE - correzione della rotazione del cp_out

[RX_Reordered_1, RX_Reordered_2, f_axis_norm] =
Correzione_rotazione_cp_out (Selecting_Channel_bandwidth, RX_Reordered, cp_out, nFFTSsize, N_symb, n_slot);

- **Search of PSS:**

LTE - PSS search

[index_max_PSS_1, index_max_PSS_2, max_PSS_1, max_PSS_2] = PSS_search (PSS, RX_Reordered_1, RX_Reordered_2, n_slot, N_symb, Occupied_Sub_carriers);

- **Evaluation of PSS correlation:**

LTE - evaluation correlation PSS

[RX_Reordered, index_max_search, flag_error, errori] =
evaluation_correlation_PSS(max_PSS_1, max_PSS_2, index_max_PSS_1, index_max_PSS_2, Rx_Sync_Symb, RX_Reordered, nFFTSsize, CP_1, CP_remaining, cp_out, N_symb, n_slot, f_axis_norm, Occupied_Sub_carriers, flag_error, errori);

- **Search of SSS:**

LTE - SSS search

[RX_Reordered] = SSS_search (RX_Reordered, secondary_prob, SSS_sub_0, SSS_sub_5, index_max_search)

- **Channel estimation:**

LTE - Stima del Canale

[Rx_RS, h_interp, Rx_Resource_Grid_equal, h, h_interp_p, Frequency_interp] =
.ChannelEstimate(RX_Reordered, RX_Reordered, RS, n_slot, N_symb, N_rb, Selecting_Channel_bandwidth, tx_Reordered_Resource_Grid);

- **Extraction of physical channel and signal:**

LTE - Estrazione dei canali e dei segnali fisici

[RX_PSS, RX_SSS, RX_RefSignal, RX_PDCCH, RX_PBCH, RX_PDSCH] =
Extraction_Channels_and_Signals(Selecting_Channel_bandwidth, Rx_Resource_Grid_equal, Occupied_Sub_carriers, n_slot, N_symb, N_rb);

- **Calculation of EVM:**

LTE - EVM Error Vector Magnitude

```
[ind_evm,EVM_max_PDSCH(CP_remove),EVM_rms_PDSCH(CP_remove),EVM_rms_PDCCH(CP_remove),EVM_rms_PBCH(CP_remove),EVM_rms_SSS(CP_remove),EVM_rms_PSS(CP_remove),EVM_rms_RS(CP_remove),PSS_tx,SSS_tx,RS_tx,PDCCH_tx,PBCH_tx,PDSCH_tx ] =
EVM_1 ( Selecting_Channel_bandwidth,
Resource_Grid,RX_RefeSignal,RX_PSS,RX_SSS,RX_PDCCH,RX_PBCH,RX_PDSCH,Occupied_Sub_carriers,n_slot,N_symb,N_rb,power_desidered_lin,Average_power_lin );
end
```

- **Visualization:**

LTE - Visualizzazione dei canali e segnali ricevuti

```
visualize_RX (RX_RefeSignal, RX_PSS, RX_SSS, RX_PDCCH, RX_PBCH, RX_PDSCH, RS, PSS, SSS_sub_0, SSS_sub_5, dataMod_PDCCH, dataMod_PDSCH, dataMod_PBCH_simb_0, power_desidered_lin, Average_power_lin, EVM_rms_PDSCH, name);
```

3.4) MERGING PROGRAMS

In order to use both programs together, some modifications on the code have been implemented. Basically, at the beginning, the pre-distortion program on Matlab was developed to work with imported transmitting and receiving signals.

Our goal is to implement the same procedure seen in predistortion analysis, but using the LTE signal, generated by the LTE simulator program. The idea is to create an LTE frame with random data, forming a structure of three identical frame concatenated. The LTE frame sequence generated is loaded from the PC to the Anritsu board.

The schematic of the link is the following:

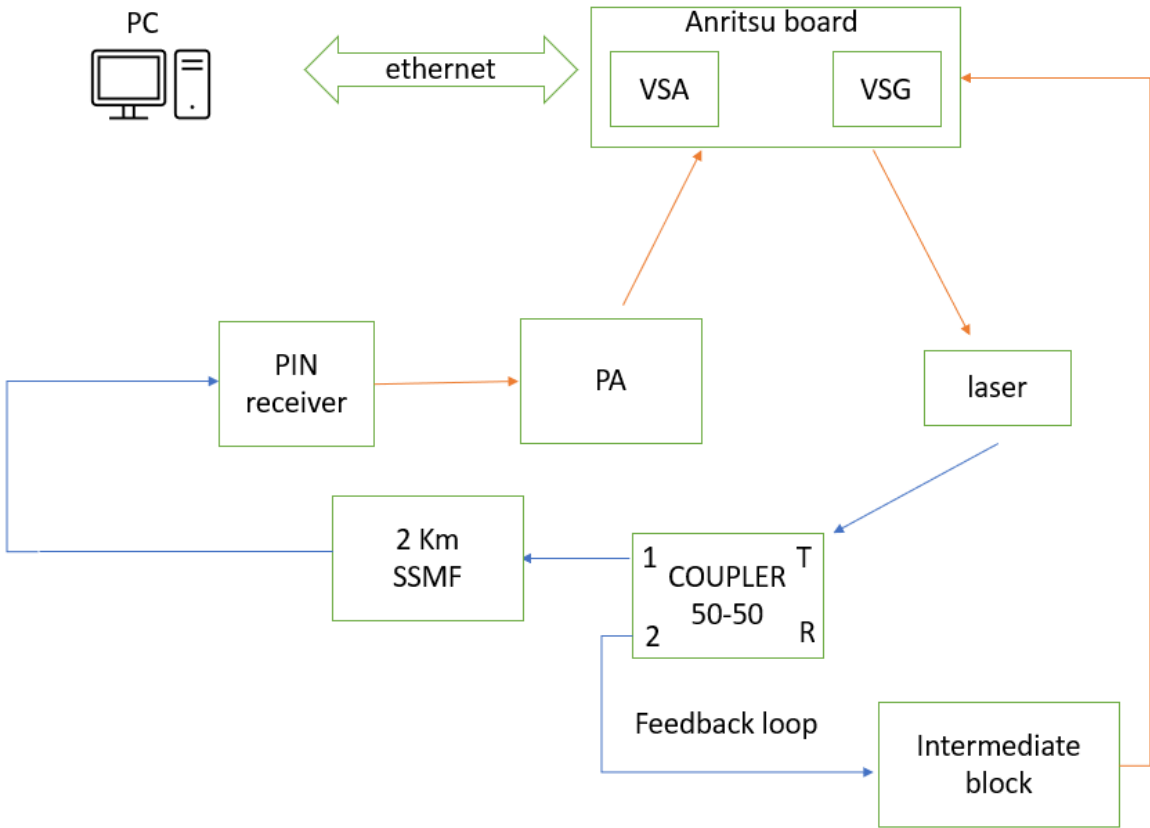


Figure 52: schematic of the link implemented.

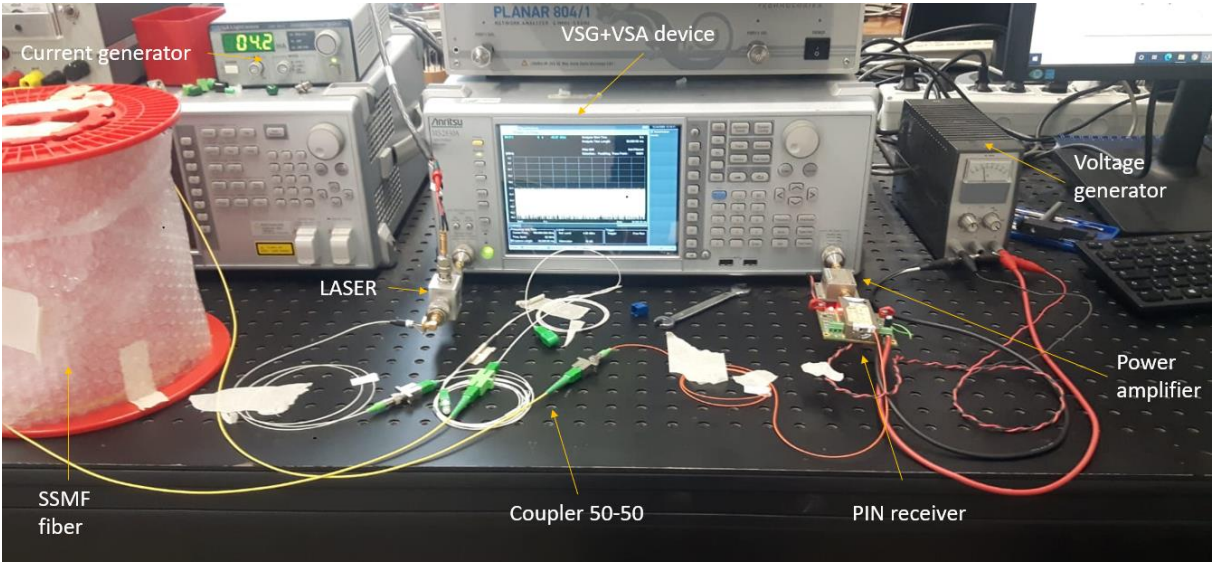


Figure 53: image of the link built used for the measurements.

Once the file is upload to the VNA a signal is generated and transmitted using a VCSEL 850 nm into a coupler 50-50 as analysed in chapter 1.

The configuration T1 of the coupler is connected to a 2 Km SSMF G-652; then we have the PIN receiver, the amplifier, and go back to the Anritsu.

At this point, the Anritsu board load the received signal into the matlab environment, and the received signal is created.

The signal received is pass to the DPD program that realizes his function, as already seen in chapter two. This cycle is repeated for each iteration of the predistortion program and, in each iteration, the value of EVM, ACPR, NMSE and spectra are reported to check the evolution of the predistortion algorithm on the generated LTE sequence.

The one presented is the basic set up but actually, the final goal of this dissertation, is to train the pre-distorter using a feedback loop, exploiting the T2 configuration of the coupler. This particular configuration, has never been tested, but it presents some interesting aspects since in this case, the predistortion loop, can be realized just after the transmitting laser. In fact, a typical problem of this solution is that the predistortion loop without the coupler, should be realized with the signal at the output of the 2 km fiber and then carried back to the transmitter, but this introduces some dB of losses and an extra amplification is required. The advantage of the coupler is that we can exploit the feedback link just after the laser and this solve the previous technical complications.

Anyway, the Anritsu board used in the lab, has only one receiving port so, to realize such application, we first need to train the pre-distorter on the feedback loop and then, use the results of the predistortion analysis for the direct link and check the reference value of EVM, NMSE, ACPR.

3.5) TRAINING OF THE ALGORITHM

For the realization of the system the first trials have been carried out using a simpler link, just composed of a laser and a direct connection to the PIN diode. Then an amplifier has been added at the end, and other experiment has been carried out. Those simplified test were performed to get, step by step, to the final link, explained in the previous section.

Since the first test, an aspect that has been highlighted, is the importance of the training the pre-distorter using the proper coefficients sequences.

In fact, depending on the specific link analysed, the sequence of K and Q coefficients vary in non a non-predictable way. If the wrong coefficients are chosen, the algorithm stops to work

because in the estimation of the coefficients, the condition number of the matrix results ill-conditioned, as already explain in chapter two.

To find out the proper coefficients sequence, a training has been implemented in the matlab code, in order to check different configurations, to find out the best one. This is the simplest approach, and is call Exhaustive search, but presents the disadvantage of requiring a lot of time since all the combinations of coefficients have to be tested.

3.5.1) MOTIVATION

The PA is the most linear components in radio transmitter and consume a lot of power, for this reason, the efficiency, is one of the most important aspect to deal with.

The problem is that the efficiency is obtained at price of poor linearity, especially for wideband signals with high PAPR. As already seen, PA not just introduce nonlinearities but also memory effects, due to electrical and electro-thermal couplings [16].

The principle of DPD is to apply a pre-correction on the signal, so that the cascade of DPD + RoF link is linear and memoryless, as the ideal case.

An important aspect to underline is that the PA, can be driven toward high efficiency region without compromise the linearity of the system; this is particularly important because the PA is the most power consuming device in the chain and the efficiency has a dominant role to reduce the total power consumption.

To better understand this concept, we consider a graph that put together the linearity and the efficiency of the PA.

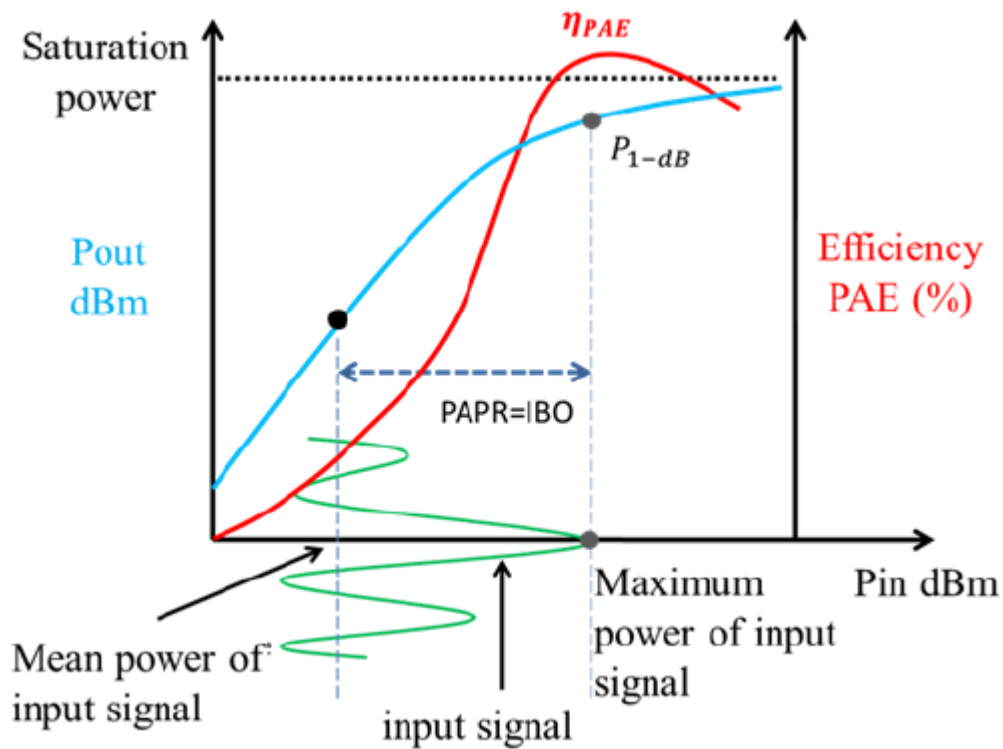


Figure 54: trade-off between linearity and efficiency [16].

The blue line is the output power, the red line instead, represents the power added efficiency, both in function of the input power. For reaching high efficiency, is better to operate near saturation zone, but the signal is subject to nonlinearity and distortion starts. To avoid spectral distortion, the operation point has to be back-off from the saturation zone.

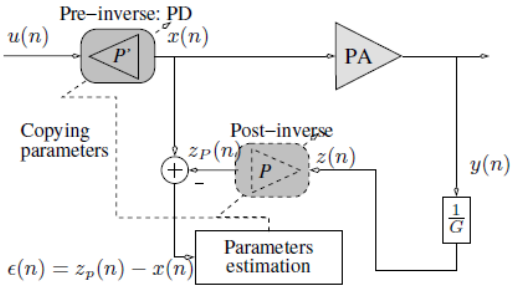
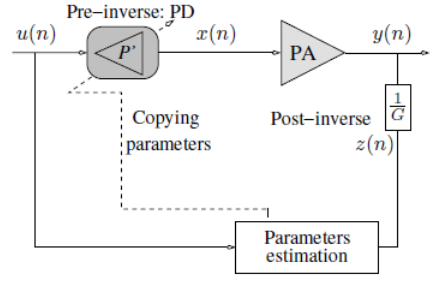
An interesting aspect of this approach is that a behavioural modelling of the PA just sees it as a black box, and it works without knowing the RF circuit functionality. As we have already seen in chapter two, exist a lot of models for this purpose, most of them derived from Volterra series like MP or GMP.

Another method is represented by the Block-Oriented Nonlinear-system in which the non-linearity and the memory effects are studied separately, like Hammerstein or Wiener.

All the models considered are linear combination of some basis functions.

Another promising technique is the adoption of neural network for the DPD modelling because of the ability to learn any arbitrary nonlinear behaviour.

As already seen, there are 2 estimation approach, ILA and DLA.

ILA	DLA
<p>Schematic:</p>  <p>Figure 55: ILA architecture. [12]</p> <p>Post-inverse is first identified and used in pre-distorter. The model is linear with respect to their coefficients and this simplify the coefficients estimation procedure. In matrix form we can express the relation in-out as follow:</p> $Z_p = Zc$ $Z = \begin{bmatrix} \Phi_{1,1}(z(n)) & \dots & \Phi_{K,1}(z(n)) & \Phi_{1,2}(z(n)) & \dots & \Phi_{K,L}(z(n)) \\ \Phi_{1,1}(z(n-1)) & \dots & \dots & \dots & \dots & \Phi_{K,L}(z(n-1)) \\ \vdots & \dots & \dots & \dots & \dots & \dots \\ \vdots & \dots & \dots & \dots & \dots & \dots \\ \Phi_{1,1}(z(n-N+1)) & \dots & \dots & \dots & \dots & \dots \end{bmatrix},$ <p>The algorithm adopted is the least square LS and the coefficients are evaluated as follow:</p> $[Z^H Z]c = Z^H x$ <p>This procedure minimizes the LS cost function expressed by the following equation:</p> $C = \sum_{n=1}^N z_p(n) - x(n) ^2$	<p>Schematic:</p>  <p>Figure 56: DLA architecture. [12]</p> <p>In this case the error to minimize is directly the difference between the DPD input and the PA output normalized by the gain $z(n)$.</p> <p>The coefficient c_k of the k-th basis function is updated applying stochastic gradient algorithm.</p> <p>In this approach, a model of PA needs to be identified at the beginning.</p> $x = Uc$ <p>U represents the matrix of basis function.</p>

3.5.2) STRUCTURE OPTIMIZATION ALGORITHM

In this case, the idea is to find the best dimensions for the nonlinearity and memory. We consider a GMP model, that has a more complex structure compared to MP, but the same concepts hold also for the simpler case MP.

As already seen in chapter two, the GMP has eight sizing parameters, each one independent from the others. For a GMP, using the exhaustive search as we do for the MP, it takes a long time, since, when a new basis function is added, impacts all the other due to the non-orthogonality and the model coefficients have to be evaluated.

For the MP, considering K and Q as dimension of NL and memory, the total number of structures to be checked is 2^{K-L-4} ; for a GMP considering a set of value from 1 to 10 for each parameter we have 10^8 configuration; complexity explodes!

Genetics algorithms (GA) have been applied for the identification of the coefficients in DPD.

Another effective method is the Particle swarm optimization (PSO), it is often also used in MP sizing.

3.6) IMPACT OF PA GAIN CHOICES

The choice of the reference gain G is between two possible value:

- G1, small signal gain
- G2, peak power gain

In this work the G1 is chosen as gain of the system in the pre-distorting procedure and the value is extracted during the AM/AM AM/PM procedure (amampm function) that generates the graphs and also a structure with inside different fields, including the small signal gain.

The concept can be easily seen in the following figure:

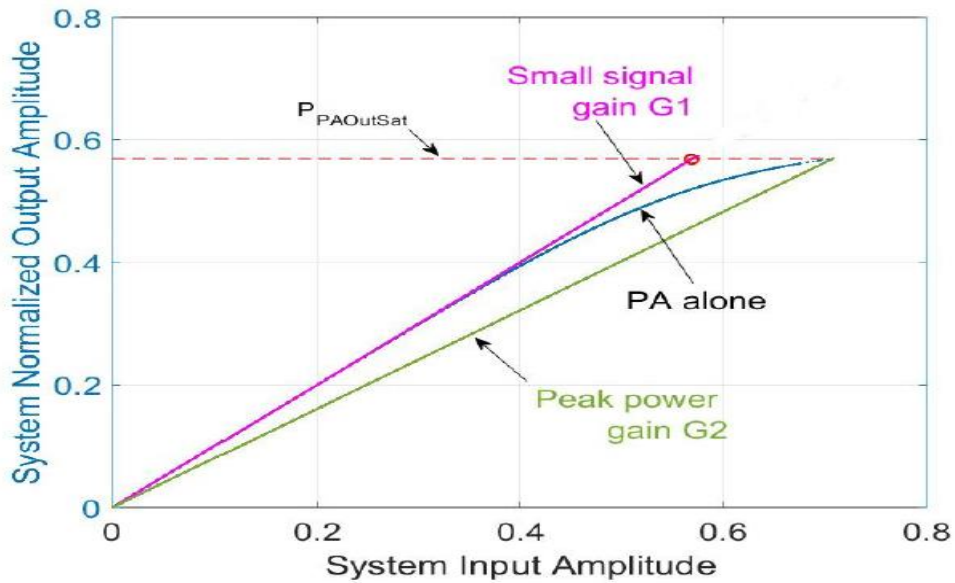


Figure 57: graphical representation of G1 and G2. [16]

The choice of gain is arbitrary, anyway using G1 require an extra calibration step. If we consider the ILA architecture, as already seen in chapter two, at the first iteration the signal $x(n)=u(n)$ since the starting coefficients are set as a 1 followed by all zeros. The post inverse block is calculated and then, the coefficients are applied to the pre-inverse block for the following iteration. Let consider the AM-AM plot of the generic PA as follows:

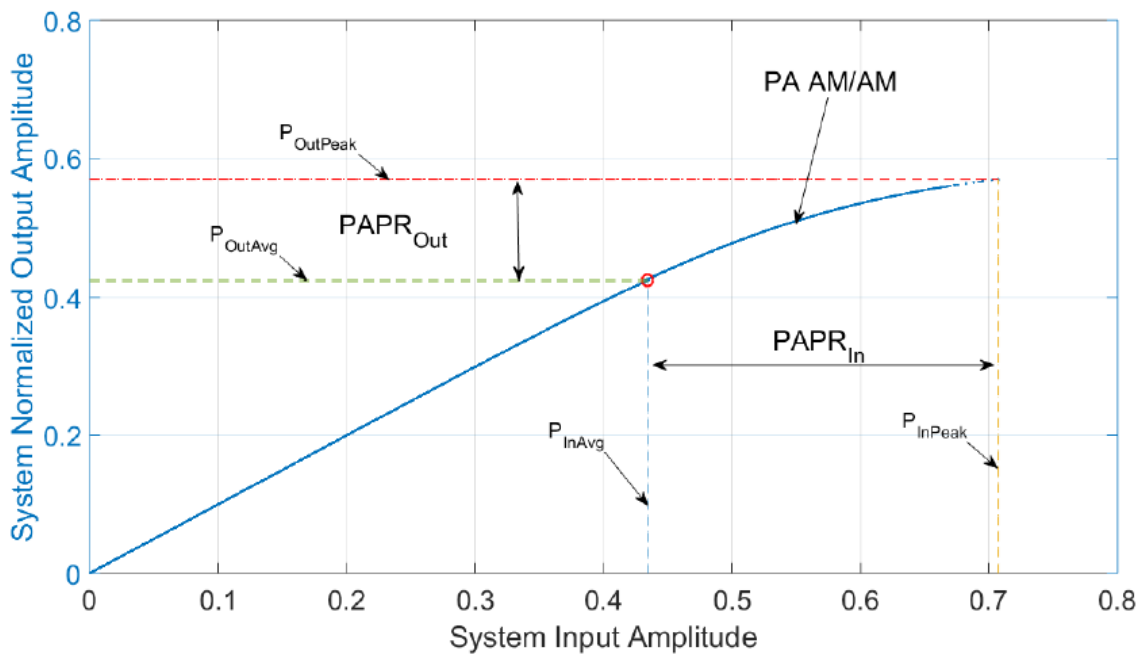


Figure 58: input of PA vs output of PA. [16]

As can be seen in the figure, because of the NL of the PA in the saturation zone, the PAPR of the output signal is compressed with respect to the input signal. This means that $PAPR_u > PAPR_z$ so the input signal of the pre-inverse and post-inverse are different. The signal $z(n)$ is normalized by the gain G and the choose of the gain can influence this step $\rightarrow z(n)=y(n)/G$

Considering the average or peak power we can formulate [16]:

AVERAGE POWER:

$$E(P_u) = \frac{E(P_y)}{G}$$

PEAK POWER:

$$\max(P_u) = \frac{\max(P_y)}{G}$$

3.6.1) LINEARIZATION G1

In the case of the small signal gain, $G1$ is evaluated using low amplitude input signals and referring to the average power we can make the following approximation: $E(P_u) \approx E(P_z)$.

We can see in the figure the AM/AM plots of the DPD, the green curve, and the one of PA, the blue curve, as follow:

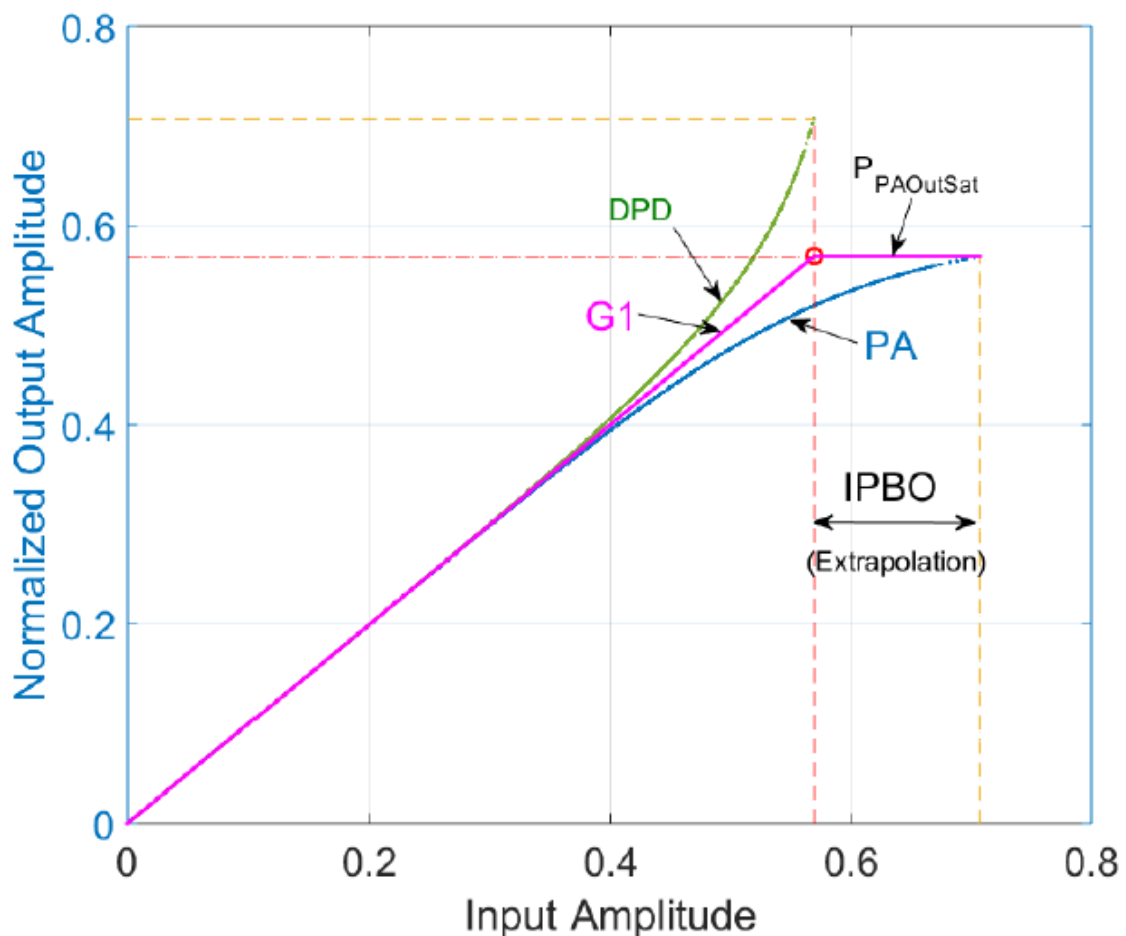


Figure 59: small signal gain G1 case. [16]

The results of the cascade of DPD and PA is the pink line, we can see that the output signal is saturated when the input signal amplitude is larger than $P_{PAOutSat}$.

It is necessary to apply an input back-off (IPBO) in order to limit the dynamic range of the input signal. In this linearization method, the average power of the input signal is maintained to a constant value. At each iteration, the signal $z(n)$ has peak power equals to $E(P_u) + PAPR_z$. In the next iterations, the DPD model is fed with a signal having peak power equals to $P_{th} = E(P_u) + PAPR_u$. As we already observe, $PAPR_u > PAPR_z$, so the DPD model cannot cover the whole range of the input signal. In this case an extrapolation of the DPD characteristic function is required for all the signal that presents power larger than $E(P_u) + PAPR_z$ and this carry to a lowering of the system performance.

In conclusion, if we choose G1, the performance of the first identified DPD is degraded by the extrapolation procedure. The countermeasure to be taken are:

- Post-inverse model M1 identified without IPBO.
- At the second iteration IPBO is applied on the input signal and the previous model is applied as DPD, in order to find a new post-inverse model M2.

We can see the two steps in the following figure, on the left the first step, on the right the second one:

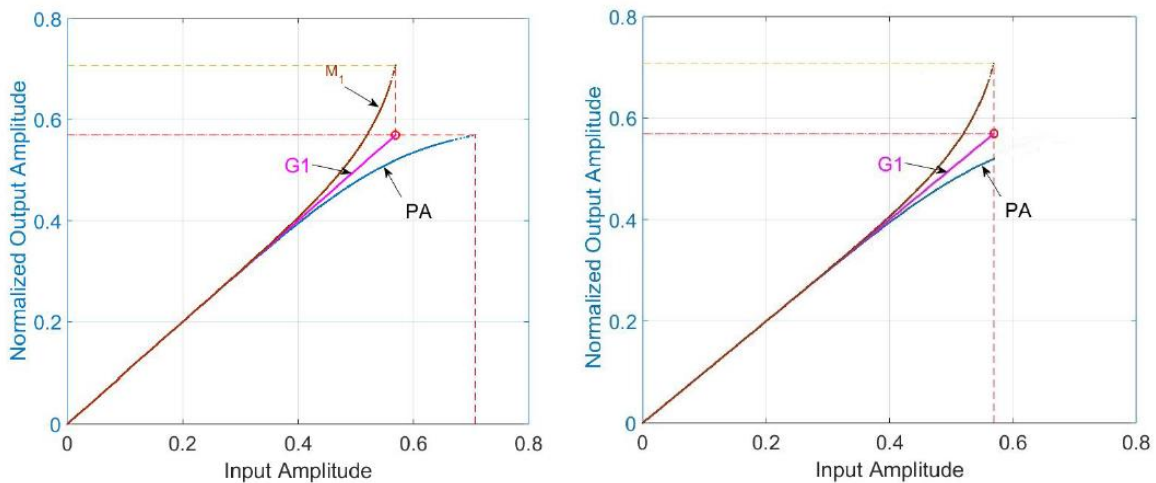


Figure 60: on the left there is the identification procedure without back-off. [16]

On the right side there is the identification with back-off.

This concept is present also in our simulation environment on matlab, where a scaling procedure is applied when the input power level raise above a certain threshold. The mathematic procedure applied to the signal is the following:

$$x = x * PA.LimitPD / \max(abs(x))$$

The scaling procedure improve the linearization performance but reduce the output power too!

3.6.2) LINEARIZATION AT G2

If the peak power gain is chosen, the gain is evaluated in the maximal amplitude of the signals at input and output of the PA $\rightarrow G_{peak} = \frac{P_v}{P_u}$

The good aspect is that there is no need of IPBO, and u(n) and z(n) share the same peak power. The negative aspect of this approach is that there is an average power difference between u(n) and z(n).

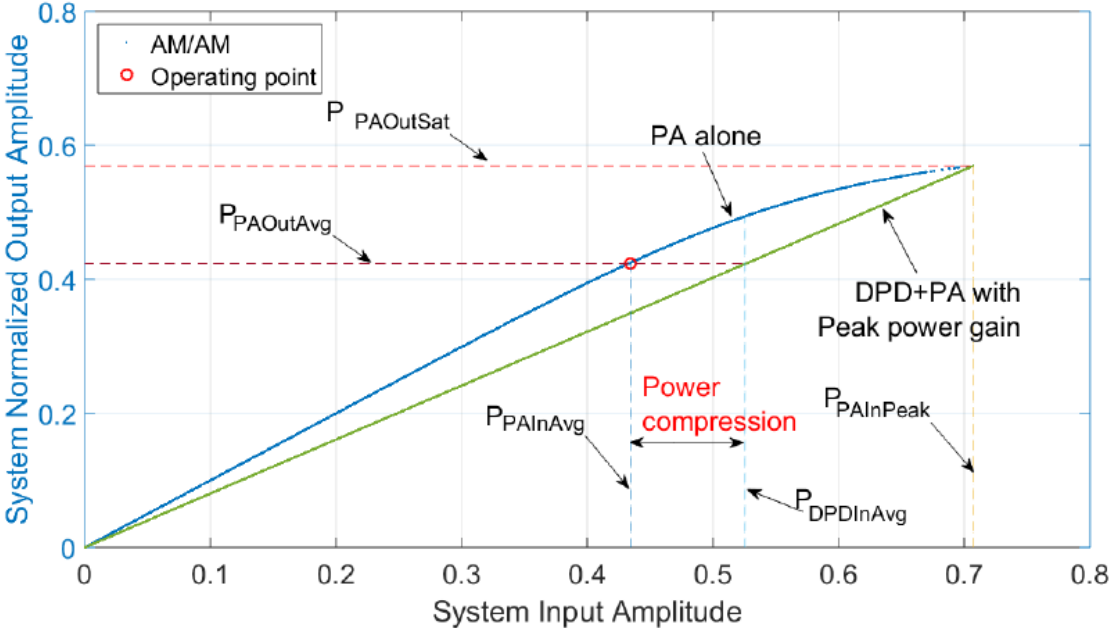


Figure 61: peak power gain G2 case. [16]

It is clear from the graph that the DPD compress the power, almost the same behaviour of the clipping procedure explained in the previous section.

3.7) EXPERIMENTAL RESULTS

As already presented in the beginning of this chapter, the experimental work has been realized as a step-by-step procedure, starting from a directly connected link with no amplifier, just the transmitter, the fiber, and the receiver; arriving to our final system with the feedback loop for the predistortion. Not all the experiments were reported because, the major parts of them, were performed just to better understand how the system works and how to fix some problem in the code, using simpler configurations. All the tests have been performed adopting a band of 5 MHz and 16 QAM modulation format.

An important aspect is that all the measure were performed at 700 MHz due to an instable noise behaviour observed at 800 MHz.

In this section will be reported the results of:

- **Intermediate configuration:** transmitter + 1 m SSMF fiber + receiver + 22 dB power amplifier. This link corresponds to a much simpler configuration with respect to the final system implemented.
- **Full link using coupler 50-50:** in this case were performed different measures, with and without clipping, direct and feedback trained.
- **Full link using coupler 90-10:** the same measure of the previous coupler has been performed to make a confront between the two couplers.
- **Final test:** performed on coupler 50-50 feedback trained, using a 256 QAM modulation format.

3.7.1) INTERMEDIATE LINK

We start from a simple link that can be schematized as follow:

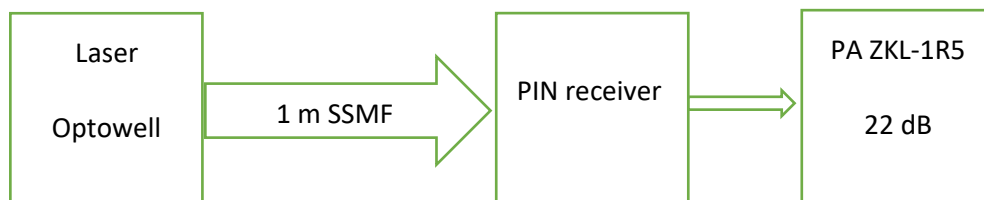


Figure 62: schematic of the intermediate link.

The Optewell laser is biased at 4,2 mA, while as amplifier we have used a ZKL-1R5 minicircuit, used in a working point near to the 1 dB saturation in order to trigger the non-linearity, since the LTE signal generated has a PAPR around 10 dB. The receiver is plugged to the voltage generator at the operating point of 12 V.

This initial procedure has been realized using a different configuration with respect to the other tests. In fact, in this case we adopt K from 0 to 10 and Q from 0 to 5. It is not the usual configuration in which K and Q are limited to lower value like 3 or 4.

Another peculiar aspect is the number of iterations, set to 10 in this case. The reason of this number is because we want to observe a stable behaviour after the first 3 or 4 iterations, to check the stability of the system. The measures were performed transmitting the LTE signal at 7 dBm and the results collected are:

- **Starting AM/AM AM/PM:**

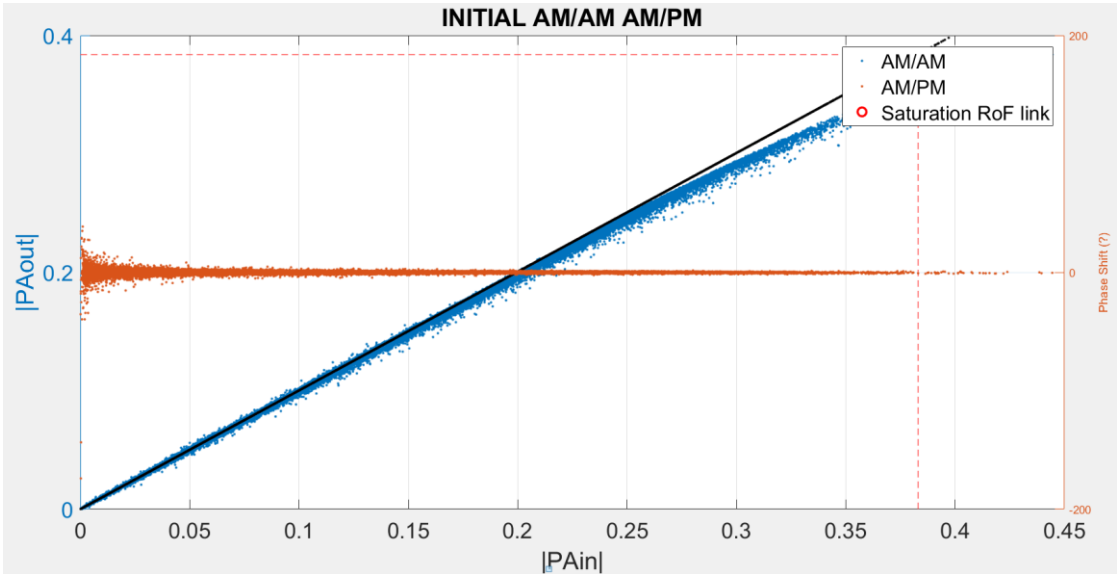


Figure 63: starting AM/AM AM/PM graph.

- **Final AM/AM AM/PM:**

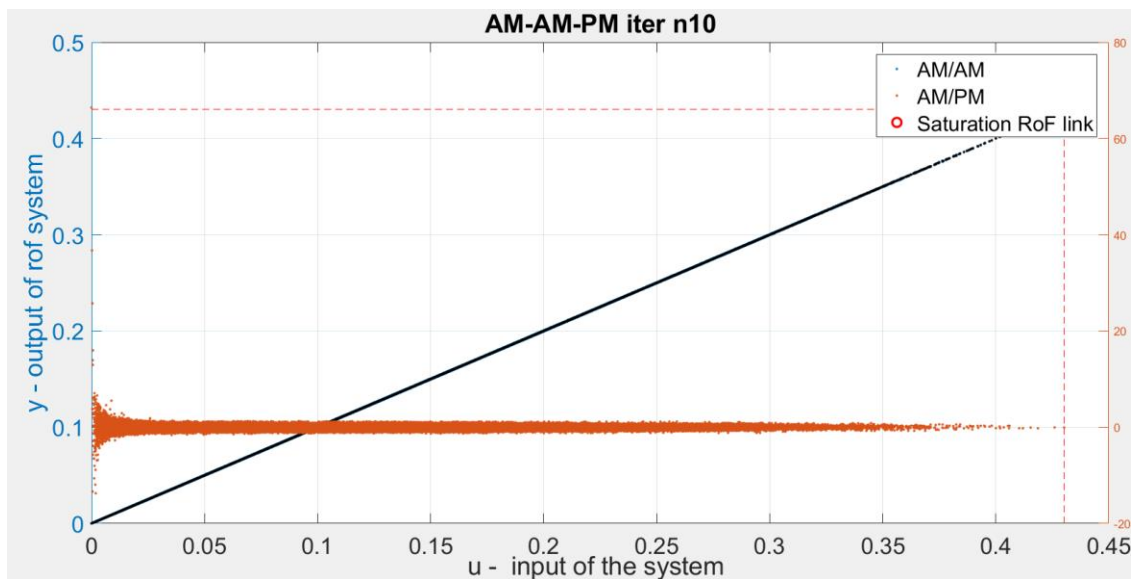


Figure 64: final AM/AM AM/PM graph after the linearization procedure.

- **Pre-distorter/ post-distorter characteristic:**

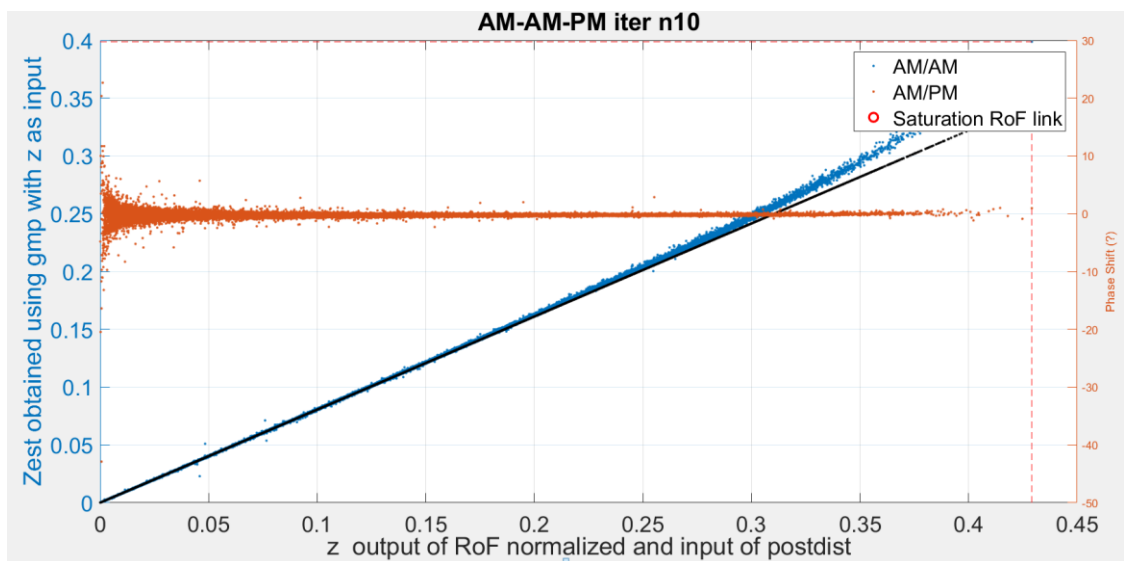


Figure 65: AM/AM AM/PM graph of the post-distorter and pre-distorter.

- **NMSE progression:**

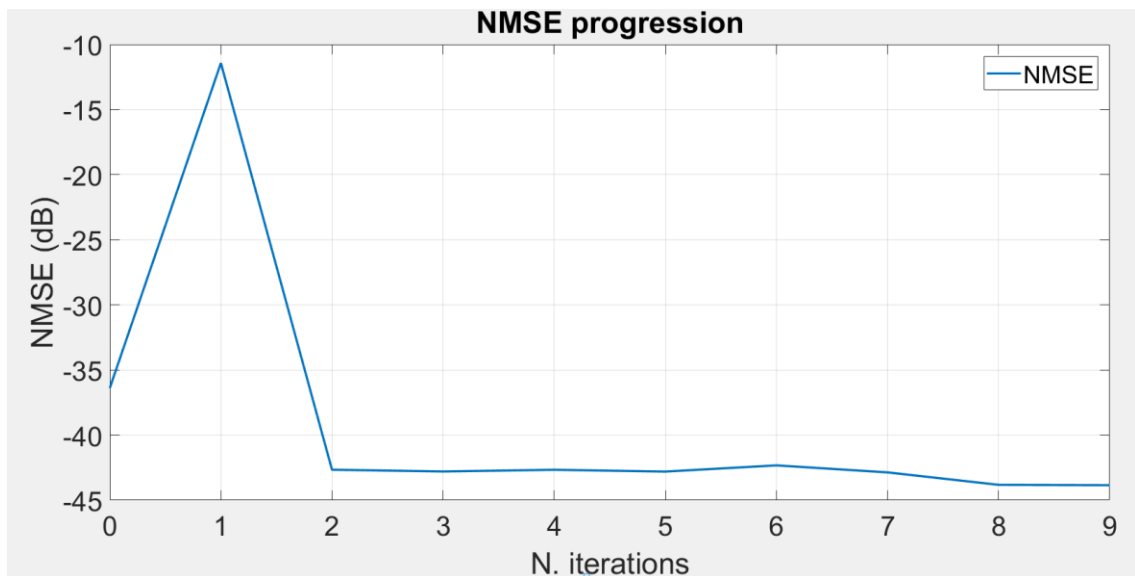


Figure 66: NMSE progression during the iterations.

The reason of the initial peak is due to the fact that, at the first iteration the coefficients of the model are set to 1 + all zeros, so no predistortion is applied. As we have already seen the NMSE is evaluated between the signal x , output of the pre-distorter, and the signal z_p , output of the post-distorter. The problem is at the second iteration, when we calculate the NMSE inside the code using the x of the previous iteration, where no predistortion is applied so is still $u=x$, while the z_p has changed because now the coefficients have been evaluated by the `gmpidentifier` and the new signal is estimated by the `gmp` function. In the next iterations the system enters in a regime state and the NMSE improve up to almost -45 dB.

- **EVM progression:**

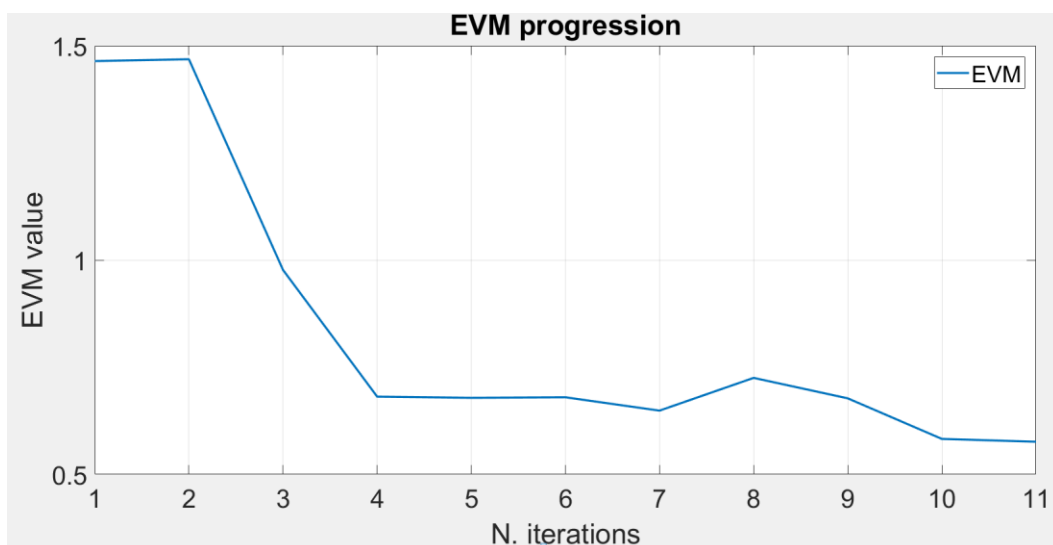


Figure 67: EVM progression during the iterations.

3.7.2) FINAL LINK COUPLER 50-50

This configuration represents the final goal of the whole dissertation and different measure were performed to check the behaviour of the system in different working situations. We have two kind of measures:

- **Direct:** the DPD procedure is applied directly at the end of the link with no feedback loop implemented. We can see the practical implementation in the following figure:

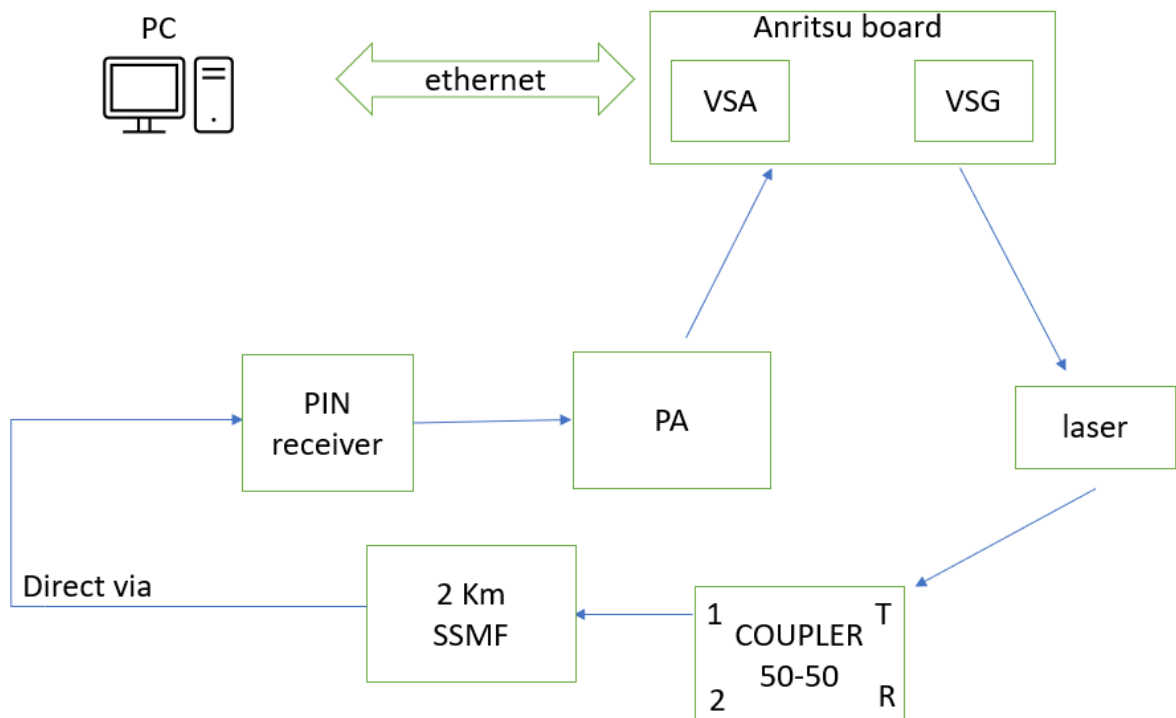


Figure 68: experimental set up for the direct via measures.

- **Feedback:** the DPD procedure is applied to the T2 output of the coupler, plugged to the Anritsu board, that has previously said, has only one receiving port. Once the DPD is applied to the feedback path, we have connected to the receiving port the direct link that is pre-distorter, according to the coefficients evaluated on the feedback path, and we analyse the performance.

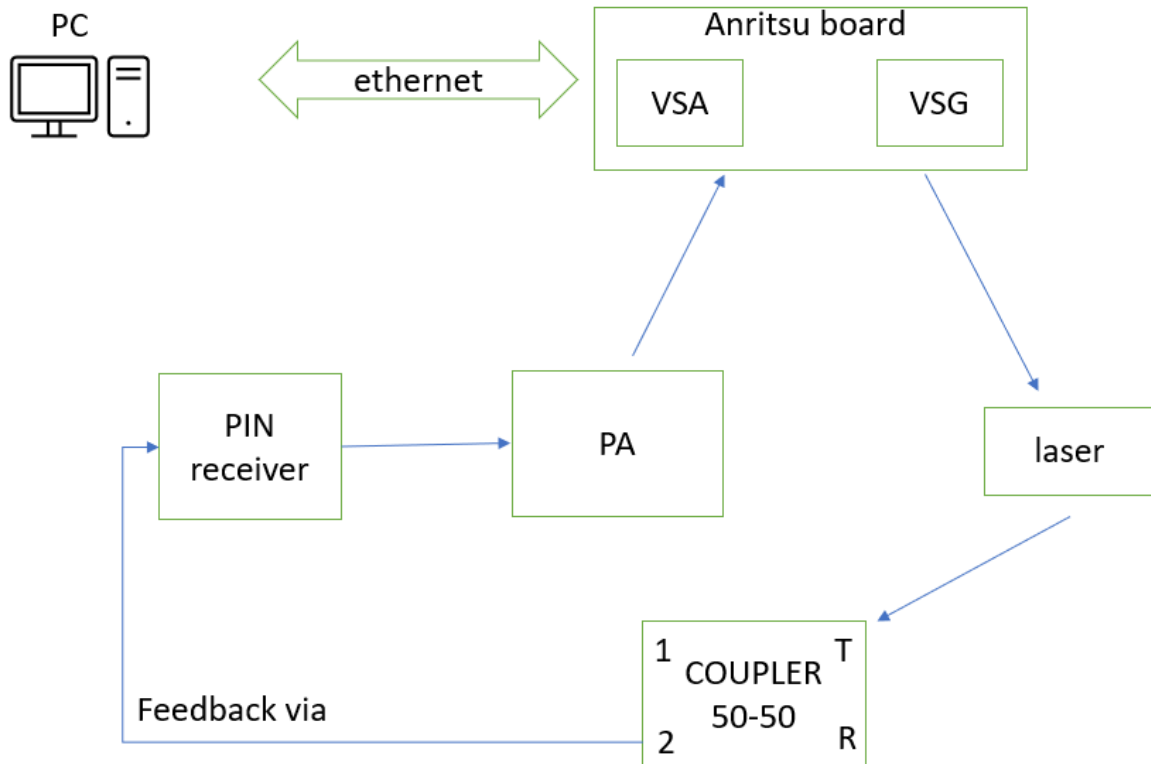


Figure 69: experimental set up used for feedback via measures.

To analyse the differences between the direct trained and the feedback trained, we perform both the measurements set. Furthermore, an evaluation with and without scaling is performed to better understand the importance of this procedure, and how impact the performance of the system. The link can be schematized as follow:

All the test performed in this section were using $K=1$ and $Q=3$. It may seem a strange configuration, but we find out using the exhaustive search algorithm, as presented in the previous sections. An initial set of measures regarding the EVM has been realized in order to find the classical behaviour of the EVM in function of the input power.

The result is a curve with 'U' shape as follow:

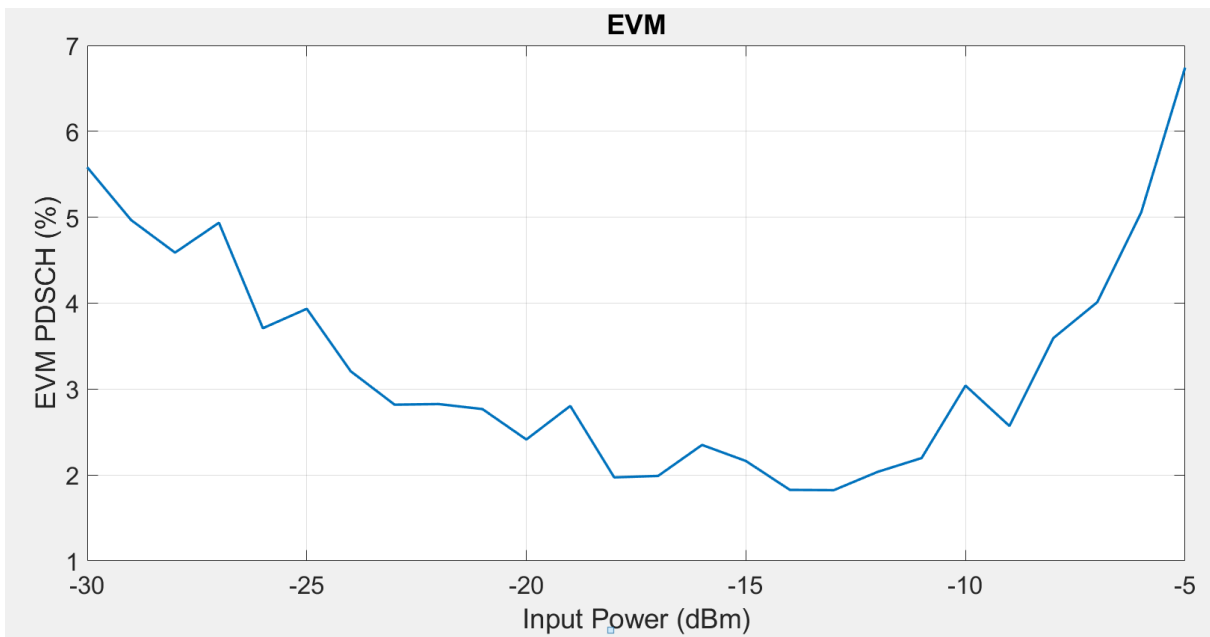


Figure 70: EVM value for the different input power levels from -30 to -5 dBm.

The reason of this behaviour is that in the first part of the graph, where the power is low, the system is dominated by the noise; instead in the right part, where the power increase, the nonlinearity starts to become dominant, increasing the EVM.

At this point, we have considered the deep of the curve, corresponding to an input power of -13 dBm, and from this point we have evaluated the direct and feedback trained mode, with and without clipping, from -13dBm to 5 dBm.

The four curves extracted during the measurements will be put onto the previous graph in order to check the improvement of each configuration.

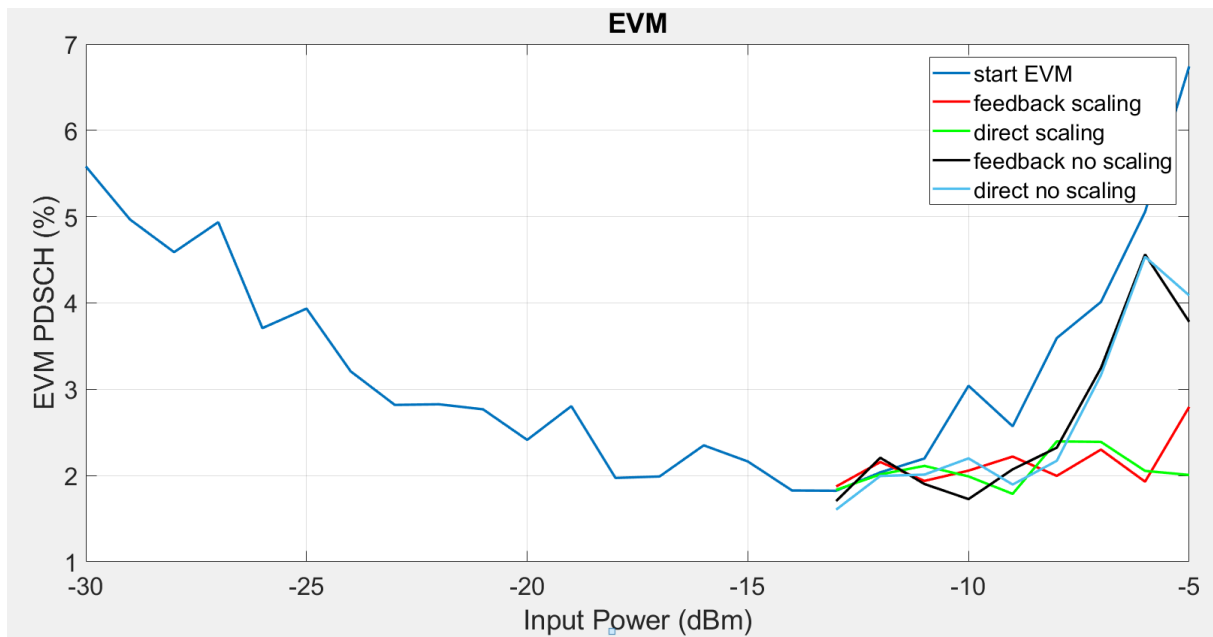


Figure 71: results achieved in term of EVM for the 4 configurations tested.

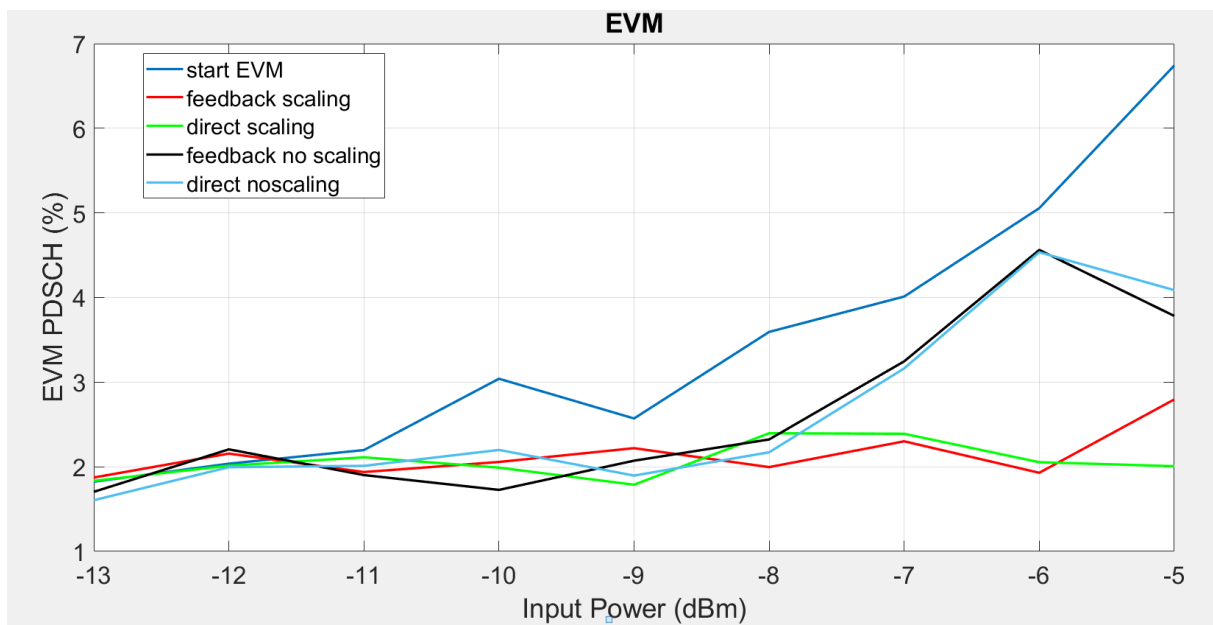


Figure 72: Zoom on the analysed region.

Here in this final graph, we can see together the four different configurations. As we have already seen, the scaling improves the performance of the system in a significative way as the graph suggests. The direct training in general is better, since the procedure is applied directly but actually, if the system is developed properly, it does not make a big difference and the feedback can be exploited almost in the same way.

In the same way we have also checked how the ACPR change with and without the scaling procedure.

The first results presented is the case with scaling:

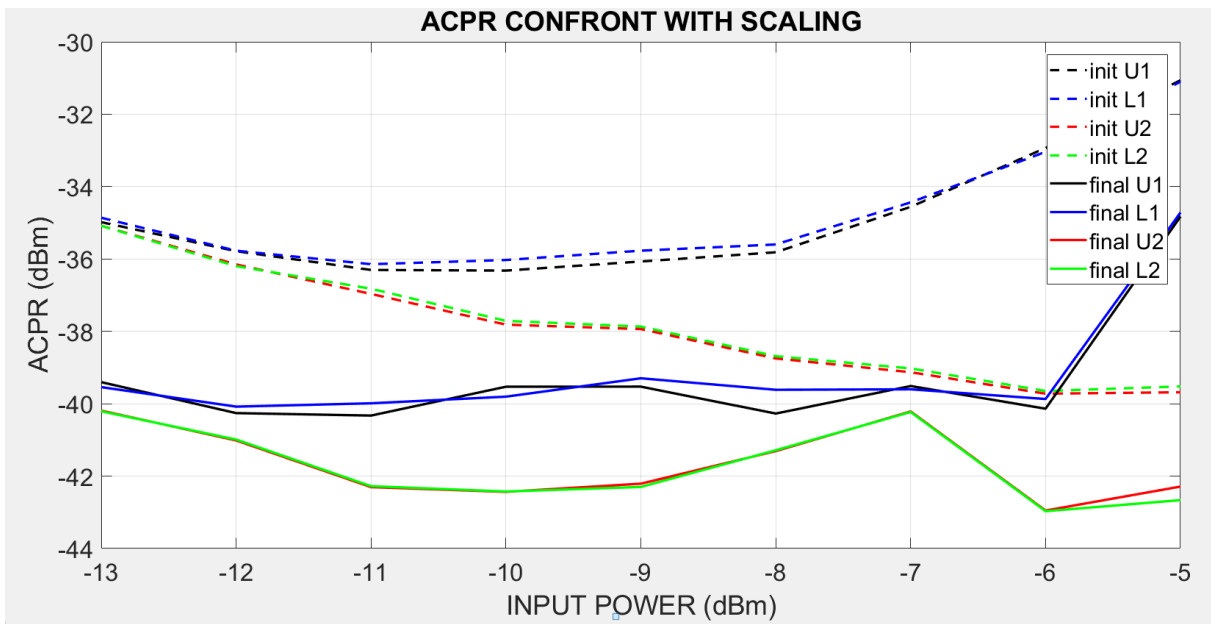


Figure 73: ACPR improvement with scaling.

Then the same kind of measure has been repeated for the case without clipping, to check the difference between the two cases.

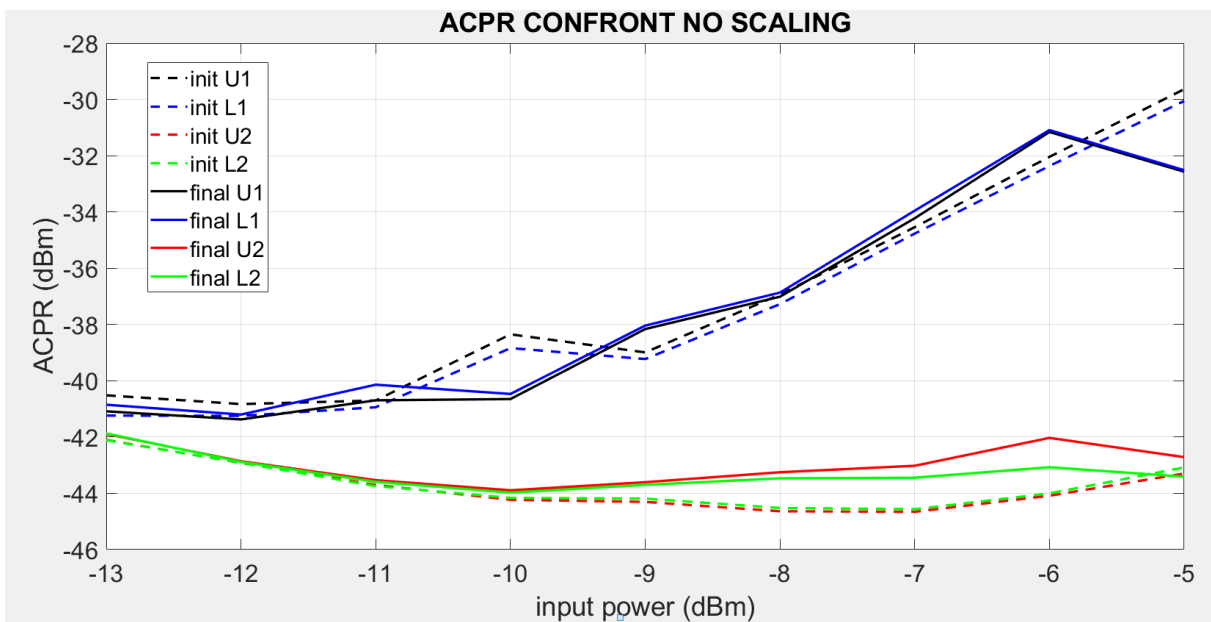


Figure 74: ACPR improvement no scaling.

From this analysis we can conclude that both direct and feedback with and without clipping, improve the basic performance in term of EVM. The clipped solution carries to the best results both in term of EVM and ACPR. The solution without clipping produce is an intermediate result for both the EVM and ACPR.

3.7.3) FINAL LINK COUPLER 90-10

The same analysis that has been realized for the coupler 50-50 is repeated for the 90-10 coupler. We first extract the behaviour of EVM for the basic link:

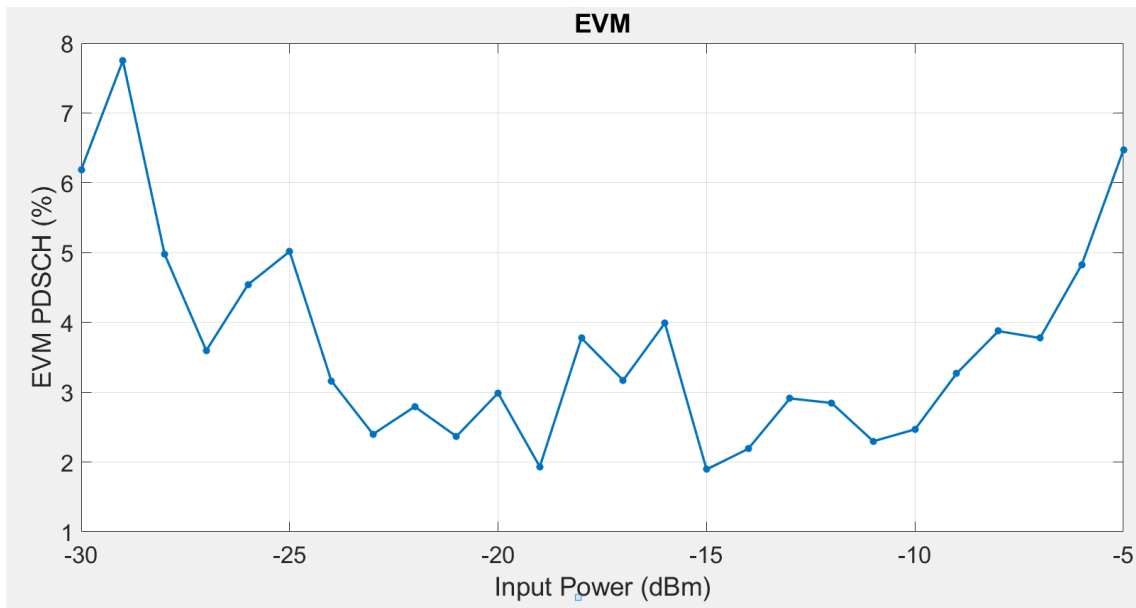


Figure 75: EVM value for the different input power levels from -30 to -5 dBm.

This time the behaviour of the EVM is less stable than in the case of coupler 50-50, anyway after -11 dBm of input power the line follows the classical ‘U’ shape.

Starting from -11 dBm, we have repeated the same set of measure as before, direct and feedback, with and without clipping.

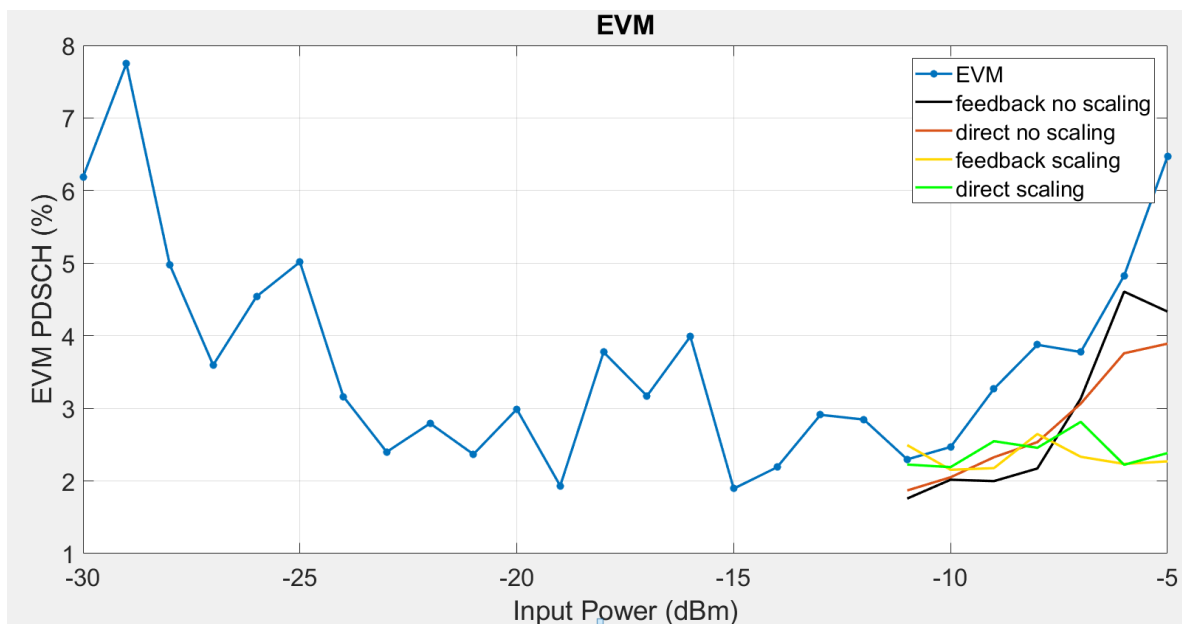


Figure 76: results achieved in term of EVM for the 4 configurations tested.

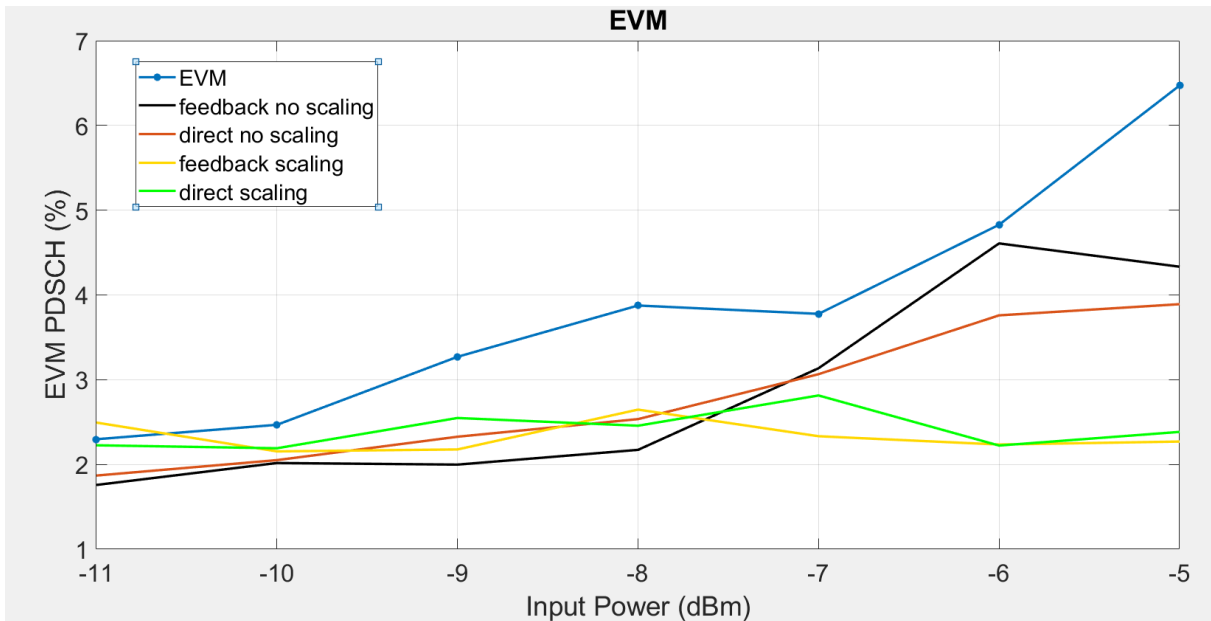


Figure 77: Zoom on the analysed region.

Then we proceed with the ACPR confront with scaling:

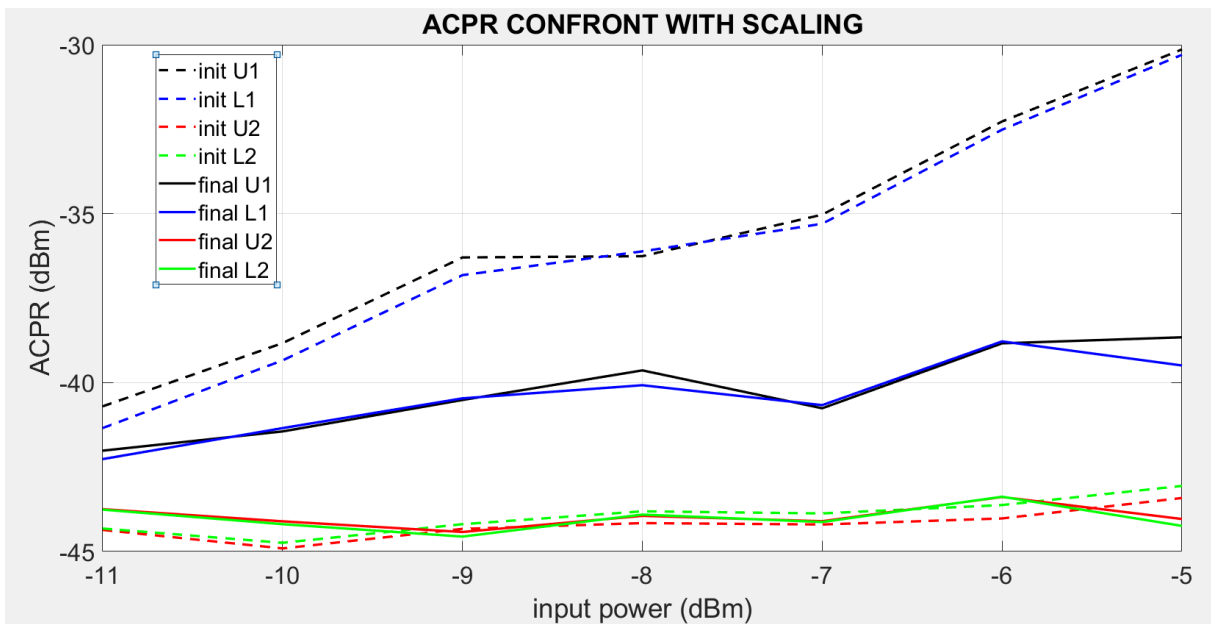


Figure 78: ACPR improvement with scaling.

and without scaling:

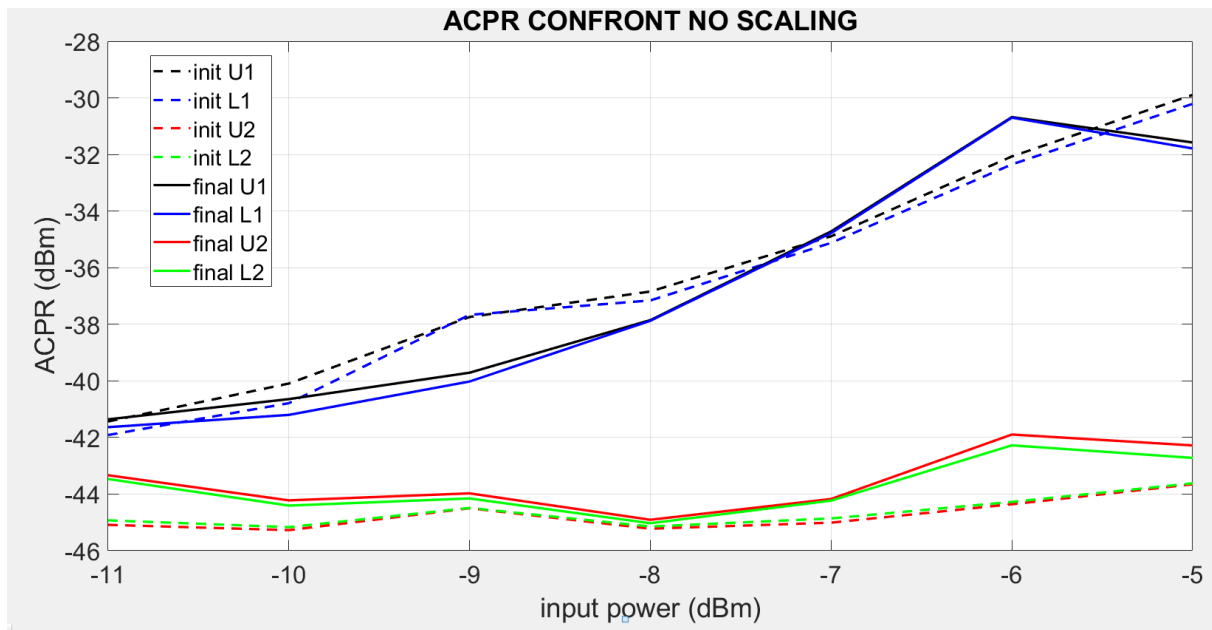


Figure 79: ACPR improvement no scaling.

The conclusions are the same as before, in fact the results of scaling are better both in term of EVM and ACPR with respect to the case with no scaling.

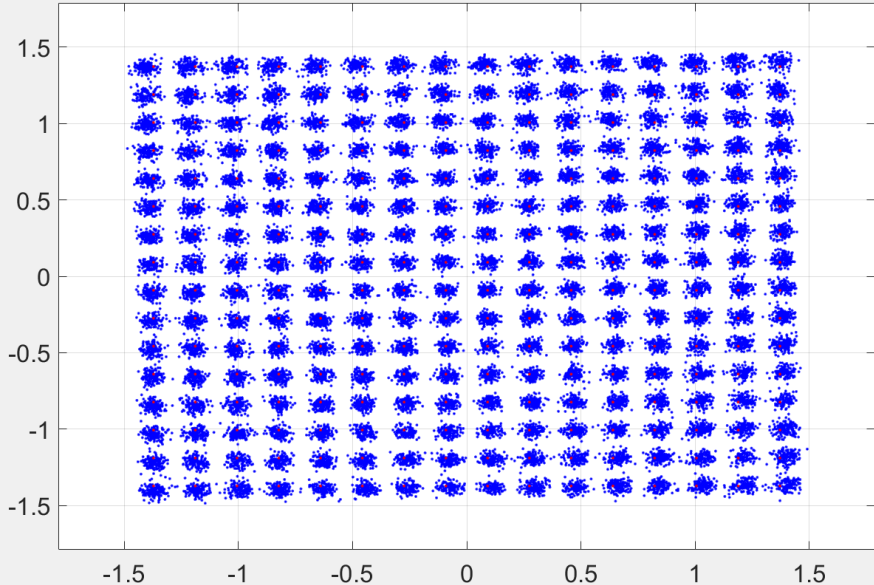
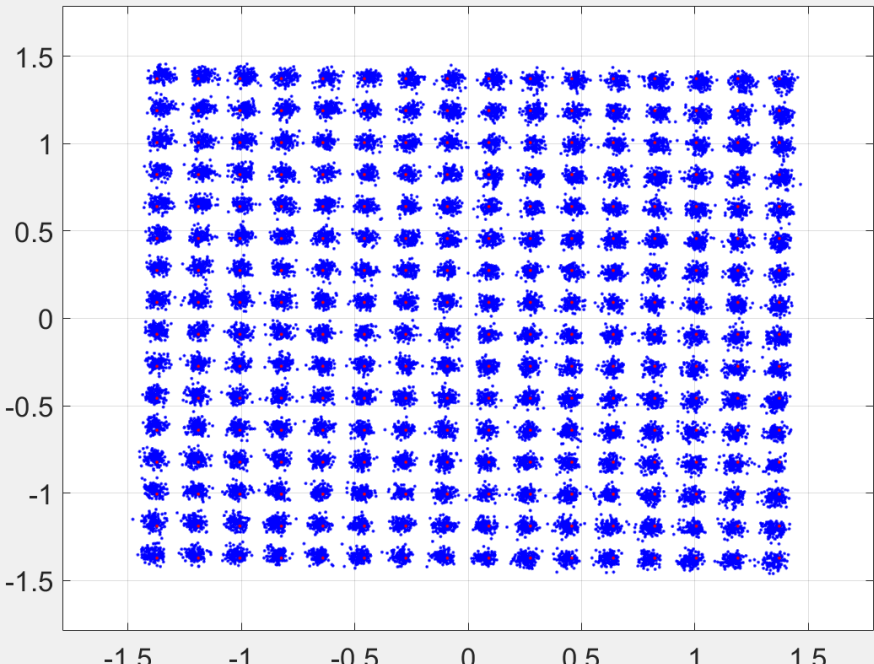
The system can work even with the coupler 90-10, even if the behaviour is not as stable as the coupler 50-50.

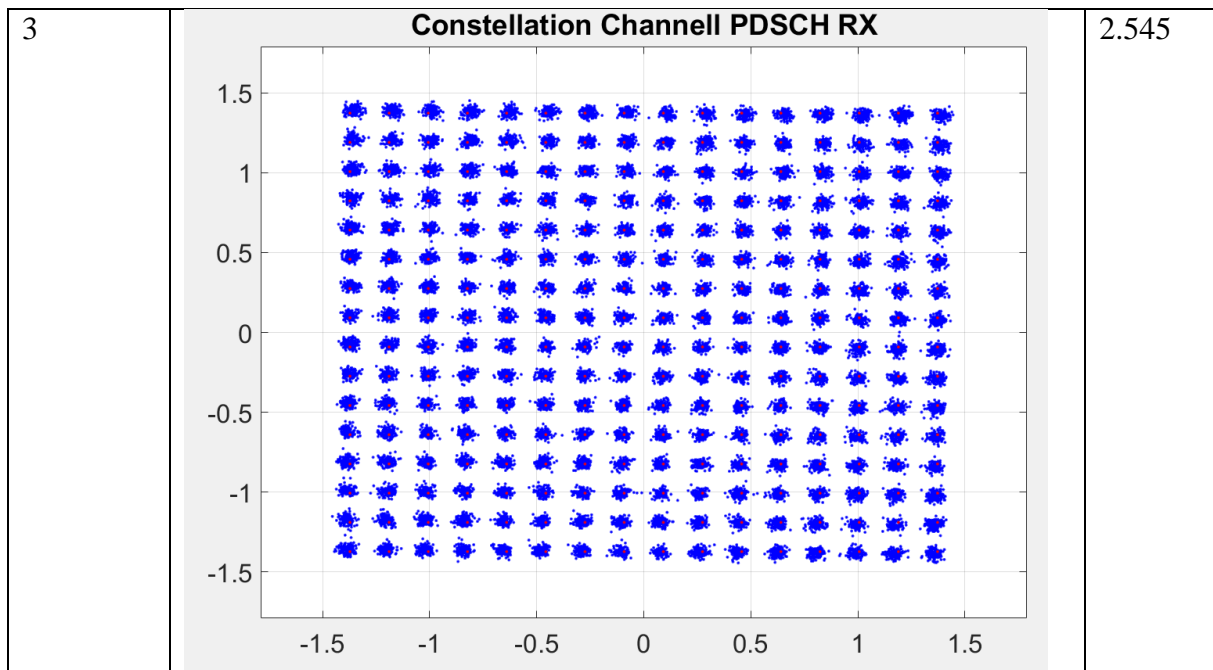
Both the experiment carried with different couplers confirm that, the system can work in direct way, so applying the predistortion algorithm on the direct data stream, but the performance, maintain almost the same even in the case where the training is executed on the feedback (T2 configuration of coupler) and then use the results of the predistortion analysis on the direct link. This is an important result, because it confirms that the predistortion can be applied directly at the transmitting laser using just a commercial coupler, with no complex retroaction link.

3.7.4) TEST 256 QAM IN DIRECT PATH

The final experiment was realized in three sets of measurements for -8, -7 and -5 dBm in order to check if the algorithm just provided can be exploited with higher modulation format. We present the two extremes case for -8 dBm and -5dBm.

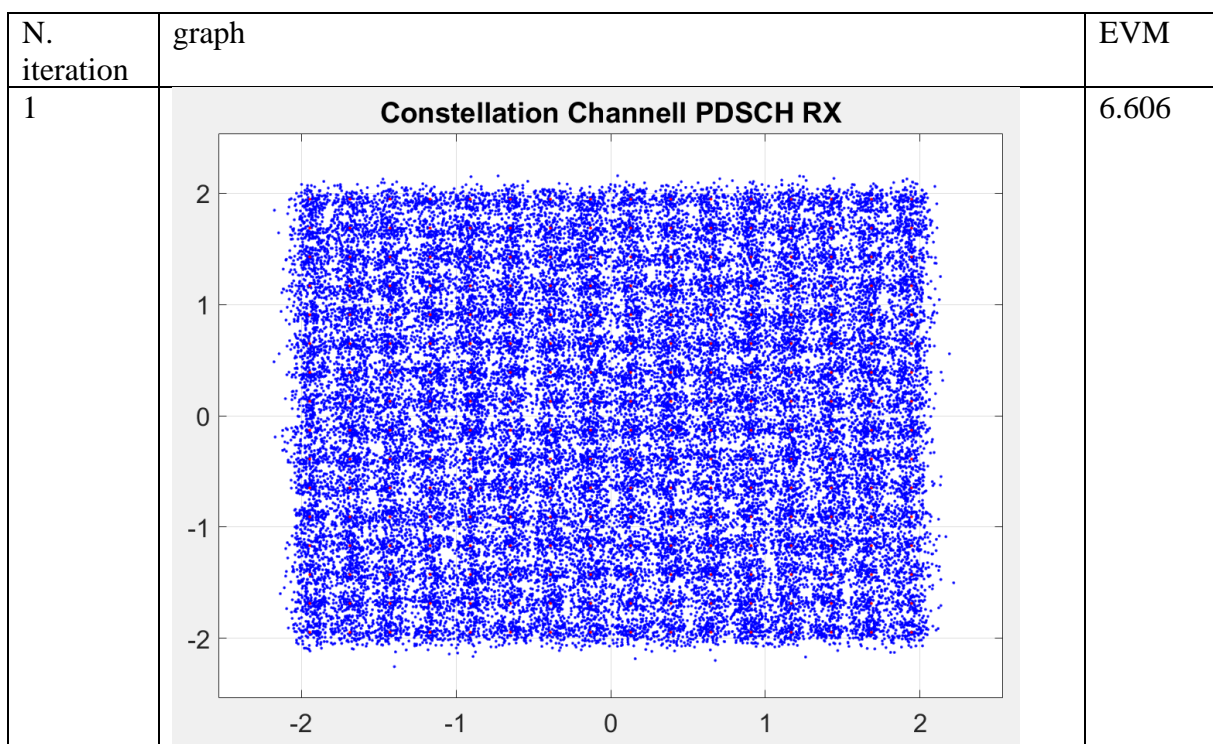
If we consider for instance the case with -8 dBm input power, and check how the EVM and the constellation improve iteration by iteration we get the following results:

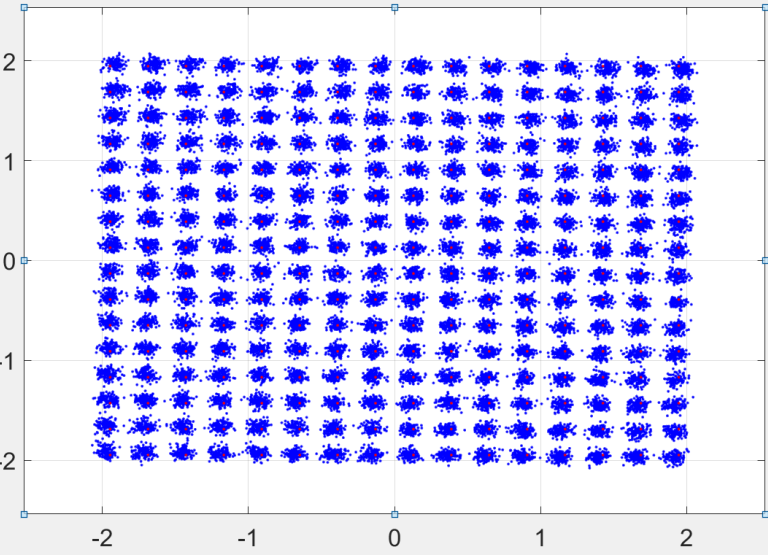
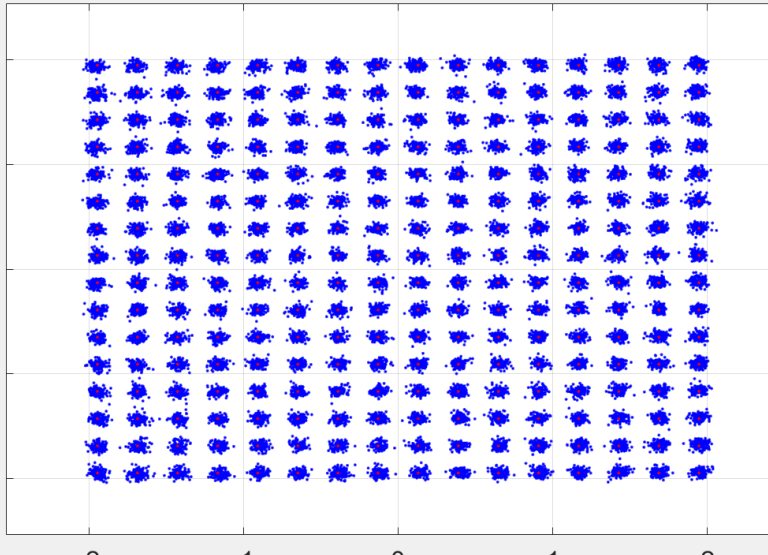
N. iteration	graph	EVM
1	<p style="text-align: center;">Constellation Channell PDSCH RX</p>  <p>The plot shows a 16x16 grid of blue points representing a QAM constellation. The axes range from -1.5 to 1.5. The points are significantly jittered, indicating high error vector magnitude (EVM).</p>	3.423
2	<p style="text-align: center;">Constellation Channell PDSCH RX</p>  <p>The plot shows a 16x16 grid of blue points representing a QAM constellation. The axes range from -1.5 to 1.5. The points are more tightly clustered around their grid positions compared to iteration 1, indicating a lower error vector magnitude (EVM).</p>	3.129



Now if the -5 dBm case is considered, in which the nonlinearities are obviously more than before, the algorithm has more correction to implement. Since the level of distortion increase, we expect to start with a constellation very chaotic that iteration by iteration get closer and closer to the constellation observed in the -8 dBm case in which all the points can be associated with their respective symbol.

In this case the pre-distorter has to correct a lot of error, let's see how the performance improve:



2	<p style="text-align: center;">Constellation Channel PDSCH RX</p> 	3.339
3	<p style="text-align: center;">Constellation Channel PDSCH RX</p> 	2.339

We can see that iteration by iteration the constellation and EVM improve in a considerable way. This result confirm that the procedure just presented can work even with the higher modulation format, so can support LTE in each of his modulation without worsening the performance.

CONCLUSION:

This dissertation has the scope to propose a new technical solution to exploit 850 nm optical system. The first part of the study has focused his attention to the propagations aspect to deal with in systems that exploit VCSEL single mode operating at 850 nm and the single mode fiber SSMF.

As we have seen the main problem to face is the bimodal propagation that takes place inside SSMF when excited with signal operating at 850 nm. This is given by the fact that actually, the SSMF is single mode with signal at 1550 nm, but in case of system working at 850 nm we have the presence of LP01 and LP11 modes. The presence of two modes causes detrimental effects due to intermodal dispersion and modal noise, and a countermeasure has to be found. There exists already some technical solution to this problem, like inserting a small portion of truly single mode fiber SMF 5 μ m between the transmitting VCSEL and the SSMF patch.

In this dissertation we have worked into another direction, exploiting commercial coupler designed to operate at 1550 nm as mode filter. A deep study has been performed adopting this kind of optical device, in order to understand if can work properly as mode filtering devices. The adoption of the commercial coupler, not only is interesting from a filtering point of view, but also allow to create a system integrable with already existing infrastructure operating at 1550 nm, as we can see in the following figure:

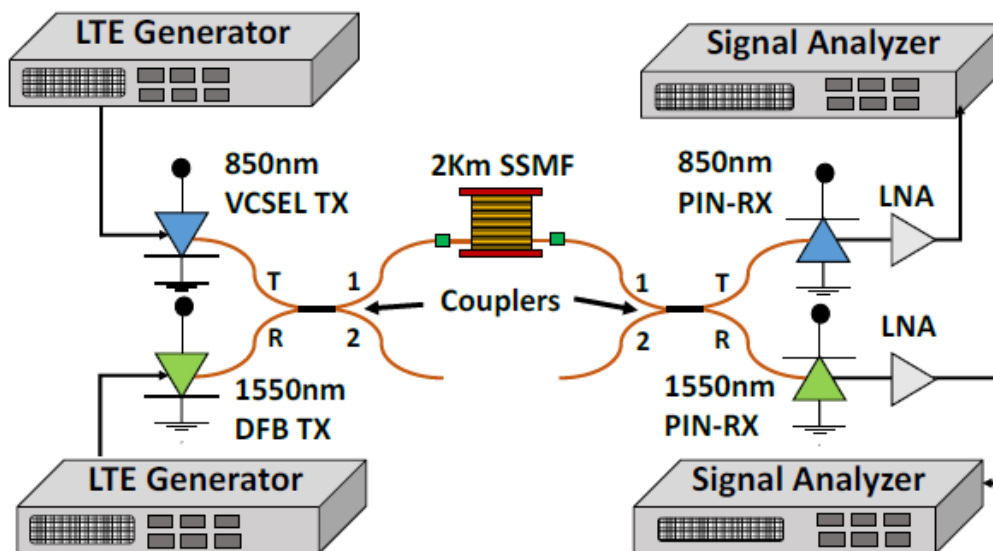


Figure 80: Experimental setup for the characterization of the multi-service WDM 850nm/1550 nm RoF system.[4]

There is more, in fact, using commercial 1550 nm coupler, allows also to exploit the output of coupler unused as feedback loop for DPD algorithm in order to improve the EVM performance. This last aspect is particularly important for the second part of the work realized.

In fact, the second chapter of the work is focus on exploiting the feedback loop using DPD algorithm to improve the EVM, ACPR and NMSE.

The digital predistortion analysis is based on the memory polynomial and can be extend to the generalized memory polynomial. More in specific, we have exploited the ILA structure, using in the pre-distorter and post-distorter the MP in order to characterize the non-linearities and memory effects of the entire RoF link, and enhance the linearization performance. A theoretical analysis of the ILA and the MP model has been performed and then we focus our attention on the Matlab program that applies those concepts for LTE signals.

In the third part of the work, we focus our attention on the realization of such system working with random LTE frame generated by another matlab program. A merging of those two programs has been realized to do that. The idea is to generate an LTE signal carrying random data generated by the program, then this signal is applied as direct modulation on a VCSEL single mode operating at 850 nm over SSMF employing the coupler as mode filter and for the feedback loop. Then the signal is received by a photodiode and then pass through an optical amplifier. At this point the signal goes back to the Anritsu board at the receiving port, and the data are passed to the PC. The data are then imported in matlab, that applies the DPD algorithm and evaluate the model coefficients. Then a new sequence of data is generated using the coefficients evaluated in the previous iteration and all the procedure restarts.

The results in term of EVM and ACPR are then put in confront with the different configurations tested, showing a very good improvement of the performances. This work has shown the potential of this kind of systems and opens the door to new study and applicative scenarios of the digital predistortion in RoF systems.

One of the critical aspects to deal with, is the sizing of the MP or GMP, where the problem is even harder. An improvement to this work could be the realization of program, able to find the correct coefficients configuration, to find the best trade-off between complexity and accuracy. The procedure to find the best settings of the model can be realized with neural network or different kind of new algorithms like Hill-Climbing Heuristic and many others.

In conclusion this work presents different innovations like the use of the commercial 1550 nm coupler and the feedback loop for DPD algorithm, showing very interesting results, and definitely opens the door to new technical solution for the realization of low-cost, low-power consumption RoF system for medium and short connections, like the one present the MFH of the mobile networks or for DAS.

BIBLIOGRAFY

- [1] Jacopo Nanni, Francesco Pizzuti, Giovanni Tartarini, dipartimento di Ingegneria dell'Energia elettrica e dell'informazione "Guglielmo Marconi" University of Bologna, "VCSEL-SSMF-based Radio-over-Fiber link for low cost and low consumption Wireless Dense Networks".
- [2] Jacopo Nanni, Jean-Luc Polleux, Catherine Algani, Simone Rusticelli, Federico Perini and Giovanni Tartarini, "VCSEL-based Radio-Over-G652 Fiber System for Short-/Medium-Range MFH Solutions".
- [3] Jacopo Nanni, Simone Rusticelli, Carlos Viana, Jean-Luc Polleux, Catherine Algiani, Federico Perini, and Giovanni Tartarini, "Modal Noise Mitigation in 850-nm VCSEL-Based Transmission System Over Single-Mode Fiber".
- [4] Jacopo Nanni, Lorenzo Baschieri, Andrea Giovannini, Enrico Lenzi, Jean-Marc Lahuerte, Jean-Luc Polleux, and Giovanni Tartarini, "Efficient Solution to Bimodal Propagation Effects in Low-Cost 850 nm Radio over G-652-Fiber Systems".
- [5] David Garcia-Rodriguez, Maria Morant, Juan L. Corral, Roberto Llorente, "Modal selectivity at 850 nm employing standard single-mode couplers: Theory and experimental demonstration".
- [6] Muhammad Usman Hadi, Jacopo Nanni, Pier Andrea Traverso, Giovanni Tartarini, Olivier Venard, Geneviève Baudoin, Jean-Luc Polleux, "Experimental evaluation of digital predistortion for VCSEL-SSMF-based Radio-over-Fiber link".
- [7] Xiupu Zhang, Ran Zhu, Dongyan Shen and Taijun Liu, "Linearization Technologies for Broadband Radio-Over-Fiber Transmission Systems".
- [8] Luis C. Vieira, Nathan J. Gomes, Antony Nkansah, Frédéric van Dijk, "Behavioural Modeling of Radio-over-Fiber link Using Memory Polynomials".
- [9] F. Fuochi, M.U. Hadi, J. Nanni, P.A. Traverso, G. Tartarini, "Digital Predistortion Technique for the Compensation of Nonlinear Effects in Radio over Fiber links".
- [10] Taijun Liu, Slim Boumaiza, Fadhel M. Ghannouchi, "Deembedding Static Nonlinearities and Accurately Identifying and Modeling Memory Effects in Wide-Band RF Transmitters"

- [11] Chunjing Yin, Jianqiang Li, Hao Chen, Qiang Lv, Yuting Fan, Feifei Yin, Yitang Dai and Kun Xu, "Behavioral Modeling and Digital Compensation of Nonlinearity in Multi-band Externally-modulated Radio-over-fiber Links".

- [12] Mazen Abi Hussein, Vivek Ashok Bohara, Olivier Venard, "On the system level convergence of ILA and DLA for digital predistortion".

- [13] Dennis R. Morgan, Zhengxiang Ma, Jaehyeong Kim, Michael G. Zierdt and John Pastalan, "A Generalized Memory Polynomial Model for Digital Predistortion of RF Power Amplifiers".

- [14] Lei Ding, G. Tong Zhou, Dennis R. Morgan, Zhengxiang Ma, J. Stevenson Kenney, Jaehyeong Kim and Charles R. Giardina, "A Robust Digital Baseband Predistorter Constructed Using Memory Polynomials".

- [15] Francesco Pizzuti, Giovanni Tartarini, Jacopo Nanni, "Sviluppo di un software per la caratterizzazione di un collegamento LTE radio-over-fiber e realizzazione del relativo banco di misura".

- [16] Siqi Wang, Geneviève Baudoin, Olivier Venard, Mazen Abi Hussein, "Study on Complexity Reduction of Behavioural Modeling Digital Predistortion for Power Amplifier Linearization".